AFOSR - TR - 60-124

Final Technical Report on Contract AF 49(638)-90

ELECTRICAL, OPTICAL, AND THERMAL PROPERTIES OF THE M_2^{Vb} N_3^{VIb} SEMICONDUCTORS

Lee Gildart - Principal Investigator

October 1961

UNIVERSITY OF KENTUCKY
KENTUCKY RESEARCH FOUNDATION
UNIVERSITY STATION · LEXINGTON, KENTUCKY

Directorate of Solid State Sciences
Air Force Office of Scientific Research
Air Research and Development Command
Washington 25, D. C.

AFOSR - TR - 60-124

Final Technical Report on Contract AF 49(638)-90

ELECTRICAL, OPTICAL, AND THERMAL PROPERTIES OF THE $M_2^{Vb} N_3^{VIb}$ SEMICONDUCTORS

Lee Gildart - Principal Investigator

(Period Covered - July 1, 1958 through January 31, 1961)

Directorate of Solid State Sciences
Air Force Office of Scientific Research
Air Research and Development Command
Washington 25, D. C.

GENERAL INTRODUCTION

The research aims of this contract set forth in the contract schedule are as follow:

Statement of Work: The contractor shall, during the period of the contract, furnish the necessary personnel, facilities, supplies and materials to conduct research in the general field of the Electrical, Liquid-Solid Transformation Properties, of Systems of the Group Va and VIa Elements, * and specifically shall investigate and submit reports in accordance with the following items:

a. Determination of the electrical properties (the usual parameters for semiconductors) of the compounds and systems.

b. Quantitative study of the liquid solid transformation of the compounds and systems.

c. Correlation of the findings of (a) and (b) with supplementary data and with existing theories; determination of the type of binding and the improvising of a model or models to explain the properties and behavior of these compounds and systems.

Note of explanation: Parts a) and c) we feel have been satisfactorily developed during the course of this investigation. Part b) was not. The explanation is that 1) The investigator for part b) left the employ of the University after the first year of the contract (the work was summarized in Technical Note AFOSR-TN-58-849) and 2) The other aspects of the work became so important as to occupy the full attention of the remaining investigators. In this connection it is noted here that U. S. Patent No. 2, 968, 014, on the switching effect in stibnite was a direct result of this contract and is classified specifically under part c).

* The newer usage is to classify the elements here concerned as Vb and VIb. Specifically, the elements are: arsenic, antimony, bismuth, oxygen, sulfur, selenium and tellurium.

CONTENTS

PART I

SOME ELECTRICAL AND OPTICAL PROPERTIES OF ANTIMONY TRISELENIDE AND ANTIMONY TRISULFIDE

INTRODUCTION

Inasmuch as Sb_2Se_3 and Sb_2S_3 are semiconductors not only in the crystalline state but also in the non-crystalline (vitreous) state, one must look for a basis for the band scheme other than the periodicity of structure. Consideration of various liquid and non-crystalline solid semiconductors has led Ioffe and Regel[1] to comment that this basis may be found in the short range order, i.e., in the chemical bonds between the atoms. Similarly, Mooser and Pearson[2] have developed a "semiconducting bond" scheme to account for the behavior of various compound semiconductors. In the band picture, this semiconductivity arises from the saturation of chemical bonds resulting in filled valency zone levels.

Mooser and Pearson have briefly discussed crystalline Sb_2Se_3 and stibnite (Sb_2S_3) and we follow their scheme, extending it also to apply to the vitreous form of Sb_2Se_3. Indeed, the similarities appearing in the optical absorption band edges for crystalline and non-crystalline Sb_2Se_3 strengthen the short range order viewpoint. (In this work, "non-crystalline" and "vitreous" will be used to designate forms which appear structureless by X-ray diffraction, although we recognize that vacuum deposited films of Sb_2S_3 show some structure by electron diffraction.[3])

Changes in this short range order, where the proportion of one constituent exceeds the true stoichiometric proportion, will then be used to account for the unusual behavior of these compounds. Specifically we refer here to: (1) the resistivity "discontinuity" observed in Sb_2Se_3[4,5] and (2) the low voltage breakdown in Sb_2S_3.[6] These effects are observed only in samples whose antimony content exceeds the stoichiometric ratio. If the antimony content is less than stoichiometric, very little change in behavior is found.

CHAPTER I

SEMICONDUCTING MODEL

Because Sb_2Se_3 and Sb_2S_3 are crystalline isomorphs[7] and sulfur and selenium are alike in their electronic structure, having six valence electrons outside closed shells, it is to be expected that the same kind of model is applicable to both compounds, and for the reasons already given, the model is based on the chemical bond idea.

1.0 Crystal Structure

Both Sb_2Se_3 and Sb_2S_3 crystallize in an orthorhombic, $D5_8$, structure. The cell parameters are a = 11.62A, b = 11.77A, c = 3.96A for Sb_2Se_3[7] and a = 11.20A, b = 11.28A, c = 3.83A for Sb_2S_3[8]. The unit cell of Sb_2Se_3 is shown in Fig. 1, which is a projection onto the x-y plane, and there are four molecules per unit cell. The shaded atoms lie in the plane of the diagram and the unshaded atoms occupy a plane a distance of c/2 above and below. Columns of double molecules, Sb_4Se_6, extend indefinitely both ways in the c direction. One such column is seen in the center of the unit cell.

Consideration of a single unit cell might lead one to predict cleavage approximately along a (110) plane, but further consideration of several unit cells will show that one should rather expect cleavage along the puckered sheet parallel to the (010) plane. The large

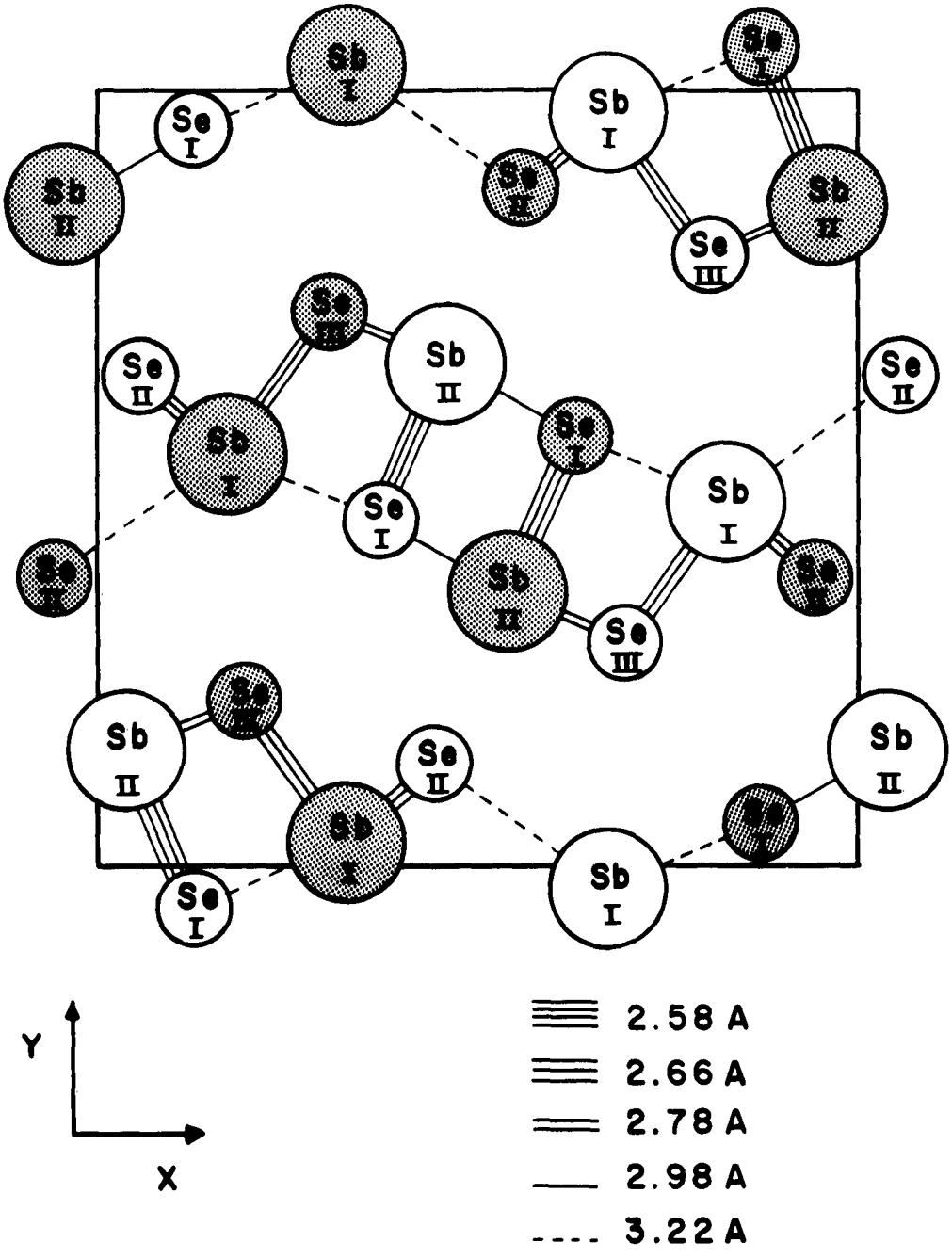

Fig. 1. The Unit Cell for Antimony Triselenide

separation of sheets compared to near neighbor separations within the sheets indicates easy cleavage. This is observed and the cleavage plane is seen to be the (010) by X-ray diffraction. The cleavage is easy and this weakness makes the handling of single crystals difficult. Particular care must be exercised in cutting perpendicularly to the cleavage plane to prevent separation of these sheets.

1.1 The Semiconducting Bond

Antimony has five valence electrons. Assuming that saturated chemical bonds are required for semiconducting behavior, we expect antimony to be a semiconductor when each antimony atom has just three nearest neighbors, i.e., forms only three covalent bonds. A semiconducting modification of pure antimony has been observed [9] in evaporated layers less than 2000 A thick. Here the atoms do have three nearest neighbors, the next nearest neighbors being sufficiently distant to permit a coordination number of three. [2] The bonds are saturated-covalent and semiconductivity is observed.

Upon crystallization the next nearest neighbors come closer, and so there is an increase in coordination number beyond the covalency requirement, and metallic behavior results, i.e., metallic bonds are formed. Similarly, saturated covalent bonds in Se and S require no more than two nearest neighbors, with the next nearest neighbors again being relatively far away.

Observation of the structure shown in Fig. 1 shows that both the Sb and Se atoms have a coordination number exceeding this covalency, and the same is true for Sb and S. The normal covalent radii[10] for these elements are given as Sb-1.41A, Se-1.17A, and S-1.04A. Tideswell et al.[7] have related bond distances to bond numbers in Pauling's[11] equation,

$$D_n = D_1 - 0.600 \log n,$$

where

D_n = observed bond distance.

D_1 = single-bond distance.

n = bond number.

Using D_1 = 2.58A for Sb_2Se_3, the sum of the bond numbers for Sb_1 (position 1) is 2.42 and for Sb_2 (position 2) is 2.49. This D_1 is the sum of the normal covalent radii of Sb and Se. If a somewhat larger radius for Se is used[7], D_1 = 2.63A. The sums of the bond numbers are then 2.97 and 2.92 for the two Sb atoms, and 1.93, 1.95, 2.02 for the Se atoms. These last sums are very nearly equal to the valences. The bonding is thus predominantly covalent. We estimate the ionic contribution to these bonds to be only 8%, from an empirical relationship[10] between the ionic character of bonds and the electronegativity difference of Sb and Se.

Bond angles of nearly 90° indicate formation of p-bonds rather than hybrid bonds, but the atoms cannot accommodate their nearest neighbors with pure p-bonds. This fact has led Mooser and Pearson[2] to postulate that semiconductivity results when the bonds on only one atom type become saturated. The Sb atom can accommodate six nearest neighbors with "p-resonance" type bonds and still allow the bonds on the Se atoms to be saturated. The empty orbital required[12] for this resonance can come from partial transfer of an electron from the Sb atom to the more electronegative Se. If the development of these resonances is between like atoms metallic behavior results.

Thus "p-resonance" bonding developed only on the Sb atoms satisfies the coordination and the bond angles, and allows saturation of the Se (or S) bonds, resulting in semiconducting behavior for Sb_2Se_3 and Se_2S_3. Evidence that this resonance is developed on the Sb atom rather than on the Se (or S) atom is found in Chapter V.

CHAPTER II

OPTICAL CONSTANTS FOR Sb_2Se_3 FILMS

Although optical constants measured on thin films do not agree with those for bulk material as well as one would like (as for instance in the case of germanium[21]) and a word of caution is to be noted,[22] we have nevertheless made our measurement on thin films (about a micron thick) for the following reasons: First, the vitreous modification of Sb_2Se_3 occurs only in thin films[13]; second, optical absorption in the high absorption region ($K \sim 10^4$ to 10^5 cm^{-1}) can only be studied in thin samples; third, it is of interest to attempt to relate the absorption constant to the spectral photoreponse observed for thin films. In passing, we note that the infrared absorption in Sb_2Se_3 has already been measured on films 0.20 mm thick[20].

2.0 Sample Preparation

The material was prepared by reacting 99.999% Se (American Smelting and Refining Co.) and 99.9% Sb (Belmont) in stoichiometric proportions in an evacuated vycor tube, and refining by a hot zone pass. This compound was then deposited in a vacuum onto clean optical quality substrates of Amersil quartz plates, 1.0 x 0.3 x 0.02 in., polished flat to one fringe. Films deposited on room temperature substrates were found to be vitreous, by X-ray diffraction, while

those deposited onto hotter (175°C) substrates were crystalline. The crystalline films were annealed at this temperature before removal from the evaporation chamber. A series of films ranging in thicknesses from 0.07μ to 1.0μ were prepared.

Film thicknesses are measured by a special method using interference fringes of equal chromatic order[23]. In the evaporation process a strip of the substrate approximately 1 mm wide is shielded from the sample deposit, producing a gap. An opaque layer of silver is then deposited onto the film, following the contour of the gap which has a depth equal to the film thickness. This is illustrated in cross section in Fig. 2a. Next a semitransparent mirror is prepared by depositing silver onto a glass slide until a transmission of around 2 per cent is obtained. These two silver surfaces are then brought close together to form an interference system as in Fig. 2a. The silver on the film eliminates the error due to the phase shift at reflection being different for the Sb_2Se_3 and silver.

A slit of white light is then imaged at normal incidence on the interference plates so that the image is perpendicular to the gap and about four or five times as long as the gap is wide. The reflection of this image is then focused on the slit of a Gaertner monochromator. The observed interference pattern is that of Fig. 2b.

The spectral order, m, of the interference fringe at λ_1,

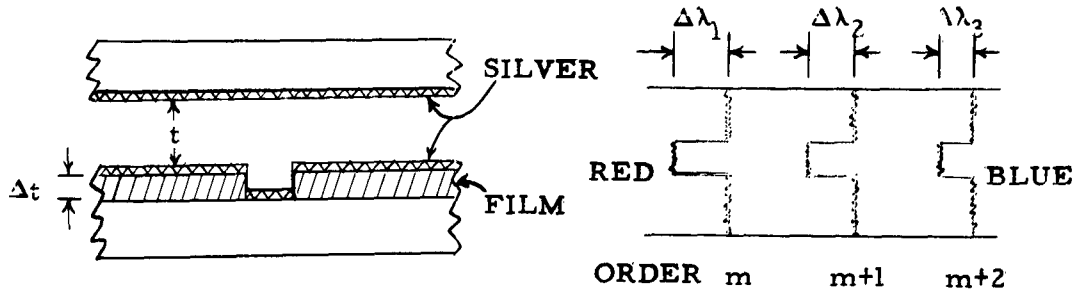

(a) Interference Plates (b) Interference Spectrum

Fig. 2. The Interference System for Film Thickness Determination

may be found from the relation:

$$m\lambda_1 = (m + 1)\lambda_2 = 2t \qquad \lambda_1 > \lambda_2, \qquad (1)$$

where λ_1 and λ_2 are the wavelengths of adjacent fringes and t is the geometric separation of the reflecting surfaces. Thus,

$$m = \lambda_2/(\lambda_1 - \lambda_2). \qquad (2)$$

As the spectral order is the same for the small displaced part of the fringe,

$$m(\lambda_1 + \Delta\lambda_1) = 2(t + \Delta t), \text{ or}$$

$$\Delta t = (m / 2)\Delta \lambda_1, \qquad (3)$$

where Δt is the film thickness.

This elementary treatment neglects the effect of the phase change suffered by the light upon reflection from the silvered surfaces. However, the phase change on reflection from silver is independent of wavelength throughout most of the visible spectrum[38] and, for spectral orders greater than 8 (as used in our measurements), the elementary treatment introduces an error of less than 0.5 per cent[23]. Using this method to measure the thickness of 100 A films, Scott et al.[39] report a precision of 5%. The root mean square deviations in our measurements, 33A for the thin films ($\Delta t \sim$ 700A) to 250A for the thick films ($\Delta t \sim$ 11,500A), are of this order.

2.1 Optical Transmission

The transmission of light through these films is observed from 2.5 μ to 0.4 μ using a Cary Model 14 spectrophotometer. This is a recording instrument sufficiently sensitive and light-tight to measure optical densities as large as 5, i.e., 10^{-3} per cent transmission. Typical spectra are shown in Figs. 3 and 4 for various thicknesses of crystalline and vitreous films. The optical density, -log T, of the substrate has been subtracted from this data. The substrate, Amersil quartz, has only minor absorption bands in this region.

The transparancies of the vitreous films in the infrared

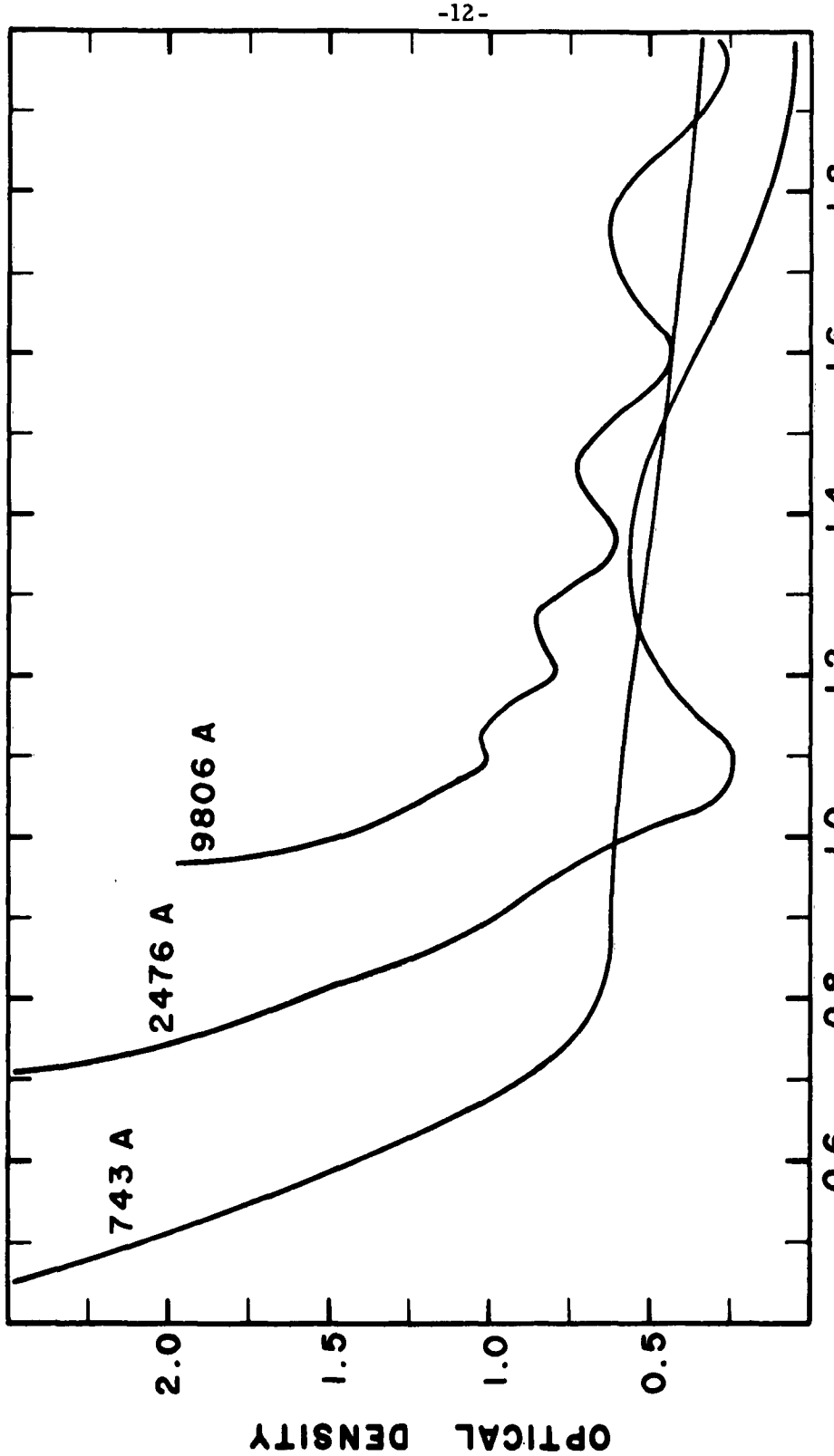

Fig. 3. Optical Absorption in Crystalline Films of Sb_2Se_3

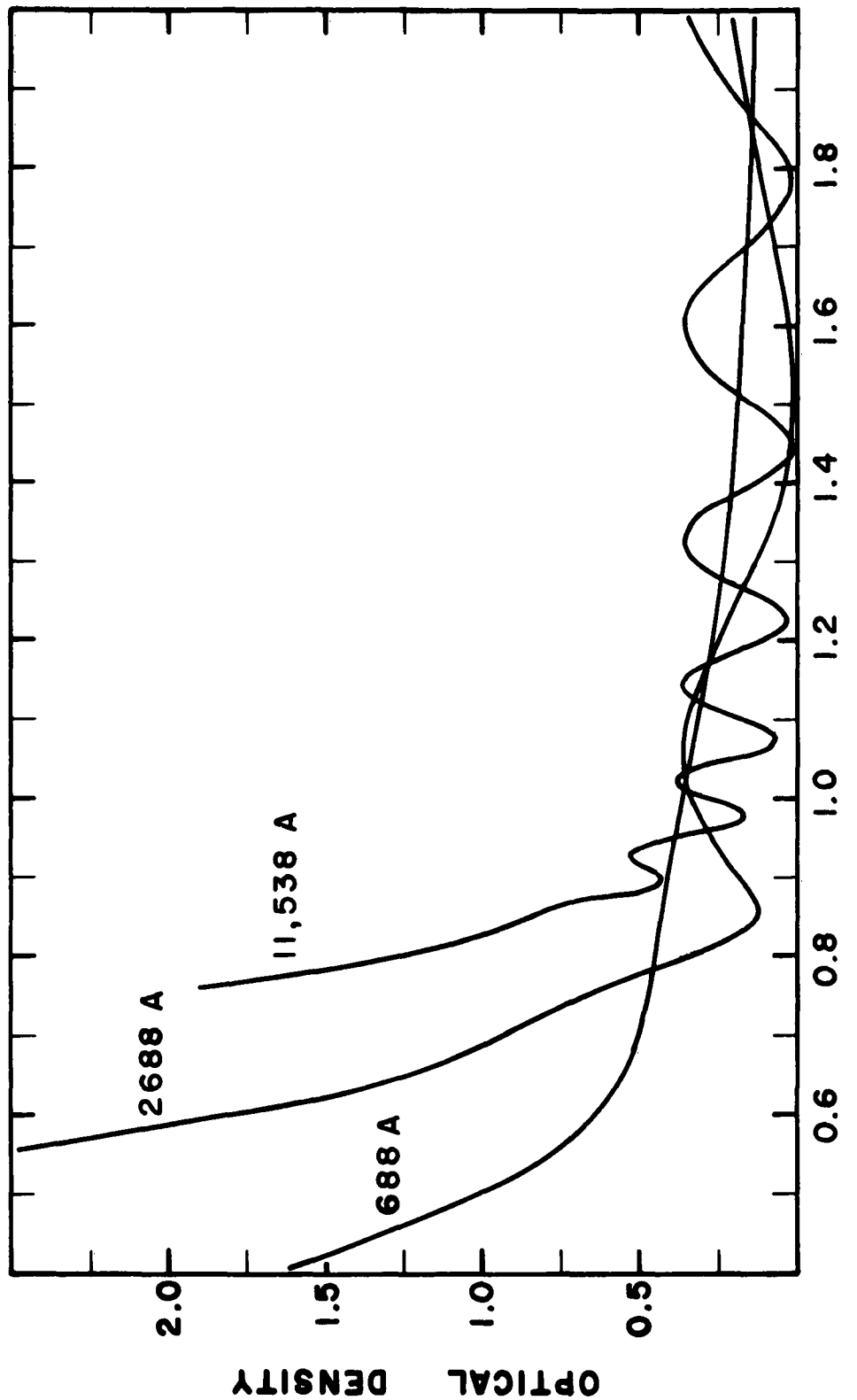

Fig. 4. Optical Absorption in Vitreous Films of Sb_2Se_3

approach 100%. Comparison of Figs. 3 and 4 show that, for the same film thicknesses, the absorption edge for vitreous films is shifted toward shorter wavelengths. The higher optical density observed in the infrared for the thinnest film is due to multiple reflections. The transmission data were obtained at normal incidence. These multiple reflections prevent using the usual method of assigning an optical density, equal to the difference in optical densities of two layers, to a layer of thickness equal to the difference thickness.

2.2 Determination of the Optical Constants

Harris, Beasely and Loeb[24] have considered the rather involved problem of transmission of light at normal incidence on an absorbing film backed by a transparent layer. They give for the transmission, T_o, in the medium of the substrate, the following:

$$T_o = \frac{4n_b}{\left| (n_b + 1)\cos(2\pi t z/\lambda) - i\left[(n_b/z) + z\right]\sin(2\pi t z/\lambda)\right|^2} \qquad (4)$$

where n_b is the index of refraction of the substrate, λ is the wavelength of the incident light, t is the thickness of the absorbing layer and z is the complex index of refraction, $n + ik$. The absorption coefficient, k, and the absorption constant, K, are related by $K = 4\pi k/\lambda$.

Taking the absolute value, (4) becomes

$$T_o = \frac{16\, n_b (n^2 + k^2)}{r^2 \{ [e^y - (s/r)e^{-y}]^2 + 4(s/r)\sin^2[x + (\theta/2)] \}} \qquad (5)$$

where

$$y = 2\pi k t/\lambda \ , \quad x = 2\pi n t/\lambda$$

$$r^2 = [(n+1)^2 + k^2][(n + n_b)^2 + k^2]$$

$$s^2 = [(n-1)^2 + k^2][(n - n_b)^2 + k^2]$$

$$\sin\theta = 2k(n_b + 1)(n^2 + k^2 - n_b)/(s\,r)$$

This differs from the equation of Briggs and Brattain[21] only in the form of the expression for θ.

The expression (5) gives the transmission within the medium of the substrate, so one must correct for the backing-air interface. Harris et al.[24] have shown that for thick subtrates, intensity addition may be used instead of amplitude addition in calculating reflectances if the incident wavelength and the substrate thickness, or both, have a sufficiently large range of probable values. In particular, they have shown that, for a wavelength of 6000A and a glass substrate, 0.02 in thick, with parallel sides, and a spread in wavelength of 100A, the reflectances calculated using intensity addition and amplitude addition differ by less than 0.015%. Correcting for the substrate by intensity addition, we have

$$T = T_o(1 - R_1)/(1 - R_1R_2) \qquad (6)$$

where

$$R_1 = (n_b - 1)^2/(n_b + 1)^2 \text{ and } R_2 = (n - n_b)^2/(n + n_b)^2.$$

Equation (5) cannot be solved for n and k explicitly, and so the Kentucky IBM 650 computer was called on to solve for these parameters by iteration. A complete description of the computer program devised for the problem is given in Appendix I, including all Fortran statements.

The method of calculation is as follows: At a particular wavelength, the known index of refraction of the base, the optical densities of the film-substrate composites, the thicknesses of two films and a rough estimate of n and k are given to the machine. The index of refraction is estimated from the multiple reflections in the infrared, and k can be taken as zero in this region. The machine calculates an optical density for one sample then compares this with that observed, and adjusts k, holding n constant, until the computed and measured values agree for this sample. The closeness of agreement can be adjusted and is generally made about the width of the noise on the paper chart trace (i.e., optical density ~ 0.01). Using this pair of n and k the computer next calculates an optical density for a second film of different thickness and compares this to the measured

value. An adjustment in n is made, and iteration on k in the first loop for the first film is again made. When acceptable values of both n and k are finally found these values are recorded on the punched cards. This procedure is followed for pairs of films over the whole wavelength range considered.

It is not always possible to fit the data by this method at every point, as for example where an interference maximum for one film coincides with an interference minimum for the other. The variation in k also tends to follow the interference pattern. This lack of agreement between calculated and observed values at interference maxima has also been noted[21] for thin germanium and silicon films. The resulting optical constants are seen in Figs. 5 and 6 for the crystalline and vitreous films respectively. These are the average values for four films of each modification, taken two at a time.

The real part of the index of refraction, n, for crystalline films seems to approach a constant value of 3.8 at about 2 μ. For vitreous films, n is about constant at 3.0 from 1.2 μ to 2.4 μ. Kostyshin[25] has determined n from multiple reflections in films of Sb_2Se_3, 10-100 μ thick. He shows n decreasing monotonically from about 3.1 at 1 μ to 2.65 at 2 μ, with n decreasing only slightly to about 2.61, from 2 μ to 9 μ. These values are near those of our vitreous films, but Kostyshin's films are absorbing whereas ours

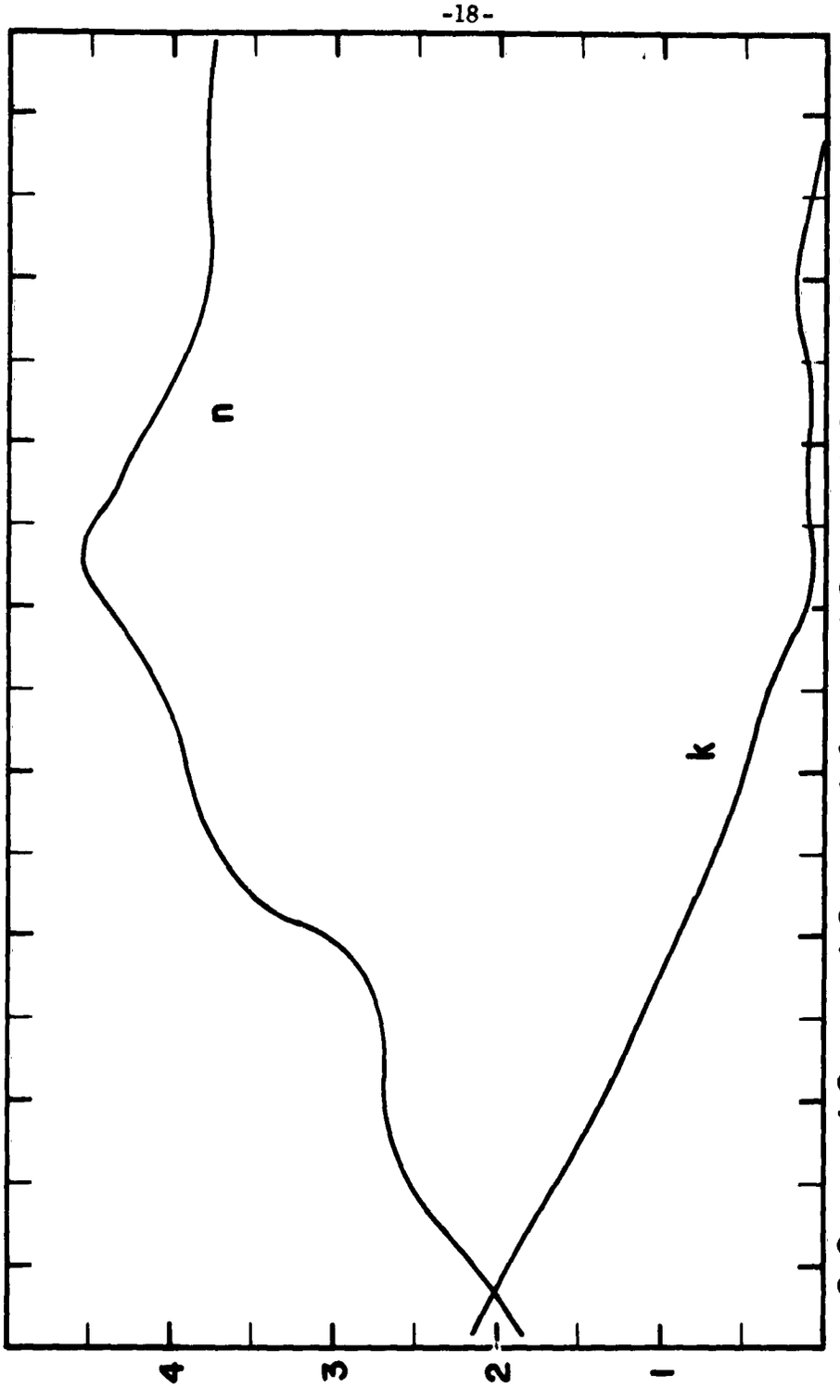

Fig. 5. Optical Constants for Crystalline Films of Sb_2Se_3

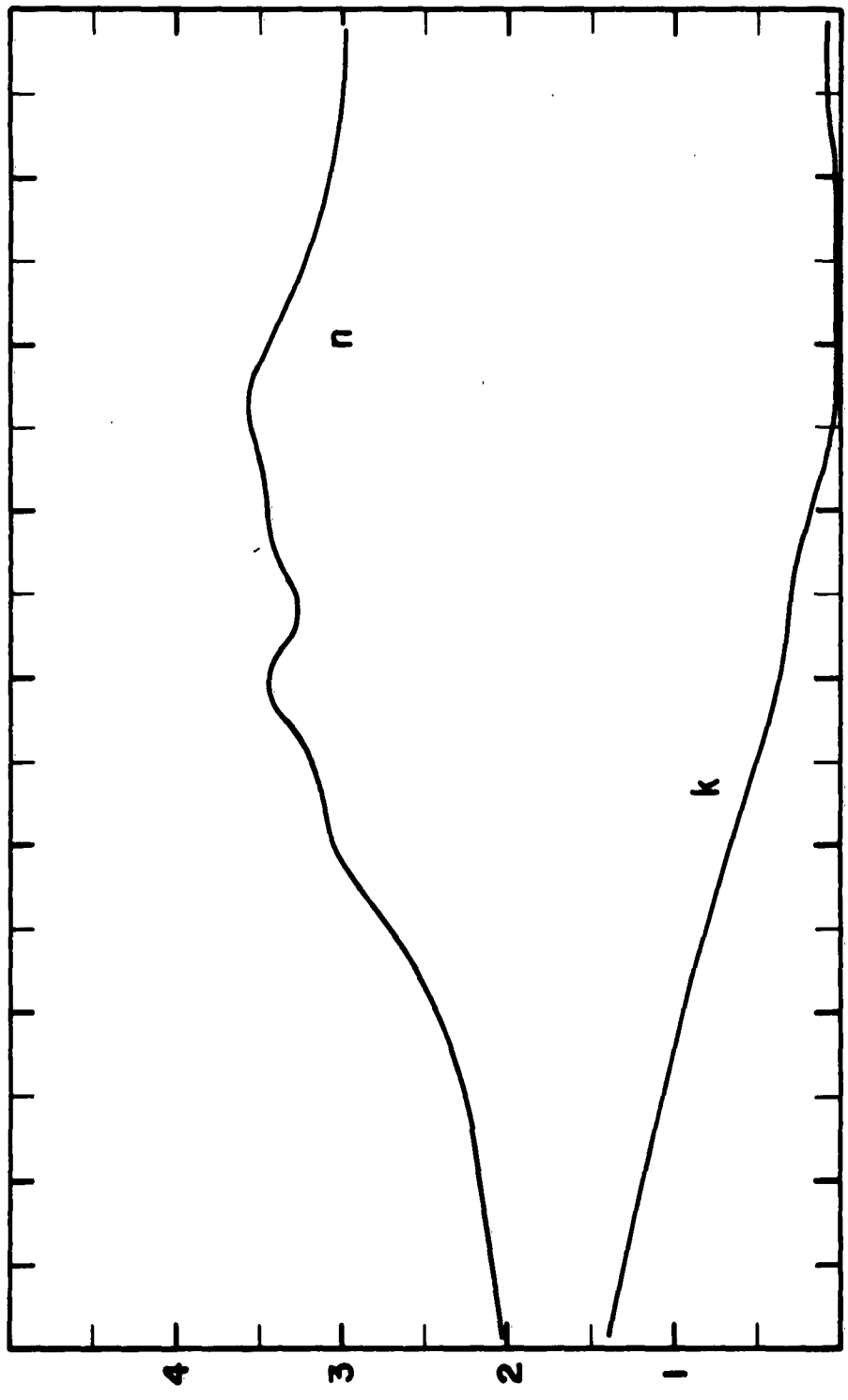

Fig. 6. Optical Constants for Vitreous Films of Sb_2Se_3

are quite transparent in the region between 1.2 μ and 2 μ. The onset of crystallization in Kostyshin's thicker films may account for the absorption in this region.

The difference (~ 12%) between our values of n at 2 μ is probably not entirely due to errors in film thickness determinations. Although we do not know the details of Kostyshin's sample preparation, a possible explanation presents itself if he used Se rich Sb_2Se_3. We have noted[13] a selective distillation of Se from the melt in the vacuum deposition of Sb_2Se_3 films. If his films contained an underlying coat of pure Se(n = 2.46 at 2 μ[28]), his value of n would certainly be less than ours.

2.3 The Absorption Edge

The square root of K, the absorption constant ($K = 4\pi k/\lambda$), for both crystalline and vitreous films is plotted as a function of the photon energy in Fig. 7. The onset of strong absorption in the crystalline films is at 1.18 eV, in good agreement with that found[20] for bulk samples of Sb_2Se_3. The onset of strong absorption in the vitreous films begins at 1.5 eV. Assuming that the band gap is a linear function of the temperature, $E_g = E_g(0^\circ K) + \beta T$, between room temperature and 78°K, β is -4.4×10^{-4} eV/C° for the vitreous films and -3.0×10^{-4} eV/C° for the crystalline films.

Black et al.[20] have given $\beta = -7 \times 10^{-4}$ eV/C° for bulk Sb_2Se_3

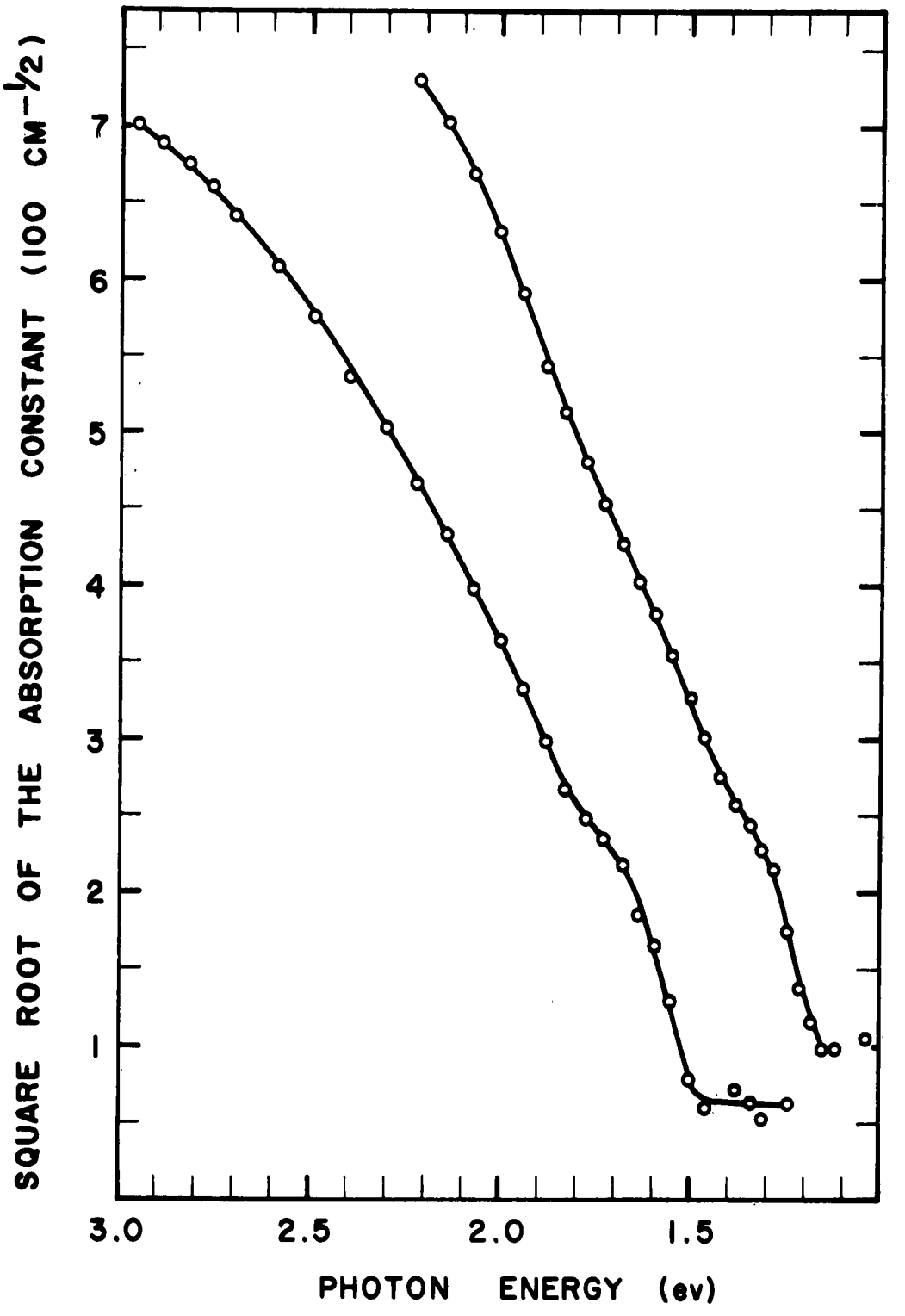

Fig. 7. Optical Absorption Band Edges for Crystalline and Vitreous Films of Sb_2Se_3

crystals.

The structure seen in both edges resembles that for the low level absorption edges of germanium and silicon[26]. The transitions are by indirect absorption (absorption accompanied by the emission or absorption of a phonon) which occurs in materials having a valence band maximum which is shifted with respect to the conduction band minimum in k-space. The long wavelength limit of photoconductivity in evaporated Sb_2Se_3 films is 0.95 μ (1.305 eV)[27] (see also Chapter III) which suggests that the absorption seen from 1.2 eV to 1.3 eV is due to exciton creation. That is, upon absorption of a photon, an electron makes a transition to a non-conducting (bound) state.

The difference between the optical energy gap, 1.18 eV, and the previously observed[13] thermal energy gap, 1.07 eV, may be due to the partly ionic character of the bonds in crystalline Sb_2Se_3. The optical activation energy is the energy required to remove an electron with the nearby atoms undisturbed[28]. The atoms move to new equilibrium positions following the absorption, the energy of the crystal being somewhat lowered in the process. The thermal activation energy is the energy difference between this final state and the original state, and thus is lower. This difference is slight for non-polar materials, but may be large for polar materials[28].

Strangely, the optically determined band gap for vitreous films

(1.5 eV) turns out to be smaller than that (1.83 eV) determined[13] thermally. Why this happens is not clear, but an interesting point for speculation is the occurence of a kink in the vitreous band edge at about 1.8 eV. Kunze[29] found a thermal band gap of 2.0 eV for amorphous evaporated films of Sb_2S_3, and a kink in the optical absorption band edge for his films appears at 2 eV, but he made no comment on this.

Of greater interest, however, is the indicated relationship between the absoprtion in the two edges in Fig. 7. The onset of strong absorption for vitreous Sb_2Se_3 (1.5 eV) occurs at the same energy as the break in the crystalline edge. Furthermore, the break in the vitreous edge ($\sim$ 1.8 eV) is accompanied by a slight break in the crystalline edge at this energy.

This is evidence that some short range order (e.g., similarly oriented short chains of molecules) in the vitreous material is preserved upon crystallization. The semiconducting properties of Sb_2Se_3 may well be mainly a result of this short range order.

CHAPTER III

SPECTRAL PHOTORESPONSE OF Sb_2Se_3 FILMS

We have observed[13] previously that the spectral sensitivities of Sb_2Se_3 films, deposited in a vacuum, are essentially flat throughout the visible part of the spectrum. Films, one micron thick, were made by evaporating stoichiometric Sb_2Se_3 at pressures less than 10^{-4} mm Hg to obtain a deposition rate of about 20A/sec. No attempt was made to sensitize the layers. Both vitreous and crystalline films exhibit this flat response, although the sensitivities vary.

The spectral sensitivity of several evaporated films is seen in Fig. 8. The long wavelength limit of photoconductivity is 0.92μ (1.35 eV.) This agrees with the value, 0.95 μ, observed by Braitwaithe[27] on evaporated Sb_2Se_3 films. The long wavelength limit is defined as the wavelength at which the response has dropped to one half of the maximum value. The closed circles in Fig. 8 represent the data for several films, both crystalline and vitreous, normalized to the maximum sensitivity exhibited by two crystalline films (open circles and crosses). We have examined with some care the region from 0.75μ to 0.4μ and find this region essentially flat.

Determination of the optical absorption constant for films thinner than those previously reported[13] indicates that K varies approximately as the square of the photon energy in this region

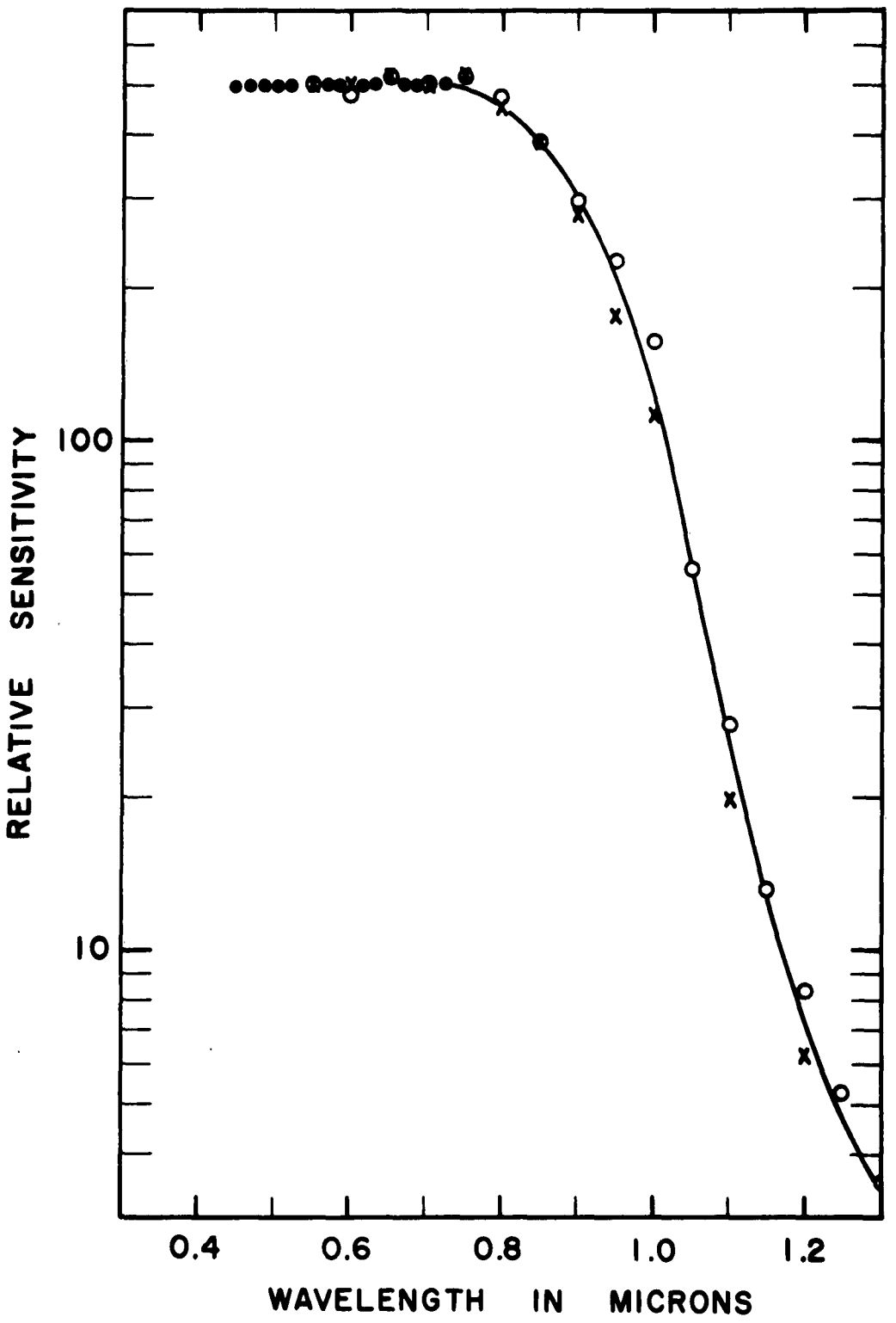

Fig. 8. Spectral Photoresponse in Films of Sb_2Se_3

(see Chapter II). Furthermore, K exceeds 10^5 cm^{-1} for wavelengths less then about 0.8 μ. Moss[28] states that one may expect linear response for low values of K, but for large ($K \sim 10^5$ cm^{-1}) values, one should expect approximately

$$N = 2(f/BK)^{1/2}, \tag{7}$$

where N is the equilibrium concentration of photoelectrons, f is the incident light flux, B is the recombination coefficient for holes and electrons, and K is the absorption constant. As K is proportional to λ^{-2} in Sb_2Se_3 in the high absorption region, we should expect from (7) that N would be proportional to the wavelength. That is, the sensitivity should fall off with decreasing wavelength. The derivation of (7) assumed equal mobilities for holes and electrons; however, thermoelectric power measurements[20] indicate a ratio of hole to electron mobility of about three. The majority carriers in Sb_2Se_3 are holes. Because the mobilities are small (see Chapter IV) one would expect the diffusion constant given by Einstein's relation, $D = \mu kt/e$, to be corresponding small. Consideration of the "lifetimes" observed in the photoconductive decay and the recombination processes involved, leads us to believe that the flat response is nevertheless due to the diffusion process.

Fig. 9 shows the decay of photocurrent in a typical evaporated

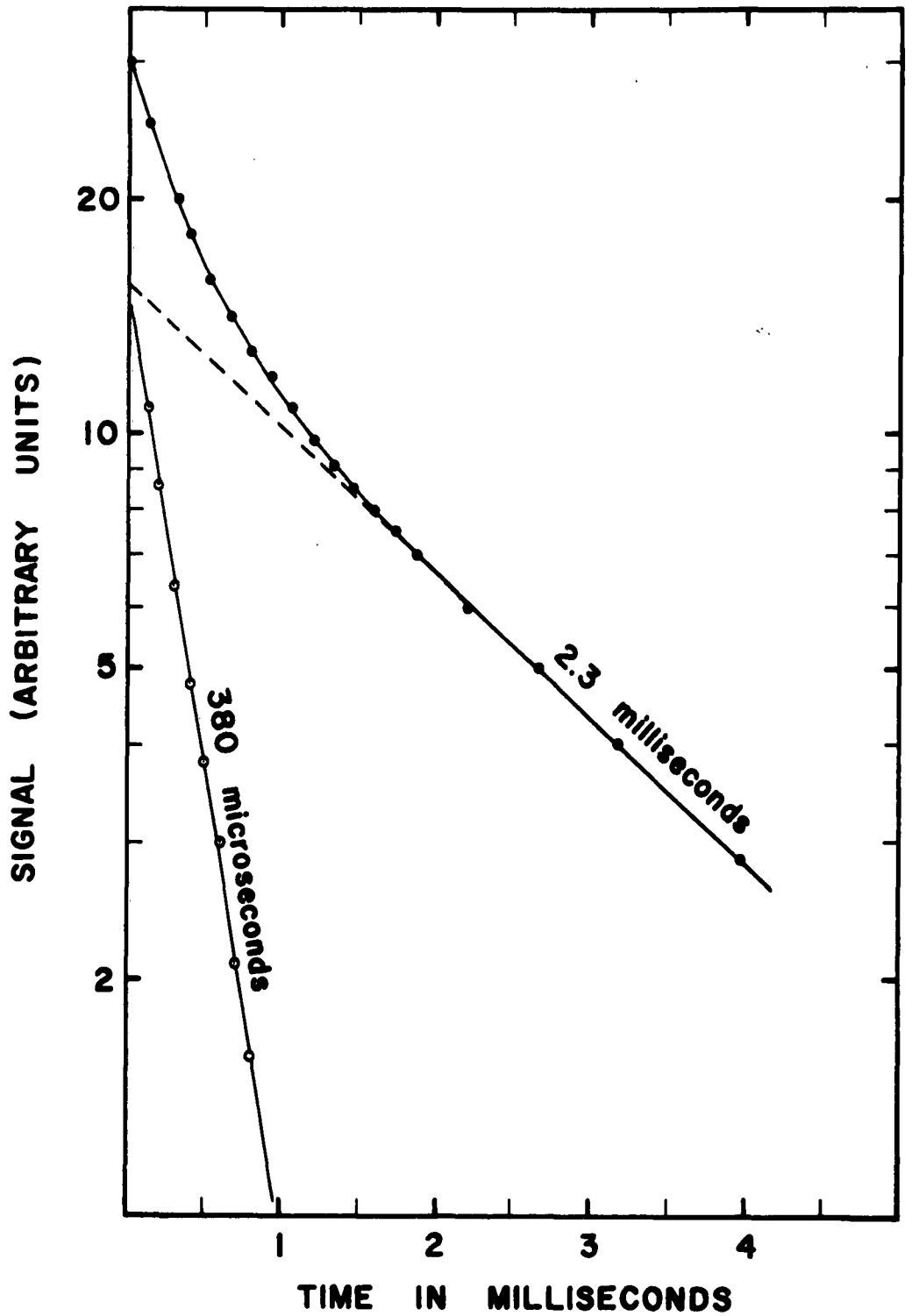

Fig. 9. Decay of the Photocurrent in an Evaporated Film of Sb_2Se_3

film of Sb_2Se_3. This decay can be resolved into two apparently independent decay times where the decay time, τ, is given by $I = I_o \exp(-t/\tau)$. Recombination in photoconductors generally takes place via discrete ground states located within the forbidden gap[30]. If the incident light flux is f, then in equilibrium, with a single level of ground states,

$$f = vs_n p_g n = vs_p n_g p, \tag{8}$$

where v is the carrier thermal velocity, s_n and s_p are the capture cross-sections of the ground states for electrons and holes respectively, p_g is the concentration of holes (electron traps) in the ground states, n_g is the concentration of electrons in ground states, and n and p are the free electron and free hole concentrations.

Equation (8) shows that the carrier lifetimes are $(vs_n p_g)^{-1}$ for electrons, and $(vs_p n_g)^{-1}$ for holes. Equation (8) also gives the carrier concentrations as

$$n = f/(vs_n p_g) \quad \text{and} \quad p = f/(vs_p n_g). \tag{9}$$

These concentrations are expected to increase linearly with light flux, f.

We have observed bimolecular recombination in Sb_2Se_3 films at the light intensities used in the observation of the decay. The

response (proportional to carrier concentration) of two typical evaporated films is seen in Fig. 10. Although these films exhibit different sensitivities, both exhibit bimolecular recombination at light levels below saturation. The flux varies as the reciprocal of the distance squared and the straight line portions of Fig. 10 shows slopes of -1 on the log-log plot; thus, p is proportional to the square root of f. From (9) we see that this requires that $p = n_g$.

It is unlikely[30] that $n_g = p_g$, i. e. the concentrations of holes and electrons in ground states are just equal. We might say then that from (8) and (9) the lifetime of the hole is $(vs_p p)^{-1}$ and the lifetime of the electron is $(vs_n p_g)^{-1}$, and note that they may be very different due to the differences in ground state concentrations and cross-sections. One might be led to believe that the long decay time in Fig. 9 is related to the hole lifetime, and the short decay time to the electron lifetime. The decay times may be greater than the lifetimes due to the emptying of shallow traps (not ground state traps)[30]. However, the equilibrium concentrations are independent of the shallow trap density and are again given by (9).

Fig. 9 shows the conduction decay, and extrapolation of the decay curves to zero time indicates that the carriers involved in the decay contribute approximately equally to the conductivity at equilibrium. Sb_2Se_3 is p-type, so one would not expect the electron

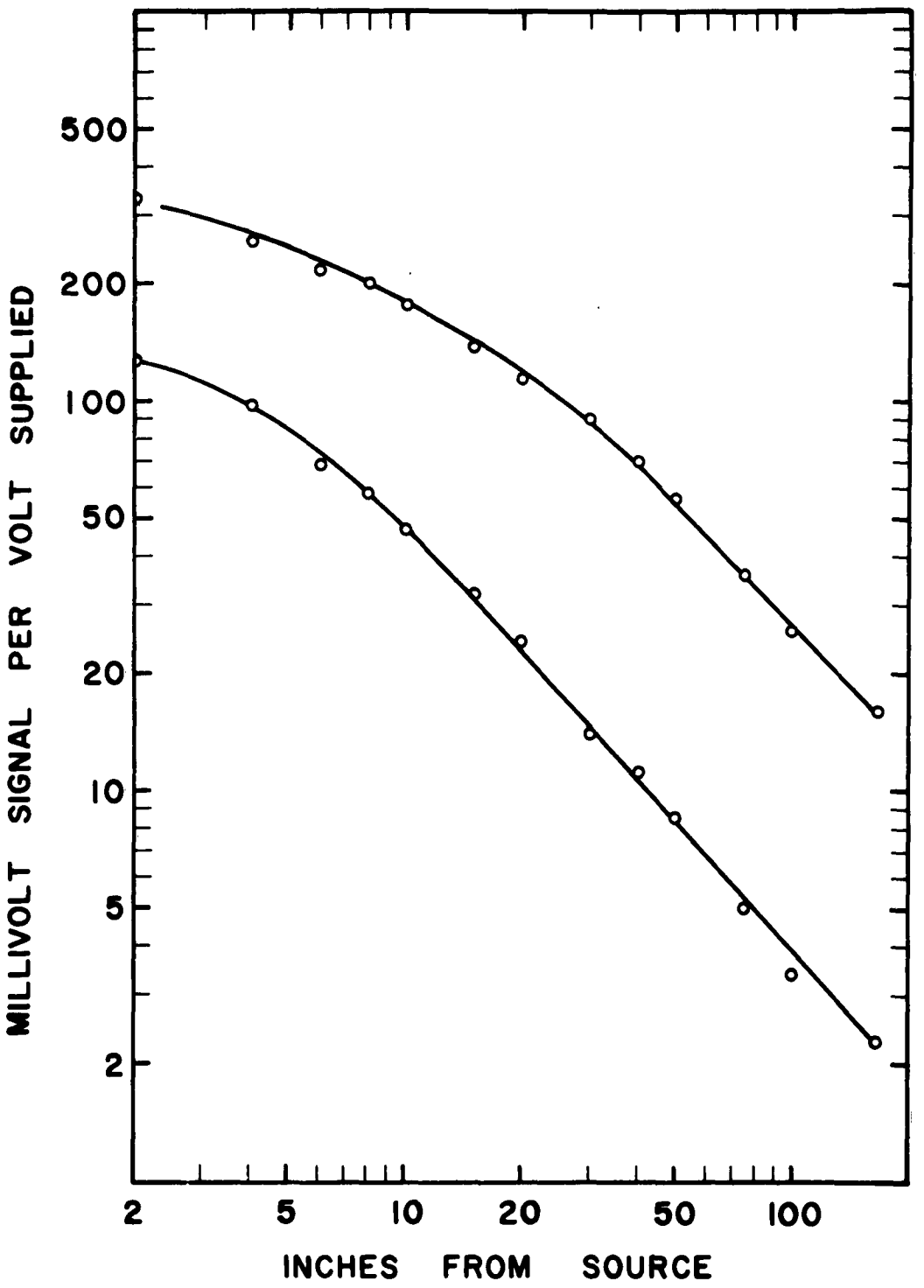

Fig. 10. Response of Sb_2Se_3 Films to the Light from a 6V-32CP Lamp

contribution to the conductivity to be as large as the hole contribution. It is our thesis that the electron lifetime is very short and does not appear in Fig. 9. Since this lifetime is $(vs_n p_g)^{-1}$, either there is a large concentration of holes in the ground states (before excitation) or the cross section for electron capture is very high. The large concentration of vacant orbitals required for the p-resonance bonding (see Chapter I) could provide the large density of holes in the ground states, supporting the first conclusion above.

If the concentration of electrons in ground states before excitation is small, following excitation, $n_g \sim p$, since a photon produces a hole-electron pair. We then have the condition for bimolecular recombination, i.e. $f = vs_p p^2$, observed in Fig. 10. This should, however, give a time dependence of hole concentration of $p \propto (1 + At)^{-1}$ rather than the exponential observed in Fig. 9, leading us to believe that the short decay time of Fig. 9 is longer than the hole lifetime. The exponential form and the longer decay time (380 μs) may be due to the emptying of shallow traps,[30] or those at about kT electron volts above the valence band.

The long decay seen in Fig. 9 we relate to a diffusion process in the following way: Most of the incident light is absorbed in a layer of depth 1/K, and since K exceeds 10^5 cm^{-1} for the region of the spectrum considered here, most of the incident light is absorbed in

the first 0.1 micron. The short-lived electrons are probably trapped in this region. The concentration of electrons in ground states (hole traps) is small before excitation; thus the majority of the hole traps are electrons trapped at the ground states near the surface. The longer-lived holes which diffuse into the film find themselves in a region containing few recombination centers. As this diffusion continues, a net positive charge accumulates opposing further diffusion, and at equilibrium the diffusion current just equals the drift current caused by this field.

Upon extinction of the light, the holes in the vicinity of the surface recombine quickly, with a decay time given by the short (380 μs) time in Fig. 9. The excess holes now diffuse back to the vicinity of the trapped electrons where recombination takes place. The decay of these holes is characterized by the long time as shown in Fig. 9. For the films investigated, the excess holes constitute about half of the current carriers as seen by the extrapolating to zero time in Fig. 9.

A similar theory has been given by Fassbender[31] to account for the lack of a fall in sensitivity for increasing K in CdS films, where the large ratio of mobilities is responsible for this behavior.

Although the mobility of the holes in Sb_2Se_3 is small it may be seen that the diffusion depth does not depend on the mobility. The

equilibrium continuity[32] equation for holes in Sb_2Se_3 under the conditions described above is

$$fKe^{-Kz} - vs_p n_g p + \text{div}(D \text{ grad } p + pF\mu) = 0 \qquad (10)$$

where f is the incident light flux, K is the absorption constant, vs_p is the recombination coefficient for holes and ground state electrons, n_g is the density of electrons in ground state traps ($n_g \sim 0$ for $z > 1/K$), p is the density of free holes, D is the diffusion constant, μ is the hole mobility and F is the field. The field in this case is given by $dF/dz = e(n-p)/\varepsilon$ and for $z > 1/K$, $n = 0$; therefore, $dF/dz = -ep/\varepsilon$. Here ε is the dielectric constant and z is the depth measured from the film surface.

Assuming uniform conditions in the plane of the film surface, we need only consider the z dependence of p and F. At equilibrium, the bracketed term in (10) is zero if recombination beyond $z = 1/K$ can be neglected. That is, no net current flows into the sample. Then

$$D \frac{dp}{dz} + \mu pF = 0. \qquad (11)$$

But $D = \mu kT/\varepsilon$ by the Einstein relation. Therefore the diffusion equation, (11), becomes

$$(kT/\varepsilon)\frac{dp}{dz} + pF = 0 \qquad (12)$$

On eliminating F from equation (12) and integrating,[28]

$$p = N_o^2 a/(1 + a N_o z)^2, \tag{13}$$

where $N_o = \int_o^\infty p dz$ and $a = e^2/(2\varepsilon k T)$. That is, the concentration of holes as a function of depth is independent of the mobility.

The majority of the electrons are trapped at any given instant due to the short electron lifetime. Electrical neutrality requires also that

$$N_o = \int_o^\infty n_g dz. \tag{14}$$

But since n_g extends only to a depth of $1/K$ we may say roughly that $n_g = KN_o$. Since the bracketed term in (10) is zero,

$$fKe^{-Kz} - vs_p KN_o p = 0 \tag{15}$$

Evaluating this at $z = 0$ with $p(0)$ from (13) equal to $N_o^2 a$,

$$N_o = \left(\frac{f}{vs_p a}\right)^{1/3}. \tag{16}$$

Substitution of (16) into (13) shows that the concentration of holes as a function of z is also independent of K. This diffusion effectthen tends to prevent a fall in sensitivity with increasing K which means that the response curve of Fig. 8 is therefore elevated above its expected value as the wavelength decreases.

CHAPTER IV

HALL EFFECT IN Sb_2Se_3

Previous attempts to measure the Hall voltage in Sb_2Se_3 have been unsuccessful due to high sample resistance and contact difficulties.[20,33] We have overcome these difficulties using a scheme adopted after that of Pell and Sproull[34] but find ourselves limited by sample and/or circuit noise.

The Hall coefficient is defined to be $R = E_y/(J_x B_z)$, where E_y is the Hall voltage which appears in a semiconductor at right angles to both the applied current density, J_x, and the magnetic field, B_z. When only one type of carrier is present, this expression may be reduced, by use of the Lorentz law, to $R = (ne)^{-1}$, where n is the carrier density. A measurement of R thus yields the carrier density directly. This is true for metals and degenerate semiconductors where the drift velocity is nearly the same for all carriers. However, for non-degenerate semiconductors, the drift velocity follows a Boltzmann distribution, and E_y compensates the Lorentz force only for carriers of average energy. This leads to a difference between the Hall mobility and drift mobility so that we must use $R = (\mu_H/\mu_d)(ne)^{-1}$. This mobility ratio is $3\pi/8$ for lattice scattering, which seems to be the predominant scattering mechanism in Sb_2Se_3[20].

The Hall mobility is generally found by measuring the conductivity, σ, and then for the predominant carrier, $\sigma = ne\mu$, and $R\sigma = \mu$. Furthermore, the conductivity is highly temperature dependent. We have therefore adopted a scheme[34] whereby the mobility is measured directly. This requires a measurement of the voltage drop across the sample, rather then the current through the sample. From this voltage, the Hall voltage, and the sample dimension, we find

$$\mu_H = \frac{(E_H)(10^8)}{E_A B_z} \tag{17}$$

where E_H and E_A are the Hall and applied fields, respectively, in V/cm, B_z is in gauss, and the mobility is in cm^2/volt-sec. For this method to succeed, the voltage drop at the current contacts must be negligible, and this is often difficult to achieve. Because Sb_2Se_3 has a large Seebeck coefficient at room temperature (1200 $\mu V/C^o$)[4], thermoelectric effects, particularly the Ettinghausen effect, may be troublesome. Since our contacts are made of different material from the sample, the Nernst and Righi-Leduc effects would also be troublesome if a dc method were used. These temperature effects are slow to build up, so they may be suppressed by rapidly reversing either the sample current of the magnetic field. Because a rapid reversal of the magnetic field is difficult, we have adopted a method wherein

the sample current direction alternates. This has the further advantage that the Hall voltage is alternating and may be easily amplified. The samples have resistances of the order of 10^6 ohms, thus requiring a high input-impedance circuit.

The form of equation (17) immediately suggests a calibration scheme. As the fields appear as a ratio, one need apply only a known fraction of the applied signal to the input circuit to get a calibration signal. The ac signal is detected in a phase-sensitive detector and the magnetic field reversed periodically so that stray signals will not be mistaken for Hall signals.

4.0 Alternating Current High Impedance Voltmeter

The measuring circuit is seen in block diagram in Fig. 11. The system is fed by an audio oscillator whose output contains negligible line harmonics. The circuit components are of sufficiently high quality to permit operation at frequencies as low as 20 cps. The input capacitance of the electrometer pre-amp determines the upper limit to this frequency.

The audio frequency signal passes through a buffer amplifier and a synchronous signal for the detector is extracted from an RC phase-shift network. This sync signal is adjusted to give maximum output signal. The sample input signal is isolated from this sync signal to permit a balance of the Hall voltage probes. We have used

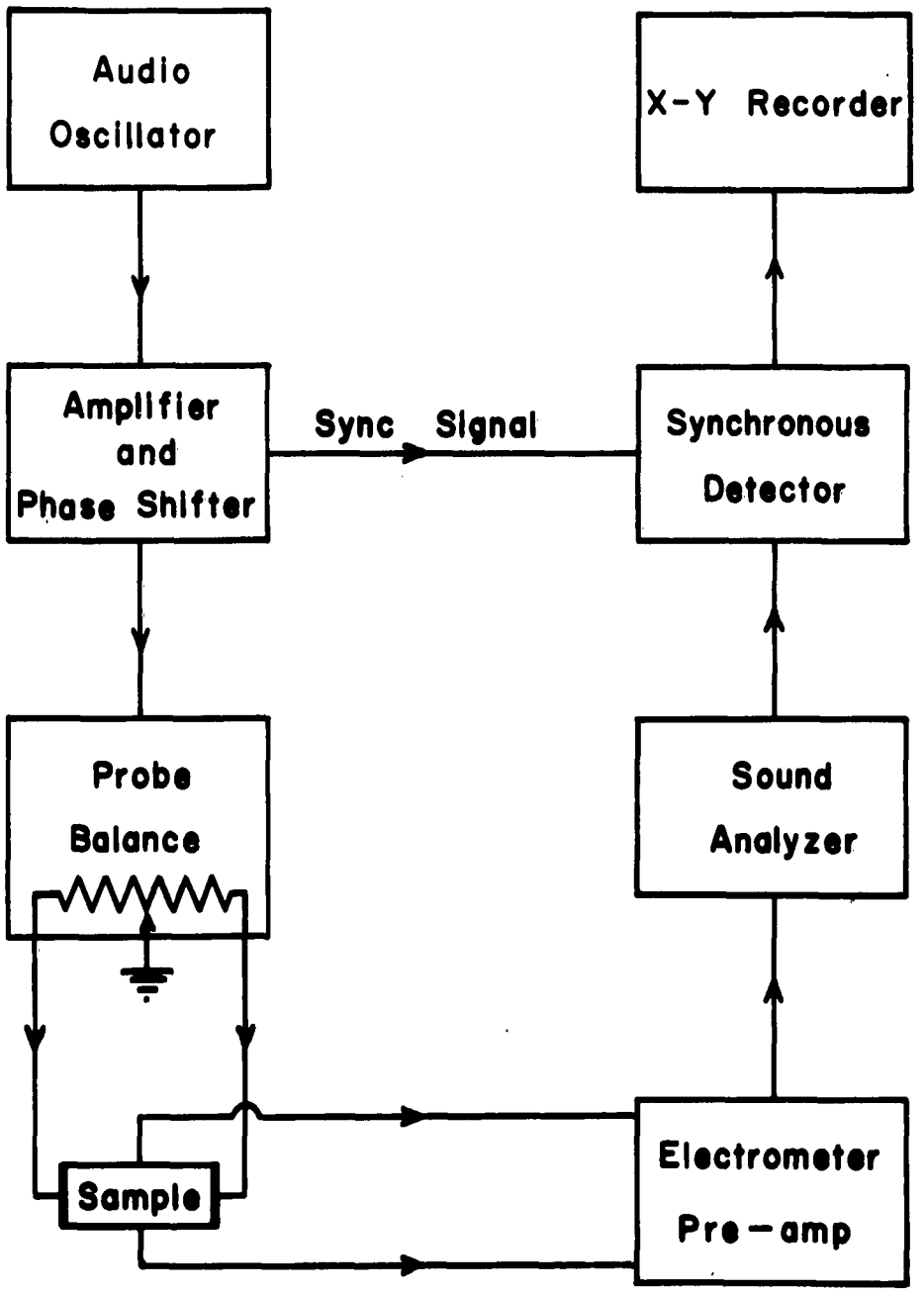

Fig. 11. Block Diagram of the Hall Voltage Measuring Circuit

the two-probe method, rather than a single probe referred to a fixed potential, so that changes in conductivity in the sample near one current electrode do not unbalance the probes. Such a conductivity change causes a single probe to change potential relative to a fixed reference, whereas two probes drift together and preserve the balance.

The samples of Sb_2Se_3 investigated had resistances generally of 10^4 to not more than 10^6 ohms. The dc input resistance of the electrometer tubes is around 10^{14} ohms and grid capacitance is about three μμf. At 25 cps, the input capacitive reactance is about 10^9 ohms.

In order to have flexibility in connecting the sample to the electrometers, various adapters are used. The connecting cable is about 16 inches long to allow spatial shielding of the electrometers from the magnetic field. The electrometer circuit is further shielded in an iron box of quarter inch walls. These leads and connections have a capacitance of about 100 μμf so that the input capacitive reactance is about 60 megohms at 25 cps. If higher resistance samples are measured, these connectors must be changed.

The electrometer output is fed into the sharply tuned circuit of a General Radio Sound Analyzer. The output of this analyzer has been modified to match the input impedance of the synchronous detector. The detected Hall voltage appears across the plates of

two vacuum tubes and so a high impedance recorder is needed. We used an Autograf X-Y Recorder, of input impedance 200 K Ω/volt.

The circuit is shown in Fig. 12. The probe balance, buffer amplifier, phase shifter, and calibration circuits are those described by Pell and Sproull[34]. The phase sensitive detector is that of Schuster[35]. It was necessary to replace Pell and Sproull's square wave generator in the sync circuit with a single stage of amplification in order to achieve the transformer coupling required by Schuster's detector.

The electrometer amplifier in Fig. 13 is based on the standard amplifier design recommended by the Victoreen Instrument Co.[40] The push-pull transformer coupled arrangement was chosen in order to allow the electrometers to operate independently of one another. This isolation is required by the probe balance and calibration scheme adopted here.

The resistors in the probe balance circuit are precision wire-wound. The coarse and fine balance controls are General Radio potentiometers ganged to have a constant resistance of 1 K ohm between contacts, allowing a probe balance while preserving a constant resistance of 2500 ohms across the sample of calibration purposes. The initial coarse adjust is made with electrometer No. 2 inoperative to prevent large voltages from appearing on the electrometers due to

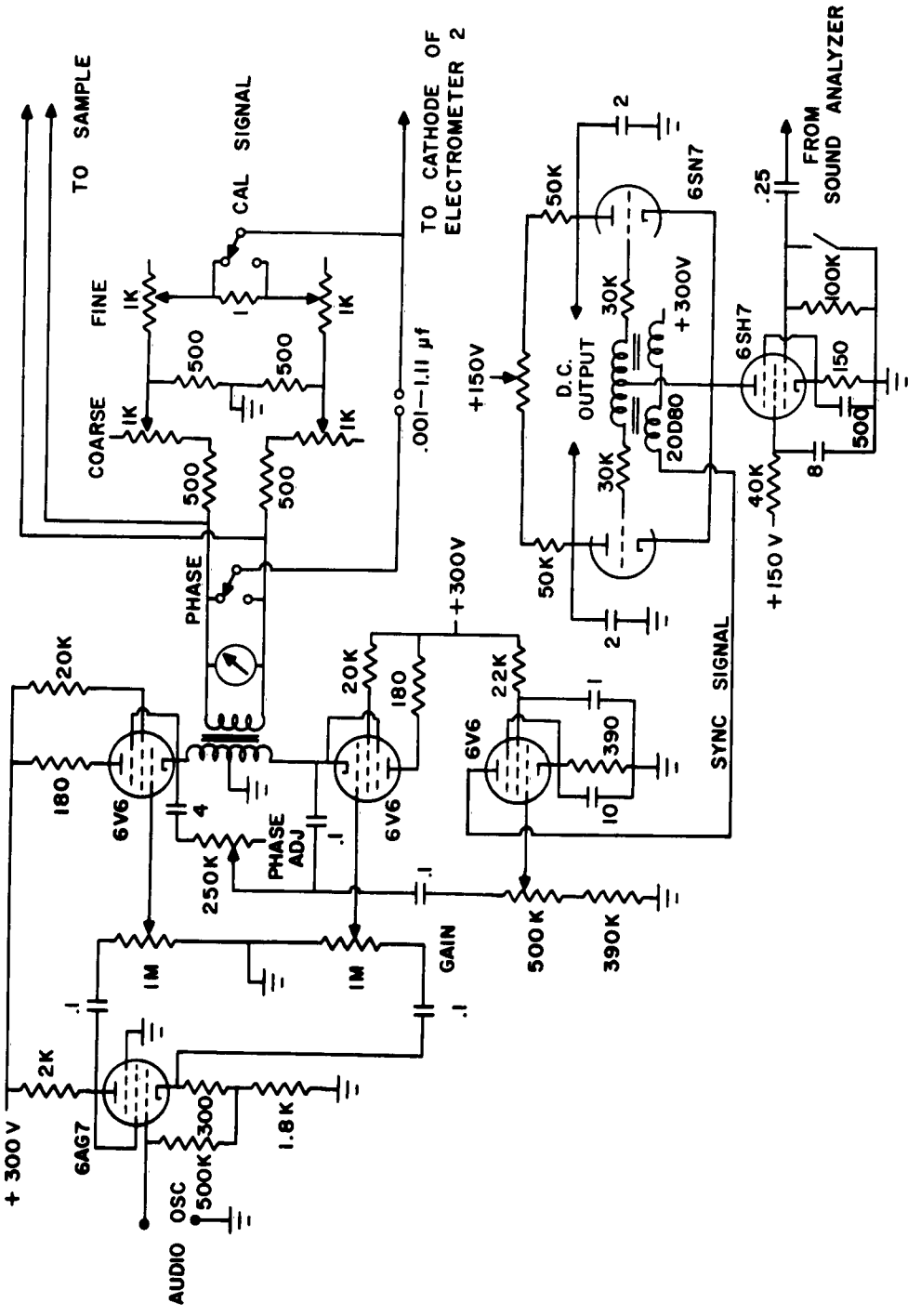

Fig. 12. Schematic Diagram of the Buffer Amplifier, Phase Shifter, Synchronous Detector, and Calibration Circuit of the Hall Voltage Measuring Circuit

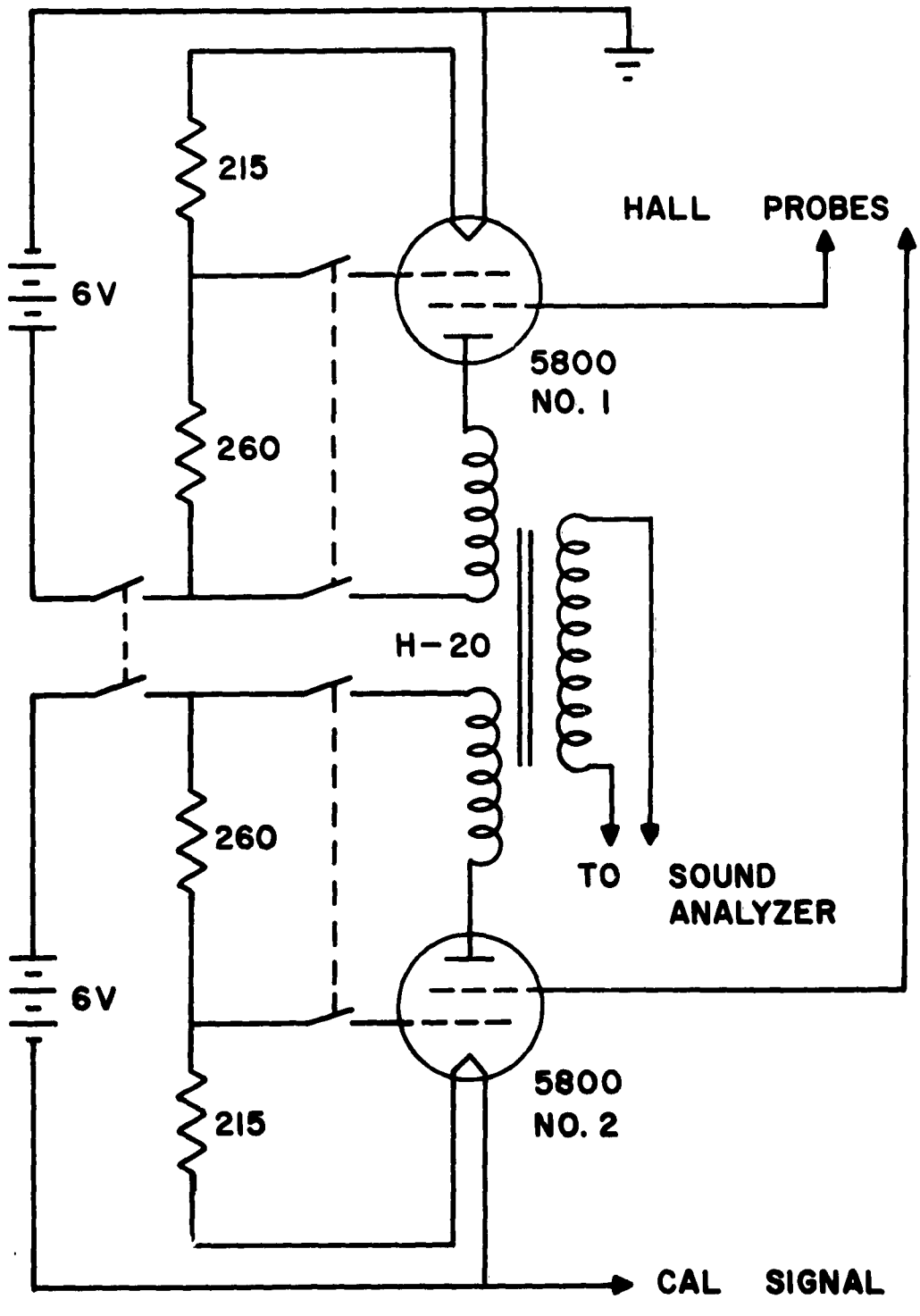

Fig. 13. Schematic Diagram of the Electrometer Amplifier

improperly positioned Hall probes. After the probes are balanced, a calibration signal of 1/5000 of the applied voltage is fed to the cathode of electrometer No. 2. The relative effectiveness of signals applied at the grid and cathode is very nearly unity for our circuit, as determined by trial.

Thus, independent of the intermediate stages of amplification, the calibrate signal equals 2.05×10^{-4} of the applied voltage. Equation (17) for the Hall mobility becomes

$$\mu_H = 20.5\ Nr/B \qquad (18)$$

where N is the Hall signal expressed as multiples of the calibration signal, B is in kilogauss, r is the length-to-width ratio of the sample and the mobility is in cm^2/volt-sec.

The detector is phase-sensitive and one must determine by experiment the majority carrier associated with the polarity of the output for a given direction for the magnetic field. A standard sample of n-type silicon (Hoffman) is used for this purpose. For the magnetic field in a given direction, and with n-type material, a definite polarity exists at the output. Reversal of the field, or use of a p-type sample yields the opposite polarity. Successive switching of the magnetic field produces a square wave output of peak-to-peak value twice the signal. In addition to doubling the output signal, this periodic field

reversal suppresses the effects of long time drifts.

4.1 Experiment

The samples prepared for measurement are single- or polycrystals of Sb_2Se_3 obtained by reacting in vacuo stiochiometric proportions of 99.999% Selenium and 99.999% Antimony (American Smelting and Refining Co.). Current and Hall leads are attached with either silver paste or welded contacts of lead. The method requires the current contacts to be low-resistance ohmic contacts so that all of the applied voltage is dropped across the sample. Care must also be taken to eliminate rectifying barriers at the Hall probes.[37] Sample lead wires (B.S. gauge No. 34 copper) are fine enough to prevent large heat conduction to or from the sample.

The sample holder seen in Fig. 14 is designed to fit over the four-inch pole pieces of an electromagnet. One pole piece is movable to permit removal of the holder. The holder may be evacuated to eliminate convection currents around the sample. The vacuum seal is made with an "o" ring fitting which seats on one of the pole pieces. The magnet used has a maximum field strength of 5000 gauss in a 1-1/2 inch gap. This field is uniform, over the one-square-inch cross section occupied by the sample, to the accuracy obtainable with a Rawson rotating coil gaussmeter (Manufacturer's specification is 1% of full scale).

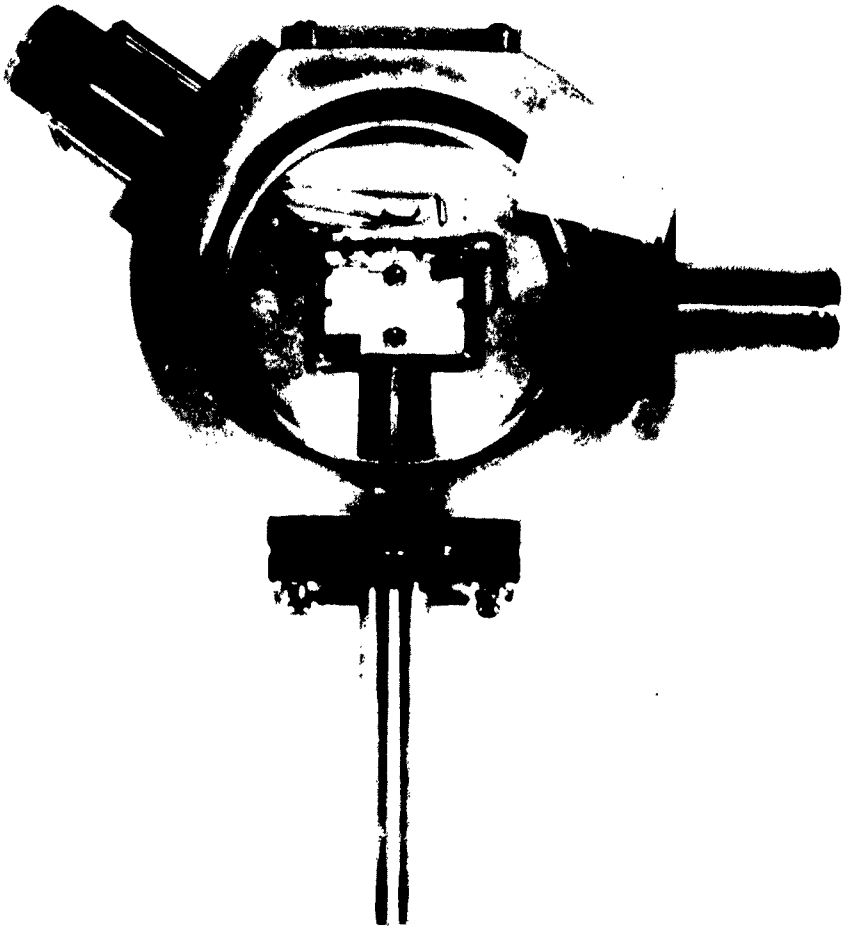

Fig. 14. Sample Holder for Hall Voltage Measurements.

The sample is contained in a radiation-shielded aluminum box in thermal contact with a 3/4 inch diameter copper rod. This rod is insulated from the holder body and acts as a heat pipe. The sample temperature is monitored by a chrome-alumel thermocouple inside the box.

Most of the samples observed were of negligible porosity although it has been shown[36] that the Hall voltage is independent of porosity. The length-to-width ratio was generally greater than 4 to prevent "shorting out" effects[36] of the current electrodes.

When both electrons and holes are current carriers, the Hall coefficient is[32],

$$R = \frac{ne\mu_n^2 - pe\mu_p^2}{(ne\mu_n + pe\mu_p)^2} \tag{19}$$

where n and p are the electron and hole concentrations respectively and the μ's are the corresponding mobilities. The quantity, μ, measured here (see equation (18)) is equal to $R\sigma$ where $\sigma = ne\mu_n + pe\mu_p$. For intrinsic behavior, n = p, and as the material is p-type, (19) reduces to

$$\mu = R\sigma = \mu_p \frac{b^2 - 1}{b + 1} \tag{20}$$

where b is the ratio of electron to hole mobility. Using b = 1/3 as determined[20] from thermoelectric data, $\mu = -(2/3)\mu_p$. The negative sign here indicates hole conduction.

The noise level is in the range of about 1/8 to 1/4 of the calibration signal. For fields up to 5000 gauss and a length to width

ration of 3 (shorting out effect $\sim$ 1.5%)[36] no intelligible Hall signal is seen. The noise level is higher for samples with smaller length-to-width ratios. Using a mobility ratio of 1/3, this gives a room temperature hole mobility of less than 6 cm^2/volt-sec. Black et al.[20] observed a decrease of about 35 per cent in their ratio of hole to electron mobility as their sample temperature was raised about 100 C^o. This made them question some of the basic assumptions used in the derivation of their thermoelectric power equation. However, if we use this lower ratio (b increased to 1/2), the hole mobility is still less than 8 cm^2/volt-sec.

This value is substantially less than the value (45 cm^2/volt-sec) obtained[20] from conductivity and thermoelectric measurements. It may be that the large thermoelectric power (1200 $\mu V/C^o$ at 25°C) is not due to a large mobility ratio. The recombination mechanisms considered in Chapter III indicate a longer hole lifetime (not to be confused with relaxation time) and thus the free hole concentration may exceed the electron concentration, even though the material is intrinsic. This equilibrium concentration difference may then account for the large thermoelectric power even though the mobilities are nearly the same.

CHAPTER V

THE RESISTIVITY DISCONTINUITY IN Sb_2Se_3 AND LOW VOLTAGE BREAKDOWN IN STIBNITE(Sb_2S_3)

A stoichiometric excess of Sb produces a resistivity discontinuity in Sb_2Se_3[4,5], and causes low voltage breakdown in Sb_2S_3.[6] Furthermore, the similarity in crystal structure and constituent atoms lead us to expect a relationship between the two effects.

5.0 Sb_2Se_3

It has been noted that the addition of 0.2 wt % Sb beyond the stoichiometric proportion (50.7%) in Sb_2Se_3 results in a resistivity decrease of about four orders of magnitude. This is accompanied by a change in temperature coefficient of resistivity from negative to positive. In the other direction, exceeding the stoichiometric proportion of Se by as much as 1% does not appreciably change the resistivity nor affect the type of majority conduction, i.e. p-type.

This latter behavior does not fit in with the usual concept of donors; where the bonds are all saturated, the substitution of a group VI atom (Se) for a group V atom (Sb) produces a localized donor site. A large density of donors should then produce a decrease in resistivity with electrons as majority carriers. Interstitial atoms in a saturated bond lattice would also be expected to produce levels

within the forbidden zone and therefore a decrease in resistivity. Consideration of the crystal structure in Chapter I shows that saturated bonds on all of the atoms is not probable. A resonance bonding scheme was proposed to account for the coordination, this resonance being developed on an empty orbital on a single atom type. If this empty orbital is on the Se atom, a Se excess would make some Se atoms nearest neighbors and result in localized metallic behavior. This is not observed. The choice of a vacant Sb orbital as the seat of this resonance therefore seems substantiated.

The excess Se atoms must occupy positions such that the saturated nature of the Se bonds is preserved. It is not probable that these occupy approximate Sb sites because of the high coordination of these positions. Furthermore very small solubility of Se in Sb_2Se_3 and the distillation of Se during evaporation[13] indicate that the excess Se atoms enter interstitally. Large interstices between layers are the most likely sites. The direction of p-bonds is such that the preferred positions of nearest neighbors to the Sb atoms, on which p-resonance is developed, are the six corners of an octahedron with Sb at the center.[10] It is quite likely then that the Se atom occupies an interstice adjacent to the Sb atoms (see Fig. 1) in approximately this sixth site and so preserves its saturated-bond nature.

Excess Sb, on the other hand, probably enters the lattice

substitutionally to form an acceptor in the usual sense. The "metallic resonance" bond of Pauling[12] is thought to develop on an empty orbital obtained by promotion of a valence electron to a higher (say d) orbital. If the p-resonance bonds are preserved in Sb_2Se_3 with excess Sb, the empty orbitals on the Sb atoms surrounding the Sb "impurity" atoms are acquired by partial transfer of electrons to the other neighboring Se atoms. The substitutional Sb would then be an acceptor site.

The transition to metallic behavior observed when Sb is the excess constituent is abrupt; there is no gradual decrease in resistivity as the transition point is approached. Mott[14] predicts an abrupt transition to metallic behavior in semiconductors when the orbitals of donors or acceptors overlap. A transition (not as sharp as predicted by Mott) to metallic behavior has been observed[15] in p-type germanium activated with gallium. This transition occurs at an acceptor density of only $5 \times 10^{16}/cm^3$ and a relatively large separation of around 270A between centers. The gallium activation energy in germanium is 0.01 eV and the dielectric constant of germanium is 16. If one considers the acceptor orbitals as hydrogen-like, we may compare Sb acceptors in Sb_2Se_3 to gallium acceptors in germanium. An excess of 0.2 wt % Sb yields an acceptor density of $6 \times 10^{19}/cm^3$, or about 25A between centers. The square of n, the real part of the index of refraction for Sb_2Se_3, is also about 16, and so the activation

energy for Sb acceptors in Sb_2Se_3 should be around 0.1 eV. We have observed only intrinsic behavior[13] in Sb_2Se_3 at room temperature (kT = .025 eV) so our quoted per cent excess at which the transition occurs is probably too high. The low carrier mobility and attendant small Hall voltage have so far prohibited a direct measurement of carrier densities.

5.1 On the Low Voltage Breakdown in Stibnite (Sb_2S_3)[6]

5.1a Observations

Dielectric breakdown in stoichiometric stibnite (Sb_2S_3) occurs at around 4×10^6 volts/cm, but stibnite containing an Sb excess of greater than 1.0 wt per cent "breaks down" at fields in the range of only 500 to 5000 volts/cm. When an electric field of the order of 10^3 volts/cm is applied to samples of stibnite containing excess antimony, it is found that the resistance drops abruptly from about 10^9 ohms to 10^4 ohms, that is, a low resistance path is established. The field strengths required are less for single crystals than for polycrystals, and less for the c direction in single crystals than for directions at right angles to this. When the field is removed, the sample retains the low resistance path. This path has metallic behavior, i.e., a positive temperature coefficient of resistivity of about $0.004/C^\circ$, and is not visually distinguishable from the matrix but may be traced by probing successive excavations. The path retains its metallic

character indefinitely at room temperature but may be returned to the high resistance state by heating the sample to around 150°C, directly or by means of a current pulse.

The temperature dependence of this breakdown has been fitted[6] to the avalanche theory of Frolich and Simpson.[16] In this theory, electrons thermally ejected from traps receive energy from the field. This energy is then dissipated in the lattice. Thus when the electron temperature exceeds the lattice temperature, breakdown occurs. The temperature dependence of low voltage stibnite breakdown indicates an average trap depth of 0.28 eV. This is not inconsistent with the observed[17] optical energy gap of 1.55 eV (intrinsic activation energy 0.77 eV) and the thermal activation energies of from 0.5 - 0.6 eV observed for our samples.

However there are two other effects for which the avalanche theory does not account. These effects are 1) an observed delay of the breakdown after application of the field, and 2) pre-breakdown pulses of approximate equal amplitude. The logarithm of the breakdown delay time is seen plotted in Fig. 15 as a function of applied field. This curve is an approximate hyperbola on a semilog plot. This indicates a delay time dependence on the breakdown field of the form, $t = A \exp(B/E)$, and therefore field emission. If the avalanche can be initiated by a local increase in electron density due to field

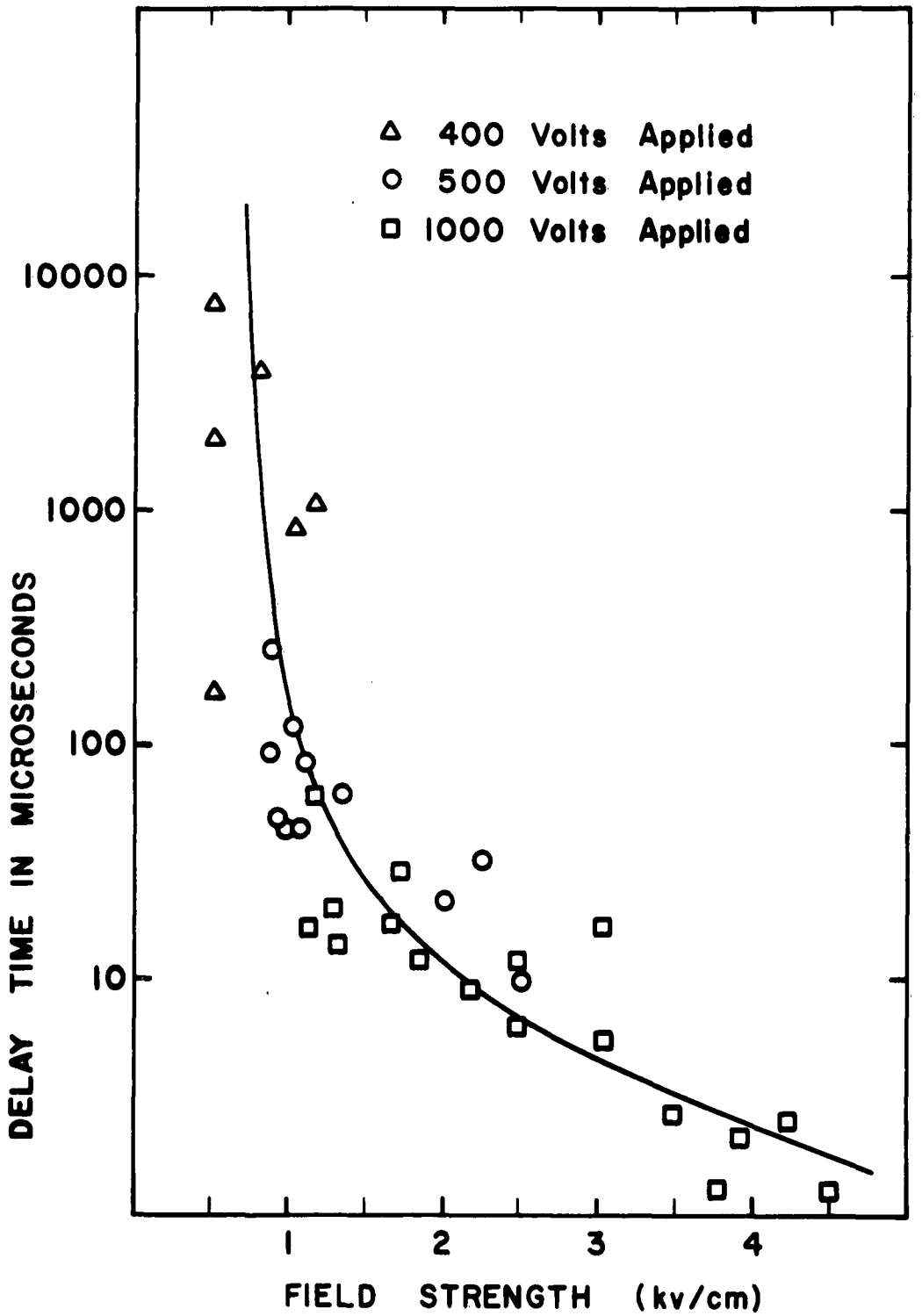

Fig. 15. The Breakdown Delay Time as a Function of the Field Applied to Stibnite (After J. R. Davis)

emission, one might expect the delay time prior to breakdown to depend on the transmission probability for field emission. Franz[18] gives the probability of emission per unit time from a trap of depth ε as

$$P = AE \exp(-B/E) \tag{21}$$

where $A = e(8m^*\varepsilon)^{-1/2}$, $B = 8\pi\varepsilon^{3/2}(2m^*)^{1/2}(3he)^{-1}$,

E is the applied field, m^* is the effective mass, e is the electron charge, and h is Planck's constant.

If the delay time, t, is equal to the mean time for emission,

$$t = 1/P = (1/AE) \exp(B/E), \text{ or}$$

$$\log(tE) = -\log A + (B/2.3)(1/E). \tag{22}$$

Fig. 16 shows log (tE) as a function of 1/E for the data of Fig. 15. The line is a least squares fit with a slope, B/2.3, equal to 1.335 kv/cm. Using $\varepsilon = 0.28$ eV, one obtains $m^*/m_o \sim 10^{-7}$, where m_o is the free electron mass. Such a small effective mass is highly improbable, indicating that some of the assumptions made in the derivation of equation (21) are not applicable in this case although the form of the dependence of t on E in Fig. 16 is characteristic of field emission.

5.1b Speculations

We have mentioned that 0.2 wt per cent excess of antimony produces a large resistivity discontinuity in Sb_2Se_3; no such dis-

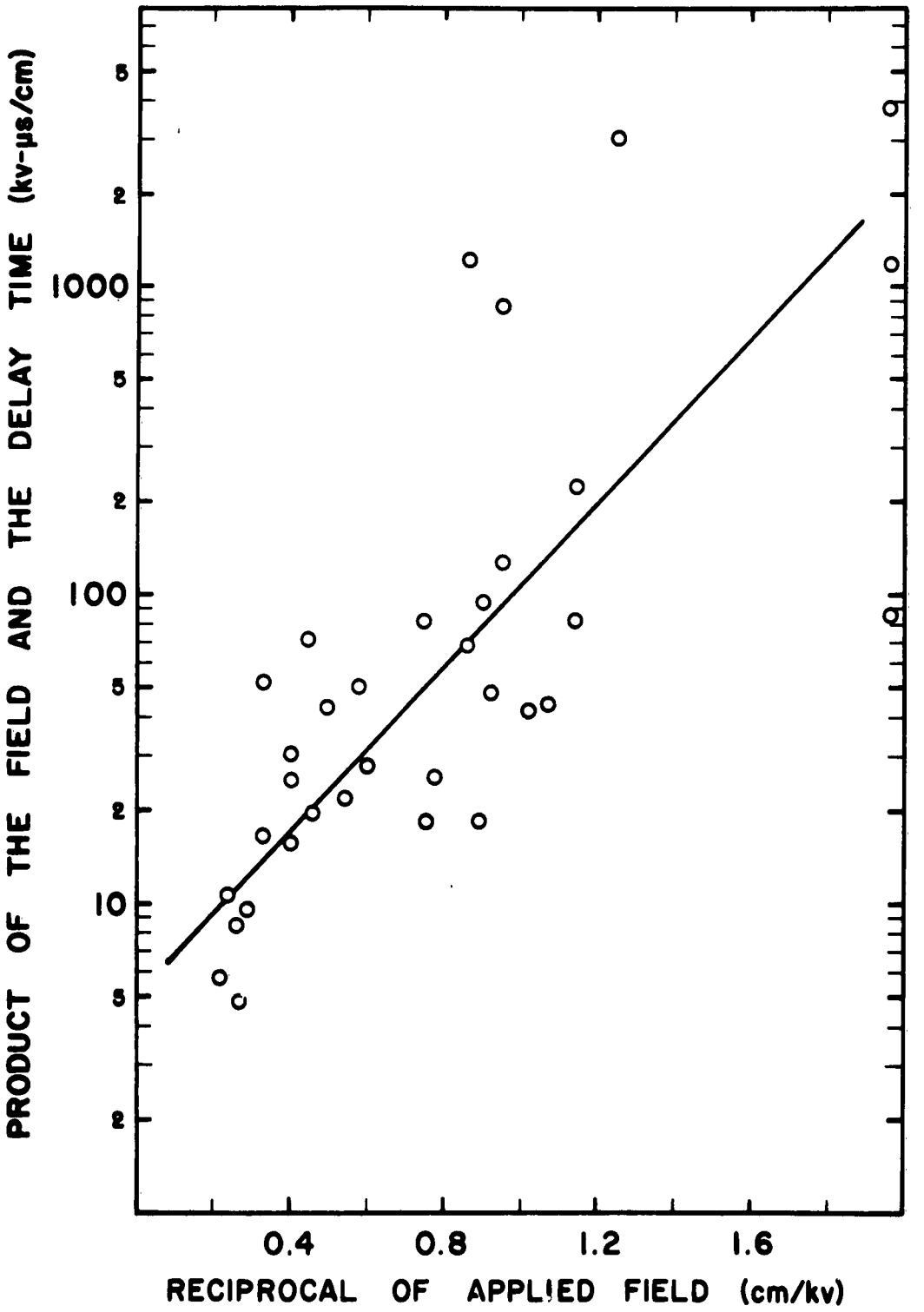

Fig. 16. The Product of the Applied Field and the Delay Time as a Function of the Reciprocal of the Field for Breakdown in Stibnite

continuity is found in Sb_2S_3 even though ten times as much excess antimony is present and despite the fact that the unit cell is smaller ($483A^3$ as against $538A^3$). We conclude therefore that, although these two compounds are isomorphs and alike in many respects, the excess antimony does not occupy the same relative lattice positions in Sb_2S_3 as it does in Sb_2Se_3.

We have proposed that Sb enters the Sb_2Se_3 lattice substitutionally for Se, and behaves as an acceptor, producing the discontinuity. A resistivity discontinuity would probably also result if the Sb went in interstitially because of resonance developed between like atoms[2]. This does not happen in stibnite, which leads us to believe that here the Sb atoms occupy their normal positions and that the antimony excess is better to be viewed as a sulfur deficit. We find that a 1.2 wt per cent excess of antimony corresponds to one sulfur vacancy for each two unit cells.

We had hoped to settle the question by means of precise density measurements, but unfortunately the results are inconclusive. Calculations show that one per cent excess antimony affects the density as follows: a) if substitutional, an increase in density of 1.0 per cent; b) if interstitial, 0.74 per cent; c) if in normal positions (sulfur vacancy), a decrease of 0.40 per cent. Meyer and Powell of this laboratory worked out a technique of the required precision

but irreducible variations in porosity of the samples masked the density changes.

If we assume sulfur vacancies do exist, we may explain the low-voltage breakdown, and subsequent recovery, as follows: The effective electrons at the sulfur vacancies are not "shared" electrons in the usual sense. The deep (0.28 eV) traps indicated by the temperature dependence of the breakdown voltage we suppose to be the valence (ground) states of the antimony atoms surrounding the vacancies. By thermal activation and field excitation these trapped electrons are promoted to higher states where they then become shared electrons, and permit the establishment of metallic resonance bonding among the antimony atoms clustering around the sulfur vacancy. This bonding change would result in further relaxion, i.e., relaxation of the Sb atoms surrounding the vacancy onto the vacancy.

This additional bonding energy is probably not great enough to overcome the attendant strain energy in the neighboring lattice when these possible metallic regions are far apart. If, however, these regions (empty p-orbitals at the sulfur vacancies) are sufficiently close together, the lower energy state may be the crystal habit of these similarly located regions being metallically bonded. Girofalco and Streetman[19], for example, have calculated the relaxion energy for the bcc structure for various forms of potentials. The problem here

would be additionally complicated by the switch in bonding type.

Our low-voltage breakdown model for stibnite is the following:

As the field is increased at a particular temperature, field emission initiates an avalanche of electrons from the deep traps located at the sulfur vacancies. The trap density must be large enough to support this avalanche. In the avalanche, a sufficiently large number of similarly located traps must be empty at the same time if a bonding switch is to occur. An avalanche of charge which did not permit this switch would appear as a pre-breakdown pulse.

To explain the restoration to the original condition we assume, only that the increased temperature, general or localized along the conducting path, destroys the metallic resonances and the regions of the vacancies return again to their original phase. The effect of the restoring (current) pulse mentioned is to provide the Joule heat at just the right location to effect the reverse switch in bond type.

The temperature coefficient of resistance for the breakdown path is $0.004/C^{o}$ or roughly that of antimony metal ($0.0036/C^{o}$), and the linear resistance of this path is around 20K ohms per mm. If one considers the breakdown path to be a filament of antimony metal (ρ = 42 microhm-cm) the cross section turns out to be 2.1×10^{6} A^{2}, corresponding to a path diameter of 130 unit cells, computed for preferred direction along the C axis.

SUMMARY

The value of 1.18 eV for the onset of strong absorption in crystalline films of Sb_2Se_3 at room temperature is in good agreement with the value of 1.2 eV observed[20] for bulk crystalline samples. Assuming that the band gap is a linear function of the temperature, i.e., $E_g = E_g(0) + \beta T$, between room temperature and 78°K, then β is -3.0×10^{-4} eV/C° as compared to -7×10^{-4} eV/C° found[20] for bulk crystals. Extrapolation to 0°K yields an optically determined band gap, $E_g(0)$, equal to 1.27 eV which is larger than the thermal activation energy of 1.07 eV observed previously[13], as might be expected for slightly polar materials. (The ionic contribution to the Sb - Se bond in Sb_2Se_3 is estimated to be 8 per cent from an empirical relationship [10] between the ionic character of bonds and the electronegativity difference of Sb and Se.) Others have observed values of from 1.4 eV[20] to 0.8 eV[4] for the thermal band gap in bulk crystals of Sb_2Se_3. The band gap obtained from the long wavelength limit of photoconductivity in evaporated films is 1.35 eV (Braitwaithe observed 1.305 eV), which suggests that the absorption seen from 1.2 to 1.3 eV may be due to exciton formation.

Vitreous films of Sb_2Se_3 exhibit an optical band gap of 1.5 eV at room temperature with a temperature coefficient, β, equal to

-4.4×10^{-4} eV/C°. This yields an $E_g(0)$ equal to 1.64 eV as compared to the thermal activation energy of 1.83 eV observed previously[13]. This latter value may be too large due to crystallization occuring in the vitreous films upon heating. As a mathematical evolution of the energy bands is not possible for vitreous materials, the semiconducting properties of Sb_2Se_3 are discussed qualitatively from the short range order viewpoint of the "semiconducting-bond" theory of Mooser and Pearson[2]. Similarities in the optical absorption band edges for crystalline and vitreous films strengthen this short range order viewpoint.

The photoconductivity of Sb_2Se_3 films, both crystalline and vitreous, is characterized by bimolecular recombination at light levels below saturation and a flat spectral response from 0.45μ to 0.75μ. Consideration of the photoconductive decay and possible recombination processes leads us to believe that the flat spectral response is due to a hole diffusion process even though the hole mobility is small.

The Hall apparatus constructed gives a direct measurement of the Hall mobility in high resistance samples, while minimizing the errors due to thermal effects. Using a hole to electron mobility ratio of three[20], and with the limitations imposed by sample and/or circuit noise, the room temperature hole mobility in Sb_2Se_3 is less

than 6 cm^2/volt-sec, as compared to the value of 45 cm^2/volt-sec derived[20] from conductivity and thermoelectric power measurements. The equation used (and questioned) by those authors[20] is based on equal concentrations of free holes and conduction electrons, i.e., equal lifetimes, whereas photoconductivity measurements indicate that the hole lifetime is larger than the electron lifetime in Sb_2Se_3. The large thermoelectric power observed[4, 20] in Sb_2Se_3 may then be due to the difference in equilibrium carrier concentrations, and the carrier mobilities may be nearly the same, thereby accounting for the small Hall signal.

The resistivity discontinuity observed[4, 5] in Sb_2Se_3 containing excess Sb may be accounted for in the usual way[14] by the concept of overlapping acceptor orbitals although the quoted excess at which the discontinuity occurs is probably too large. It had been hoped that the carrier concentrations could be obtained from the Hall voltage measurements. Stibnite (Sb_2S_3) and Sb_2Se_3 are isomorphs and the lack of such a discontinuity in stibnite containing excess Sb serves as the basis for a model used to account for the low voltage breakdown in stibnite.

APPENDIX I

Described below is a computer program devised to obtain values of n and k from experimentally determined values of T for equations (5) and (6) of Chapter II. The statements are in Fortran which may be machine translated into a object program for both the IBM 650 and IBM 701 Computers.

The symbols used in this program are as follows:

OPN = n, the real part of the index of refraction

OPK = k, the imaginary part of the index of refraction

APON = large positive number (to initiate the direction of iteration)

ADELN = initial magnitude of iterative constant in outside (n) loop

ADELK = initial magnitude of iterative constant in inside (k) loop

CN = fractional multiplier of iterative constant in outside loop

CK = fractional multiplier of iterative constant in inside loop

ACCN = accuracy of fit required in outer loop (units of optical density)

ACCK = accuracy of fit required in inner loop (units of optical density)

ADDTN = estimate of change in n expected at next wavelength

ADDTK = estimate of change in k expected at next wavelength

WL = wavelength in angstroms

BN = index of refraction of substrate at the given wavelength

D = film thickness in angstroms

ODA = observed optical density of film and substrate (1)

ODB = observed optical density of film and substrate (2)

TR = calculated transmission

A = sin θ (equation (5), Chapter II)

M = number of inner loops required for fit

L = number of outer loops required for fit

Fortran Statements

```
1   Dimension Z (2), Y(2), D(2), T(2), TR(2)
2   Read 1, PON, OPK, APON, ADELN, ADELK, CN, CK
3   Read 1, ACCN, ACCK, ADDTN, ADDTK
4   Read 1, WL, BN
5   Read 1, D(1), ODA
6   Read 1, D(2), ODB
7   OPN = OPN + ADDTN
8   OPK = OPK + ADDTK
9   NIL = 0
10  L = NIL
11  PON = APON
12  DELN = ADELN
13  M = NIL
14  POK = APON
```

```
15  DELK = ADELK
16  DO 18 I = 1, 2
17  Z(I) = (12.5664 * D(I) * OPK/WL
18  Y(I) = (12.5664 * D(I) * OPN)/WL
19  R = ((OPN - 1)*(OPN-1) + (OPK) * (OPK))*((OPN-BN)*(OPN-BN) +
        (OPK) * (OPK))
20  S = ((OPN +1)*(OPN + 1) + (OPK)*(OPK))*((OPN + BN)*(OPN +
        BN) + (OPK)*(OPK))
21  A = (2 * OPK*(BN + 1)*(OPN*OPN + OPK*OPK-BN))/SQRTF
        (R*S)
22  AB = SQRTF (R/S)
23  PIC = SQRTF (1-A*A)
24  ROB = ((BN-1)/(BN + 1))) **2
25  RBA = ((OPN-BN)/(OPN + BN)) **2
26  COR = (1-ROB)/(1-ROB*RBA)
27  Do 29 I = 1, 2
28  T(I) = EXPF (Z(I)) + (R/S)*EXPF(-Z(I))-2*(AB)*((COSF(Y(I)))
        *PIC-A *SINF (Y(I)))
29  TR(I) = (COR*16 * BN * (OPN*OPN + OPK*OPK))/(S*T(I))
30  ZER = (1 + ROB)/(1 - ROB)
31  ZERO = LOGF(ZER)
```

```
32  AXP = ODA + ZERO
33  ATR = LOGF (1/TR(1))
34  DIFF = ABSF(AXP-ATR)
35  IF(DIFF-ACCK)45, 45, 36
36  IF(POK-DIFF)43, 43, 37
37  POK = DIFF
38  OPK = OPK + DELK
39  M = M + 1
40  IF(OPK)41, 16, 16
41  PUNCH 1, OPN, OPK, DELK
42  STOP
43  DELK = - CK*DELK
44  GO to 37
45  PUNCH 1, M, OPN, OPK
46  BXP = ODB + ZERO
47  BTR = LOFG (1/TR(2))
48  DIFN = ABSF(BXP-BTR)
49  IF(DIFN-ACCN)57, 57, 50
50  IF(PON-DIFN)55, 55, 51
51  PON = DIFN
52  OPN = OPN +DELN
```

```
53      L = L + 1
54      GO TO 13
55      DELN = -CN*DELN
56      GO TO 51
57      PUNCH 1, L
58      PUNCH 1, OPN, OPK, WL, TR, A
59      GO TO 4
60      END
```

The scheme of calculation is as follows: Two data cards are prepared with the information desired in statements 2 and 3. This information is given at the beginning of a run and if adjustment of some of these constants is desired, the machine must be stopped, the adjustments made, and the program restarted. A set of data consists of the three cards of statements 4-6. These have been put onto separate cards as the calculations are made for pairs of films. For each film then, a set of data consists of cards read in statements 5 or 6. The observed optical density is that observed at the wavelength given in statement 5.

Using the estimated values of n and k given initially, the machine iterates on k, holding n fixed, until the desired fit between calculated and observed values of OD is obtained for one film. An

intermediate punch tells the number of times the "k loop" has been traversed. Using these n and k, the machine calculates an optical density for the second film, compares this to the observed, and adjusts n. Using the new value for n, the inner, k, loop is again traversed until a fit is made to film one. Again, these values are used to calculate an optical density for film two. This proceeds with adjustment of n and k until a pair are obtained which give optical densities sufficiently close to those observed for both films. Then the information of statement 58 is punched and a new set of data (statements 4-6) is read. In the event that k becomes negative, the machine punches the value of n, k, and the iterative constant and then stops.

REFERENCES

1 A. F. Ioffe and A. R. Regel, Progress in Semiconductors 4, 237 (1960).

2 E. Mooser and W. B. Pearson, Can J. Physics 34, 1369 (1956), J. Phys. Chem. Solids 7, 65 (1958).

3 S. V. Forque, R. R. Goodrich and A. D. Cope, RCA Rev. 12, 335 (1951).

4 B. D. Cullity, M. Telkes and J. T. Norton, J. Metals 2, 47 (1950).

5 D. F. Clifton and Lee Gildart, Bull. Am. Phys. Soc., Series II, 1 226 (1956). AFOSR TN 58-849.

6 J. R. Davis, Thesis, University of Kentucky (1960), AFOSR TN 61-121

7 N. W. Tideswell, F. H. Kruse and J. D. McCullough, Acta Cryst. 10, 99 (1957).

8 E. Donges, Z. anorg. Chem. 263, 289 (1950).

9 J. Cohen, Appl. Phys. 25, 798 (1954).

10 L. Pauling, The Nature of the Chemical Bond (Cornell University Press, 1940).

11 L. Pauling, J. Am. Chem. Soc. 69, 542 (1947).

12 L. Pauling, Proc. Roy. Soc. (London) A196, 343 (1949).

13 T. E. Johnson, Thesis, University of Kentucky (1957). AFOSR TN 58-849

14 N. F. Mott, Nuovo cimento X 7, no. 2, 312 (1958).

15 H. Fritsche, J. Phys. Chem. Solids 6, 69 (1958).

16 H. Frolich and J. H. Simpson, Advances in Electronics II (Academic Press, 1950).

17 S. Iluki and S. Yoshimatsu, J. Phys. Soc. Japan 10, 549 (1955).

18 W. Franz, Handbuch der Physik XVII, "Dielectric Breakdown" (Springer-Verlag, Berlin, 1956).

19 L. A. Girifalco and J. R. Streetman, J. Phys. Chem. Solids 4, 182 (1952).

20 J. Black, E. M. Conwell, L. Seigle, and C. W. Spencer, J. Phys. Chem. Solids 2, 240 (1957).

21 H. B. Briggs and W. H. Brattain, Phys. Rev. 75, 1705 (1949).

22 O. S. Heavens, Optical Properties of Thin Solid Films (Butterworths, London, 1955).

23 L. Holland, Vacuum Deposition of Thin Films (Wiley, New York, 1956).

24 L. Harris, J. K. Beasley and A. L. Loeb, J. Opt. Soc. Am. 41, 604 (1951).

25 M. T. Kostyshin, Optics and Spectroscopy 5, 71 (1958).

26 G. G. Macfarlane, T. P. McLean, J. E. Quarrington and V. Roberts, Phys. Rev. 108, 1377 (1957).

27 J. G. N. Braitwaithe, Proc. Phys. Soc. (London) B64, 274 (1951).

28 T. S. Moss, Photoconductivity in the Elements (Butterworths, London, 1952).

29 C. Kunze, Ann. Physik 1 165, 173 (1958).

30 A. Rose, Phys. Rev. 97, 322 (1955).

31 J. Fassbender, Ann. Physik 5, 33 (1949).

32 W. Shockley, Electrons and Holes in Semiconductors (Van Nostrand, New York, 1950).

33 J. A. Stamper, Thesis, University of Kentucky (1958).

34 E. M. Pell and R. L. Sproull, Rev. Sci. Instr. 23, 548 (1952).

35 Schuster, Rev. Sci. Instr. 22, 254 (1951).

36 J. Volger, Phys. Rev. 79, 1023 (1950).

37 J. Bardeen, Bell System Tech. J. 29, 469 (1950).

38 W. F. Kochler, J. Opt. Soc. Am. 43, 738 (1953).

39 G. D. Scott, T. A. McLauchlan, and R. S. Seornett, J. Appl. Phys. 21, 843 (1950).

40 J. A. Victoreen, Proc. Inst. Radio Engrs. 37, 432 (1949).

PART II

SOME SEMICONDUCTING PROPERTIES OF BISMUTH TRISULFIDE AND BISMUTH TRIOXIDE

We give here a condensation of the subject matter covered in Technical Note AFOSR-TN-60-1028, summarizing (1) The work done on the sample preparation of bismuth trisulfide, Bi_2S_3, and bismuth trioxide, Bi_2O_3, and (2) Results of electrical and optical measurements. Also included is a review of the scant data to be found in the literature on these two compound semiconductors.

The main aim of this work was to produce and study single crystals of Bi_2S_3 with composition as near to perfectly stoichiometric as possible. As a by product we have developed a new way of producing films of Bi_2O_3.

BISMUTH TRISULFIDE

A summary of results of other workers is given in Table I. Comparisons lack significance because the samples are of various forms, and the agreement of the data seems worse than should be expected, even so.

TABLE I

PUBLISHED DATA ON Bi_2S_3, VARIOUS FORMS

Observer (Type)	Eg_{th} (eV)	Eg_{opt} (eV)	σ $(ohm\ cm)^{-1}$	S ($\mu V/^oC$)	Carrier Concent. (cm^{-3})	Mobility ($cm^2/V\ sec$)
Konorov[1] (sintered)	0.77 to 400°K, 1.0 above 400°K		10^{-3} at 300°K	-1300 at 300°K		
Black[2] (poly-crystal)	~1.0 at 0°K	1.3 at 300°K	10^{-2} at 300°K	-750 at 300°K	$3x10^{18}$ at 300°K	200 at 300°K
Goriunova[3]	0.55	1.4	$2x10^{1}$			
Kolomiets[4] (thin films)		1.1 at 300°K				

1.0 Sample Preparation

Samples of bismuth trisulfide must be prepared under moderately high pressure because the compound dissociates at its melting point, 850°C, if only under atmospheric pressure. With proper precautions we find Vycor (96% silica glass) to be a satisfactory container, as explained in the Technical Note mentioned.

To produce bismuth trisulfide the constituents are weighed out in stoichiometric proportions and placed in a closed evacuated Vycor tube with one end pointed. The materials are then reacted in a specially designed safety furnace. The sample tube is rotated as the materials are melted, for better mixing and to prevent hot spots from forming along the sides of the tube.

We find that the mixture of bismuth and sulfur reacts exothermally at about 350°C, but that the resulting product is amorphous and far from stoichiometric. Furthermore unless the above-mentioned precautions are taken, heating produces sufficient vapor pressure to cause an explosion before the sample can be brought to a temperature high enough to produce a stoichiometric compound.

A further difficulty is that condensed sulfur appears in the space above the melt, and thus the sample again fails to be stoichiometric. The solution to this difficulty is to lower the sample in its Vycor tube container through a zone melting furnace, pointed end first. The large difference between the melting point of bismuth trisulfide (850°C) and metallic bismuth (271°C) insures that the excess bismuth is frozen out as the sample crystallizes. Single crystals as large as 1.5 cm in diameter and 10 cm in length can

be produced this way. They are stoichiometric to within 0.1 % or better in the lower sections of the sample.

A side product of the method is the production of dendrites or whiskers of Bi_2S_3 from the vapor phase in the space above the melt, often as large as of 0.1mm x 0.01mm x 3cm. However they are not truly stoichiometric and contain many dislocations.

1.1 Properties

a) Thermal Energy Gap, Eg_{th}.

The low resistivity of Bi_2S_3 makes it impossible to measure resistance as a function of temperature using a sample cleaved from the bulk single crystal. It was found that films of bismuth trisulfide having the necessary high resistance can be produced by heating films of bismuth, deposited on a glass substrate, in a sulfur atmosphere. These films are amorphous.

Nichrome wire electrodes are attached by means of silver paste, and the samples are run through heating and cooling cycles. Reproducible temperature vs resistance curves result. The thermal energy gap is found using the following relation for a semiconductor:

$$R = A \exp Eg_{th}/2kT$$

Fig. 1 shows a typical temperature vs resistance plot for these samples. The value of the thermal energy gap as determined from a series of these samples is found to be $Eg_{th} = 0.72 \pm 0.05$ eV in the temperature range 300 to 400°K.

b) Electrical Resistivity

Single crystal samples having dimensions of approximately 1 mm x 1 mm x 1 cm are cleaved from the bulk Bi_2S_3 crystal for resistances measurements as described in Part V. A series of

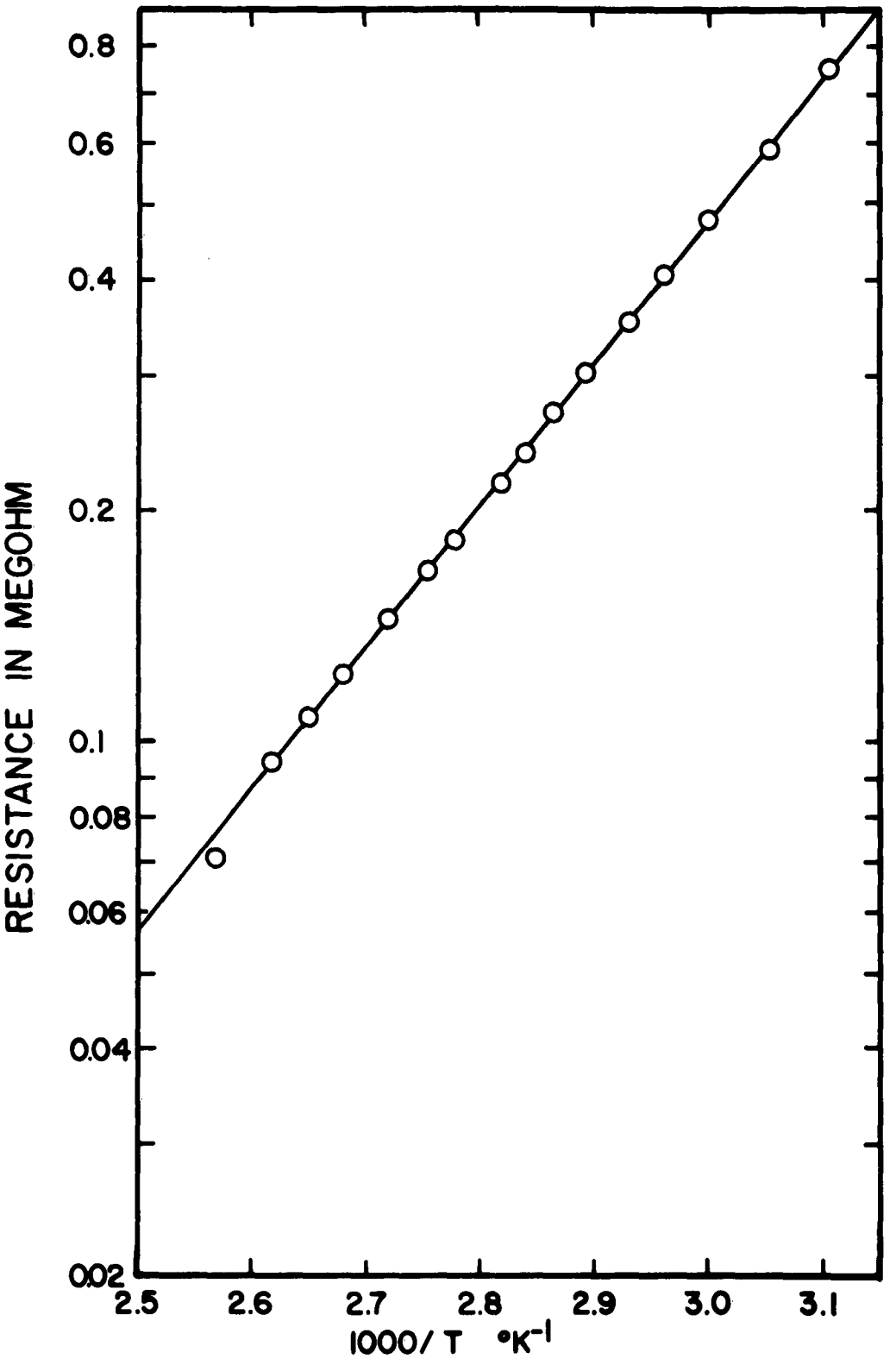

Fig. 1. Resistance vs 1000/T for Amorphous Film of Bi_2S_3 .

these samples has an electrical resistivity of 0.85 ± 0.05 ohm-cm at 300°K in a direction parallel to the cleavage planes.

c) Thermal Conductivity

Thermal conductivity of cylindrical samples cut from the bulk Bi_2S_3 single crystal are measured using the apparatus described in Part III. Results for the series of samples, show a thermal conductivity of 0.0203 ± 0.0015 watts/ cm deg at 15°C in a direction parallel to the cleavage planes.

d) Seebeck Coefficient

The Seebeck coefficient is measured using the apparatus and techniques described in Part III; when the temperature gradient is parallel to the cleavage planes, it is found to be -550 ± 50 μV/°C, at 15°C, and there is no appreciable change when the gradient is perpendicular to the cleavage planes. Polycrystalline samples of bismuth trisulfide give somewhat higher Seebeck coefficients, with typical values in the range -700 to -850 μV/°C.

e) Optical Energy Gap, Eg_{opt}.

Transmission studies are made on cleaved single crystals of bismuth trisulfide using a Cary model 14R recording spectrophotometer. The incident light is perpendicular to the cleavage planes and measurements are made at room temperature (300°K) and at liquid nitrogen temperature (77°K). Fig. 2 shows a typical transmission curve for bismuth trisulfide at 300°K. Fig. 3 shows the absorption edge at 300°K and 77°K. The absorption edge gives a value of 1.2 eV for the optical energy gap at 300°K and 1.4 eV at 77°K with a temperature dependence of -8×10^{-4} eV/°K, assuming a linear variation over this temperature range.

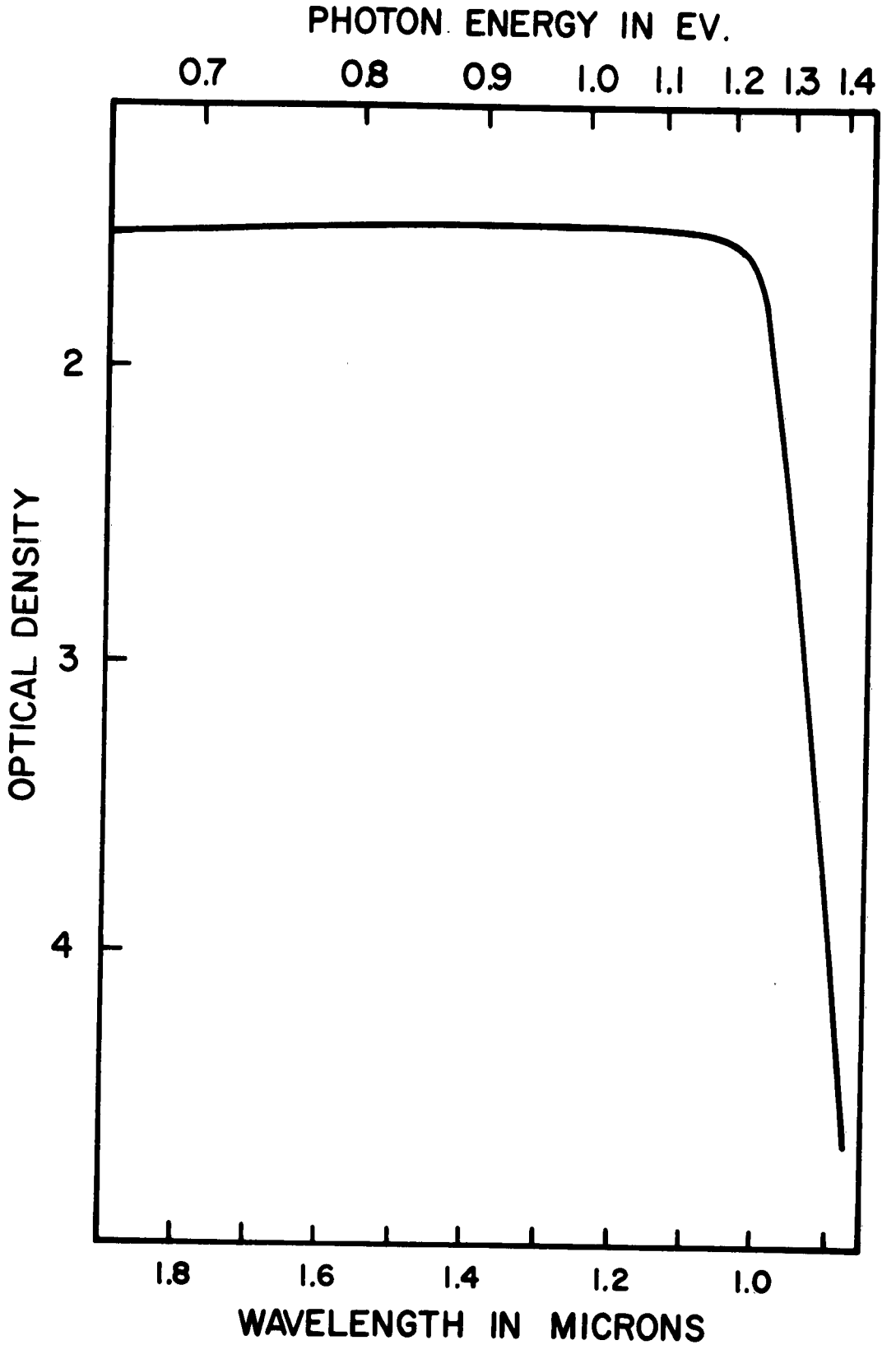

Fig. 2. Infrared Transmission of a 30 micron Thick Sample of $Bi_2 S_3$ at 300°K.

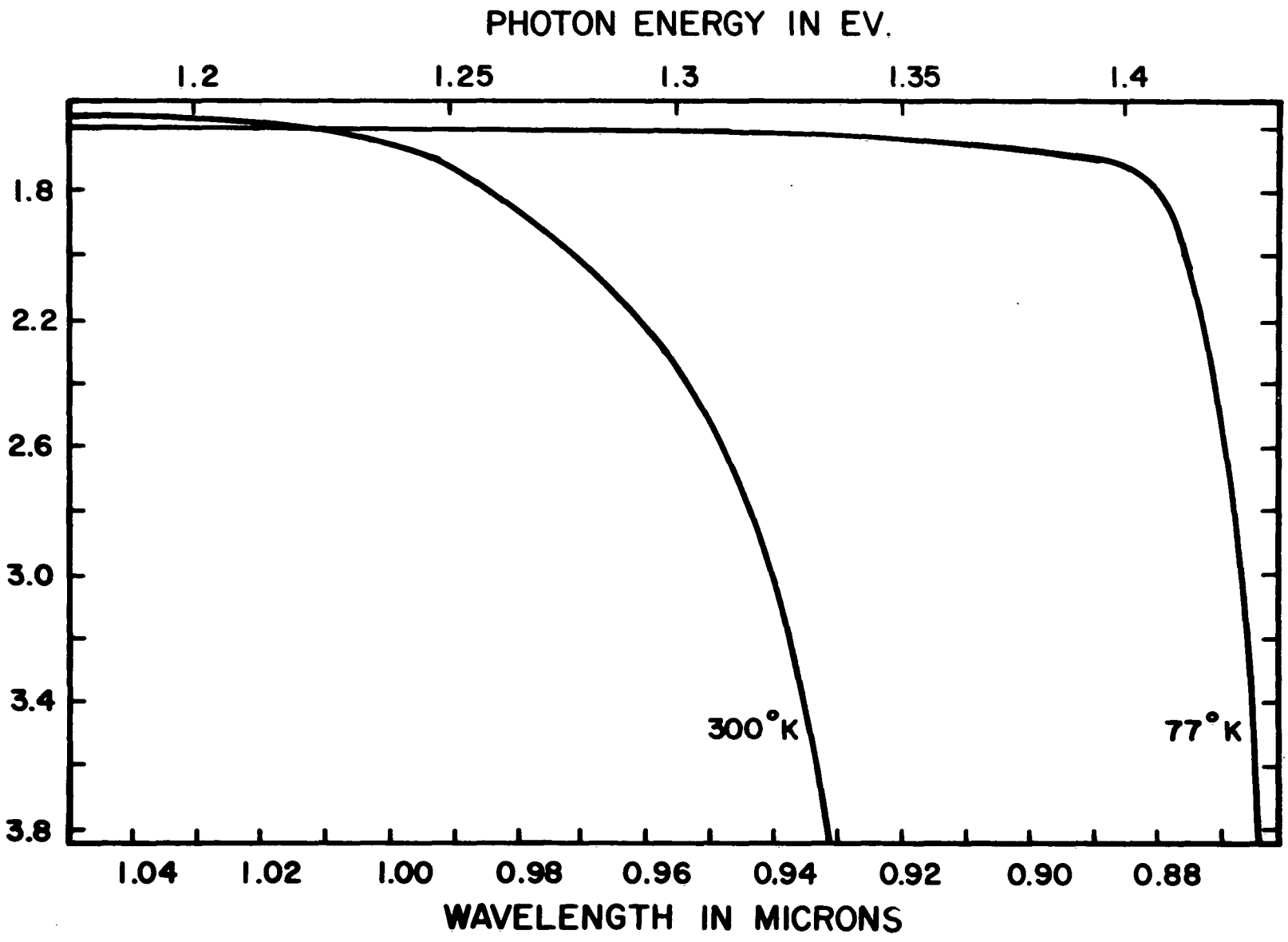

Fig. 3. Absorption Edge for 300 micron Thick Sample of Bi_2S_3.

f) Hall measurements.

Hall measurements are made using the apparatus and techniques described in Part V. The carrier concentration is found to be 1.2 x 10^{17} cm^{-3} and the carrier mobility is found to be 65 cm^2/volt sec, although the presence of noise is troublesome.

BISMUTH TRIOXIDE

A unique method of preparing polycrystalline films of bismuth trioxide (Bi_2O_3) was found during the course of the work in producing the sulfide. Since very little work had been reported on for this compound, our investigation was expanded to include studies of some of the basic properties of this compound.

2.0 Sample Preparation

The method used in the preparation of polycrystalline films of bismuth trioxide takes advantage of the large difference between the melting point of bismuth metal (271°C) and that of its trioxide (828°C). Bismuth metal is melted in a graphite crucible open to the air, and bismuth trioxide slag is formed. The temperature is raised to slightly above the melting point of bismuth trioxide and the carbon reduces the bismuth trioxide slag to metallic bismuth. The temperature is then lowered to slightly below the melting point of bismuth trioxide and a thin film of good oxide forms on the surface of the molten bismuth. The film is lifted off by means of a nichrome wire loop. (As mentioned in the Technical Note, hot Bi_2O_3 is a very active solvent, violently attacking all of the usual crucible materials.)

The films range in thickness from 10-100 microns, and areas of a square inch or greater, free from inclusion of bismuth, may be selected.

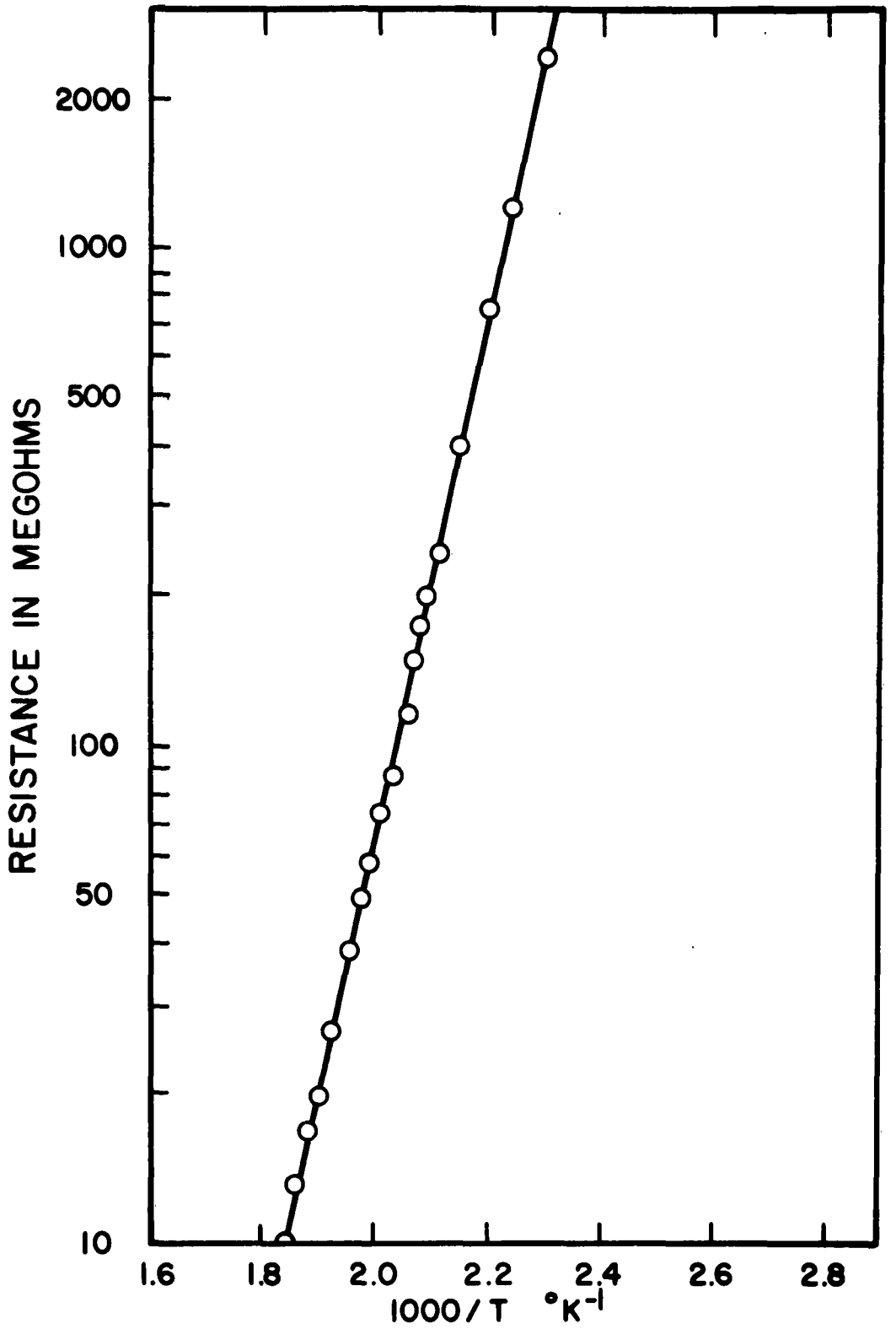

Fig. 4. Resistance vs 1000/T for Polycrystalline Film of Bi_2O_3.

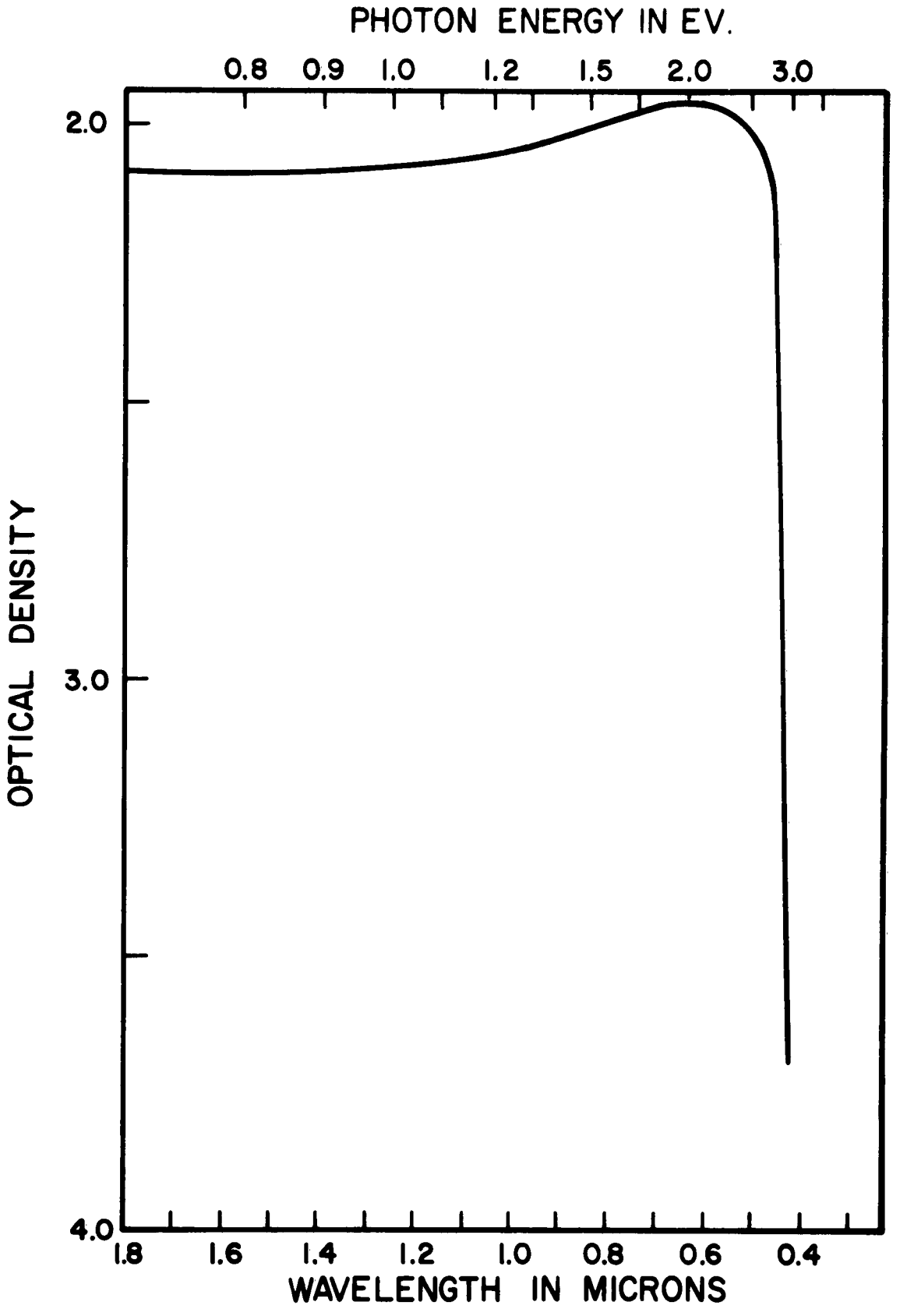

Fig. 5. Transmission of 40 micron Thick Polycrystalline film of Bi_2O_3 vs Wavelength of Incident Photon at 300°K.

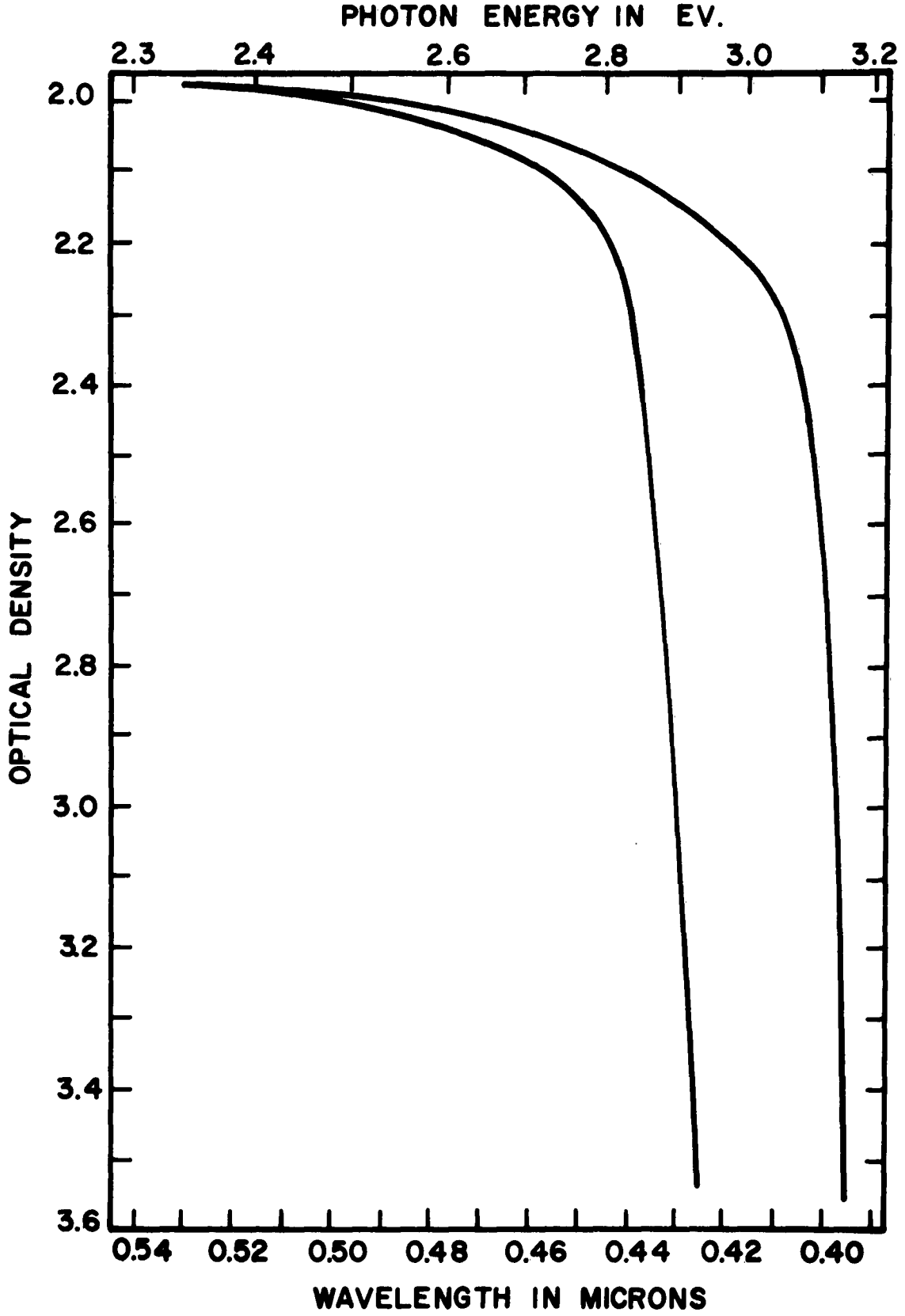

Fig. 6. Absorption Edge for Polycrystalline Film of Bi_2O_3 at 300°K and 77°K.

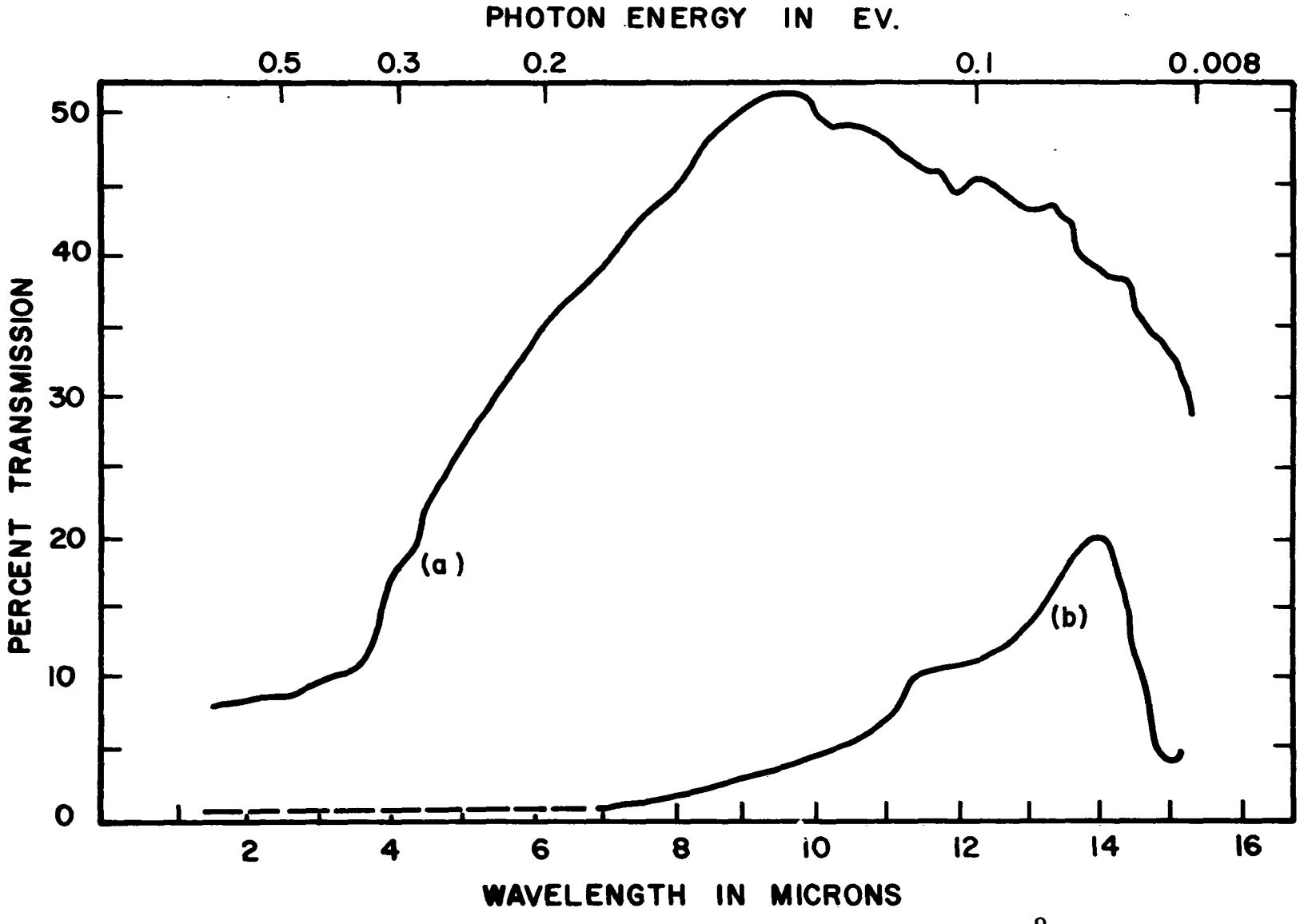

Fig. 7. Infrared Transmission of Two 30 micron Films of Bi_2O_3 at $300^{\circ}K$.

2.1 Properties

a) Thermal Energy Gap, Eg_{th}

Uniform portions of the bismuth trioxide films are connected to by means of silver paste electrodes and nichrome wire, and resistance as a function of temperature is then plotted. Fig. 4 shows a typical temperature vs resistance curve, giving a thermal energy gap of 2.07±0.07 eV, in the range 400-550°K.

b) Optical Energy Gap

Optical transmission studies are made with a Cary spectrophotometer on these polycrystalline films and Fig. 5 shows a typical transmission curve. Fig. 6 shows the absorption edges at 300°K and 77°K, which give for the optical energy gap, 2.8 eV at 300°K and 3.1 eV at 77°K, with a temperature dependence of 1.1×10^{-3} eV /°K, if we assume the variation is linear over this temperature range.

c) Infrared Transmission

Infrared transmission of the films is measured with Perkin - Elmer model 21 infrared spectrophotometer and is shown in Fig. 7.

References

1) P. P. Konorov, Zh. Tekh. Fiz. 26, 1126 (1956).

2) J. Black, E. M. Conwell, L. Seigle and C. W. Spencer J. Phys. Chem. Solids 2, 240 (1957).

3) L. Goriunova, Soviet Phys. - Tech. Phys. 1, 1583 (1957).

4) B. T. Kolomiets, Zh. Tekh. Fiz. 19, 126 (1949).

5) A. E. van Arkel, E. A. Flood and N. F. H. Bright, Can. J. Chem. 31, 1009 (1953).

PART III

THERMOELECTRIC STUDIES

INTRODUCTION

The work of Part III had three aims: First, to find the figure of merit of Bi_2S_3, a compound about which there is hardly anything in the literature; second, to measure the thermal conductivity and Seebeck voltage of a number of samples of the other compounds already prepared and studied under this contract, such as Sb_2Se_3 and Bi_2Te_3; and third, to produce if possible reliable apparatus for making the above-mentioned measurements on samples necessarily of small size.

Table I gives the results of our studies, together with some results from other workers where comparable. Table II shows the results, using the apparatus mentioned, on a series of known and unknown samples, to assess the reliability of the method.

Also included are plots of such functions as Seebeck voltage vs temperature difference, thermal conductivity vs temperature and Seebeck coefficient vs temperature for Bi_2S_3 and other compounds.

DISCUSSION

1. 0 Coefficient of Performance

Coefficient of performance is usually given as the ratio of the heat energy transferred to a thermocouple from its surroundings over the power consumption of the thermocouple. The heat energy transferred to the thermocouple from its surroundings is

TABLE I

THERMAL CONDUCTIVITY, ELECTRICAL RESISTIVITY,

AND SEEBECK COEFFICIENT OF Sb_2Se_3

AND OTHER COMPOUNDS

Sample No.	Compound	k Watt/cm deg Room temp	ρ ohm cm Room temp	S μV/deg Room temp
2	Sb_2Se_3+0.5%Se	0.0221	3.7×10^{4}	+1376
202	Bi_2Se_3	0.0230	4.1×10^{-4}	-108
231	Bi_2Te_3	0.0230	0.91×10^{-3}	+140
226	Bi_2Te_3+0.2%Bi	0.0231	1.63×10^{-3}	+202
228	Bi_2Te_3+0.1%Pb	0.0244	1.57×10^{-3}	+168
240	Bi_2Te_3+0.1%I	0.0256	0.63×10^{-3}	-184
212	Bi_2Te_3+1.0%Bi_2Se_3	0.0249	2.18×10^{-3}	+146
207	Bi_2Te_3+3.0 Te	0.0149	2.2×10^{-3}	- 75
301	Bi_2Se_3 polycrystal*	0.0201	3.5	-700 to -850
303	Bi_2S_3 single crystal*	0.0206	0.85	-550

* Denotes average value of some 10 or 15 samples.

TABLE I (Contd)

Reference	Compound	k Watt/cm deg 300°K	ρ ohm cm 300°K	S μV/deg 300°K
10	Sb_2Se_3		$4x10^4$	
11	Sb_2Se_3		$6x10^1$	
12	Sb_2Se_3		10^6	+1200
17	Sb_2Se_3		$\sim 10^5$ (25°C)	~ +1000
12	Bi_2Se_3		$5x10^{-4}$	-100
18	Bi_2Se_3		$4.7x10^{-4}$	
20	Bi_2Te_3	0.020	$0.52x10^{-3}$	+240
13	Bi_2Te_3		$0.8x10^{-3}$	+150
14	Bi_2Te_3		$2.0x10^{-3}$	
18	Bi_2Te_3		$1.3x10^{-3}$	
14	Bi_2Te_3(excess Bi)	0.021	$3.3x10^{-3}$	+210
14	Bi_2Te_3(p type)		$1.6x10^{-3}$	+170 (60°C)
14	Bi_2Te_3 + 0.1% Pb		$1.3x10^{-3}$	
14	Bi_2Te_3 (excess I)	0.021	$2.1x10^{-3}$	-180(60°C)
14	Bi_2Te_3 + 0.5%Bi_2Se_3		$2.9x10^{-3}$	
14	Bi_2Te_3 + 2.0% Te		$2.7x10^{-3}$	
15	Bi_2S_3 (sintered)		10^{-3}	-1300
12	Bi_2S_3 (polycrystal)		10^{-2}	-750
16	Bi_2S_3 (polycrystal)		$2x10^1$	

TABLE II

Material	k Watt/cm deg Room temp	k, (published) Watt/cm deg Room temp	Reference
Bi (polycrystal)	0.0837	0.08012	5
		0.0836	6
Sb (polycrystal)	0.1670	0.178	19
Bi_2Te_3 (n type)	0.0315	0.0255	9
		0.0330	7
Bi_2Te_3 (p type)	0.0231	0.0230	9
		0.0285	7
		0.0205	21

$$Q = SIT_c - I^2R/2 - K(T_h - T_c) \quad (1)$$

where $$S = S_1 + S_2 \quad (2)$$

$$R = \rho_1 L_1/A_1 + \rho_2 L_2/A_2 \quad (3)$$

and $$K = k_1 A_1/L_1 + k_2 A_2/L_2 \quad (4)$$

The subscripts refer to branch (1) and branch (2) of the thermocouple, S is the Seebeck coefficient, I the current, R the resistance, K the thermal conductance, L the length and A the cross-sectional area of the branch, ρ the resistivity and k the thermal conductivity of the branch, and T_h and T_c the temperatures of the hot and cold junctions respectively.

The power consumed by the thermocouple is given by

$$W = I^2R + SI(T_h - T_c) \quad (5)$$

thus the coefficient of performance is

$$\eta_{max} = \left[\frac{T_c}{T_h - T_c} \right] \left[\frac{(1 + Z\overline{T})^{1/2} - T_h/T_c}{(1 + Z\overline{T})^{1/2} + 1} \right] \tag{6}$$

where $$\overline{T} = (T_h + T_c)/2 \tag{7}$$

$$Z = (S_1 + S_2)^2 / \left[(k_1\rho_1)^{1/2} + (k_2\rho_2)^{1/2} \right]^2 \tag{8}$$

and where Z refers to the figure of merit of the thermoelectric cooling device. The circuit parameters satisfy the condition

$$A_1L_2/A_2L_1 = (\rho_1k_2/\rho_2k_1)^{1/2}. \tag{9}$$

The temperature difference $(T_h - T_c)$ reaches its maximum value when the cold junction is thermally insulated (i. e. $Q = 0$). Then ΔT_{max} results from solving for ΔT in the (1) and maximizing with respect to the current

$$\Delta T_{max} = ZT_c^2/2. \tag{10}$$

The efficiency for thermoelectric power generation, a function of the same parameters, is defined as

$$\xi = \left[\frac{T_h - T_c}{T_h} \right] \left[\frac{(1 + Z\overline{T})^{1/2} - 1}{(1 + Z\overline{T})^{1/2} + T_c/T_h} \right] \tag{12}$$

The quantities η, ξ, ΔT_{max} and Z are temperature dependent. The figure of merit affords a good first-order evaluation of material for Peltier cooling and heating and for thermoelectric power generation. We see by (8) that the figure of merit for one branch of a thermocouple

is

$$Z = S^2/\rho k \tag{13}$$

The larger the Seebeck coefficient and the larger the ratio of electrical to thermal conductivity, the better the device.

1.1 Thermal Conductivity

Data are presented on the thermoelectric properties of compounds of the M_2N_3 type among the Group Vb and Group VIb elements.

The thermal conductivity is measured with the apparatus shown in Fig. 1, developed in this laboratory and designed for use with small cylindrical samples of low thermal conductivity, using a comparison technique[1, 2]. The unknown sample is put in series with a standard sample between a heat source and heat sink. At thermal equilibrium the thermal gradients necessary to establish uniform heat flow through the crystal column are measured. The thermal conductivity of the unknown sample is given by

$$k_u = k_s A_s L_u (T_1 - T_2)/A_u L_s (T_2 - T_3) \tag{14}$$

where the subscript s refer to the standard and u to the unknown sample.

Temperatures T_1 and T_3 are maintained by the steady flow of water through a constant temperature bath, then through the source, then an ambient temperature cooling coil to establish $T_1 - T_3$ and finally through the sink. These temperatures are varied by regulating the water flow and the heat input to the constant temperature bath.

Iron constantan thermocouples are imbedded within the source and the sink, with the junction as near as possible to the interface[3, 4]

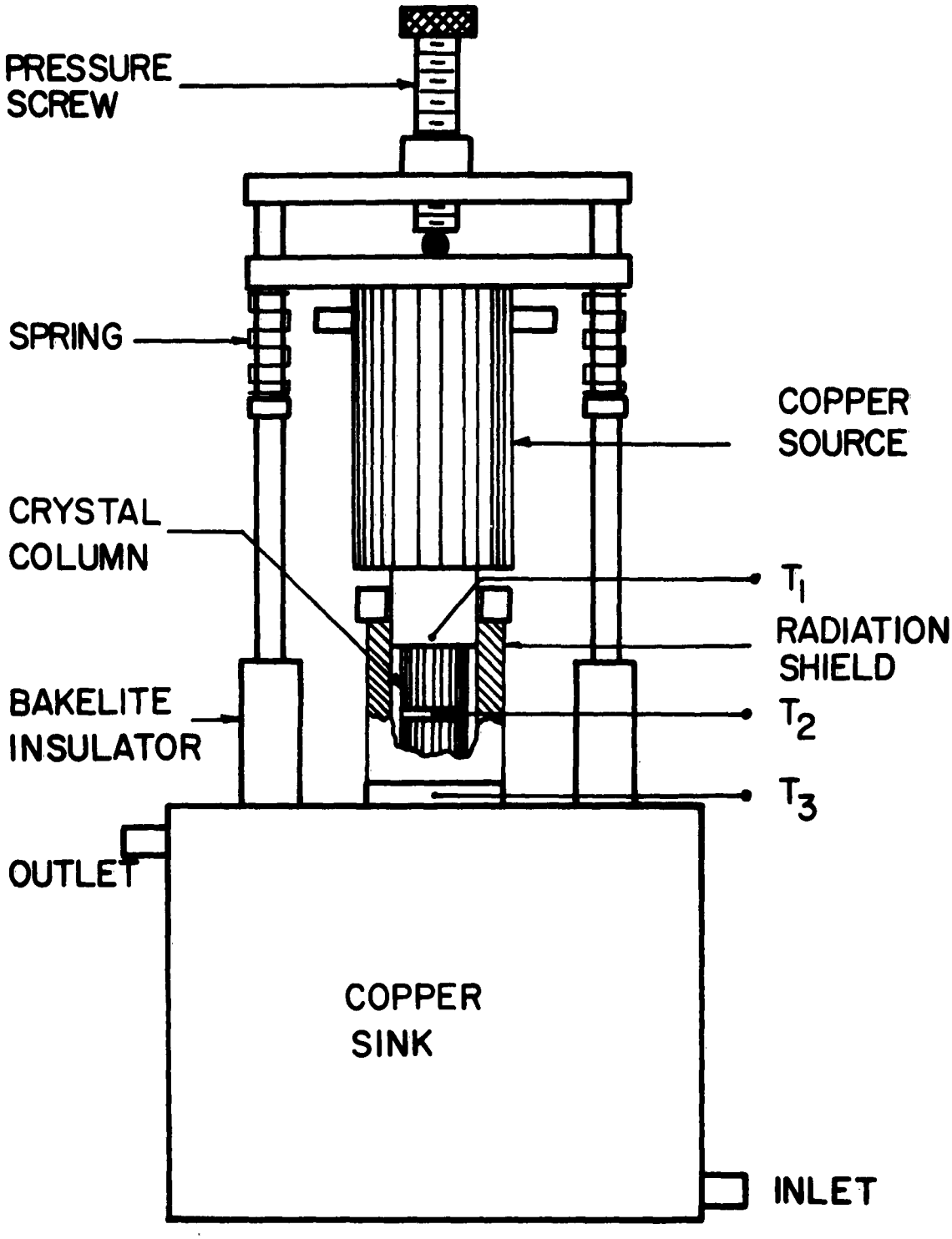

Fig. 1. Apparatus for Measuring Thermal Conductivity and Seebeck Coefficient.

so that measured values of T_1 and T_3 are essentially the temperatures at the extremities of the crystal column, see Fig. 2. Thermocouple T_2, mounted in a thin copper wafer to minimize the interface gradient, one lead in the upper surface and the other in the bottom surface, is situated between the samples. Sample faces are machined perpendicular to the cylinder axis and burnished with fine emery paper. A thin layer of vacuum grease impregnated with fine copper powder helps to minimize thermal resistance at the interfaces.

A polycrystalline bismuth shield surrounds the samples during measurement, and is also in good thermal contact with the source and sink. Thus the shield, having a similar gradient, presents a "no loss" environment for the crystal column.

Bismuth, having a value of thermal conductivity near that of the unknown, was chosen as standard. This has a thermal conductivity of 0.09426 watt/cm deg for single crystals in the direction parallel to the cleavage planes[5]. Test runs on polycrystalline bismuth, polycrystalline antimony and nearly stoichiometric n and p type bismuth telluride in place of the unknown sample, gave results which agree with those reported for these compounds[5, 6, 7]. Fig. 3 shows the thermal conductivity vs termperature curve for a typical sample of n type bismuth telluride and Fig. 6 shows k vs T curve for single crystal bismuth trisulfide.

1.3 Seebeck Coefficient

The Seebeck coefficient S, measured at temperature T_a is given by

$$S = E_s/\Delta T \tag{15}$$

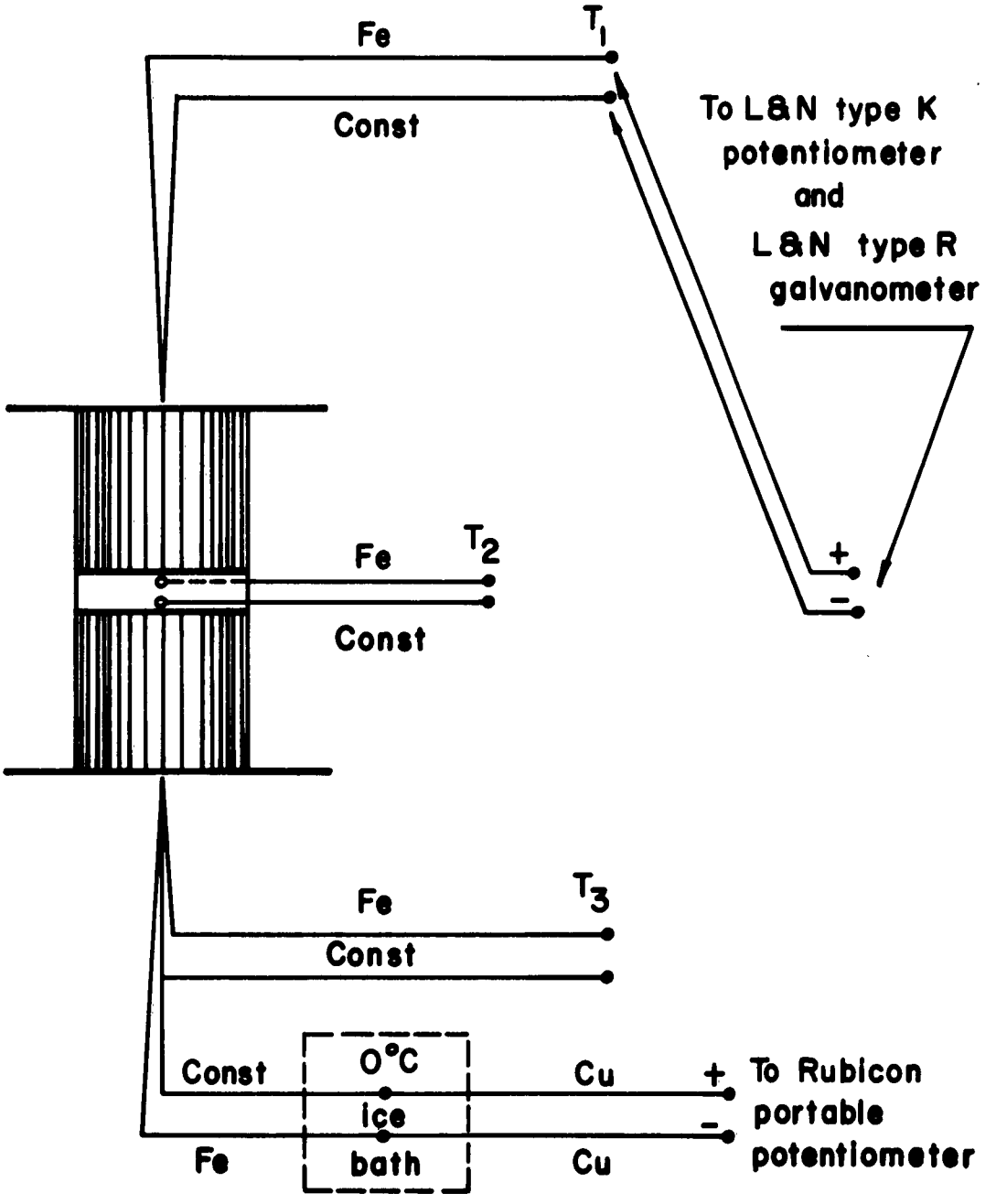

Fig. 2. Crystal Column and Thermocouple Arrangement.

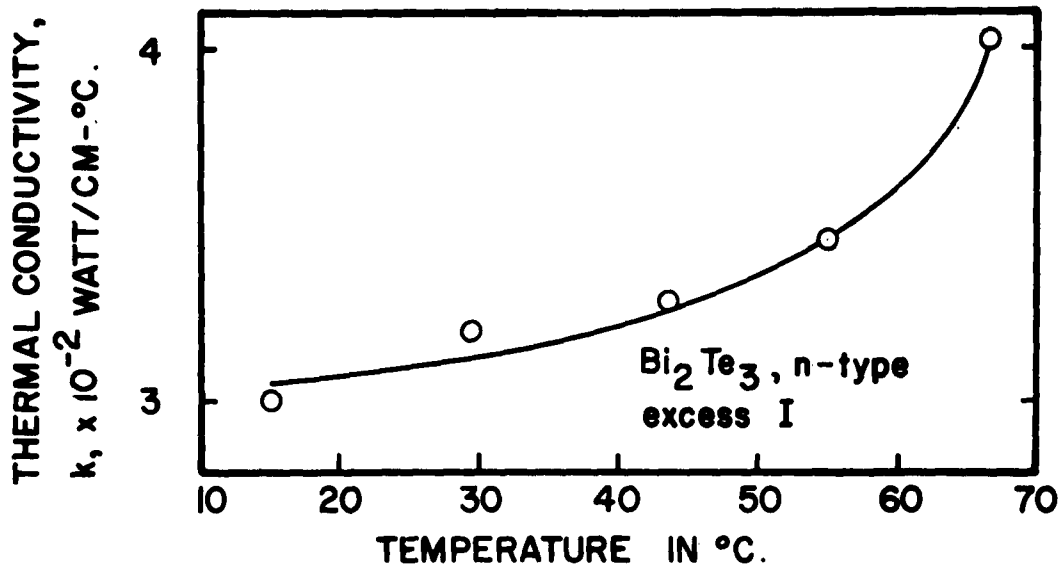

Fig. 3. Thermal Conductivity vs Temperature.

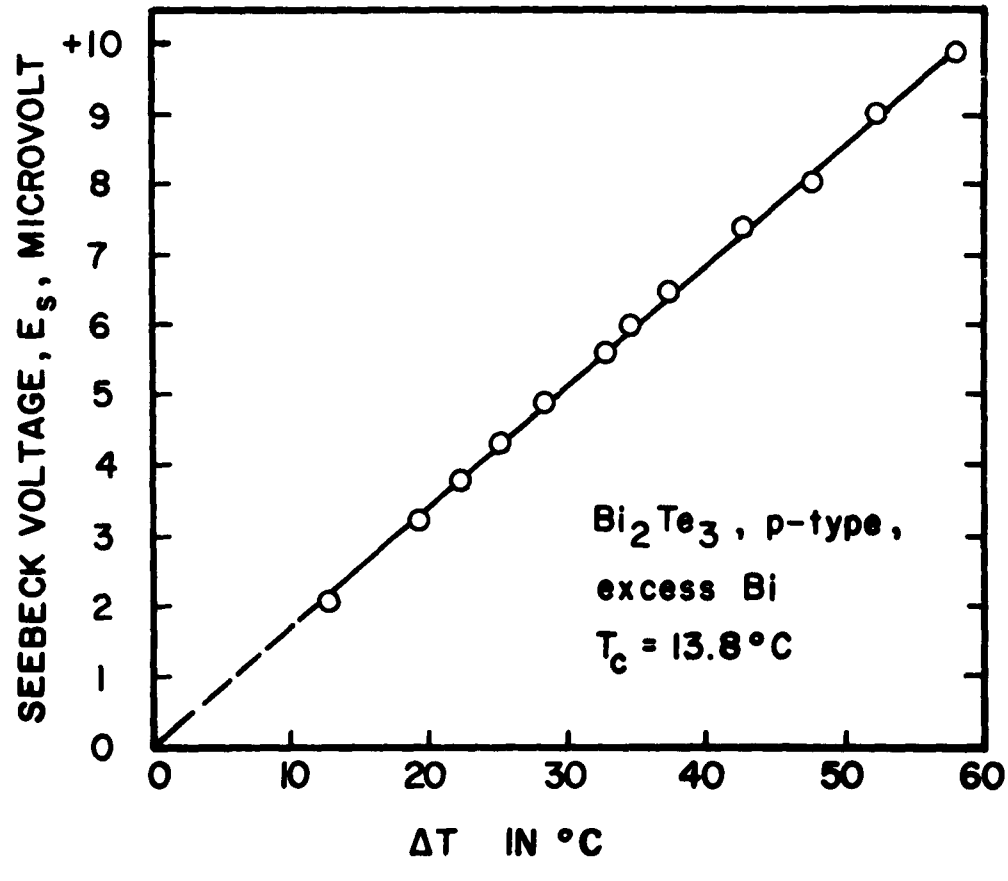

Fig. 4. Seebeck Voltage vs Temperature Difference.

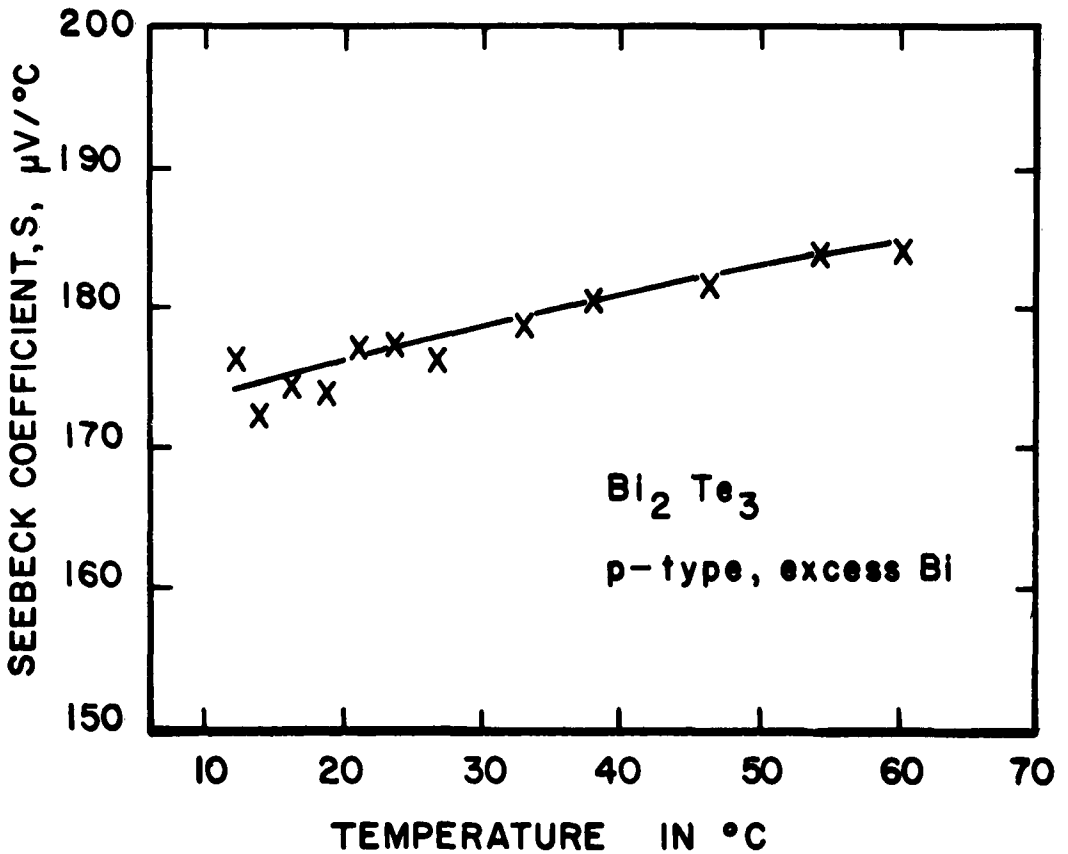

Fig. 5. Seebeck Coefficient vs Temperature

and $$T_a = T_1 + T_3/2 \quad (16)$$

where E_s is the Seebeck voltage established by the temperature difference, ΔT between the heat source and the heat sink. The Seebeck voltage, read with a Kaylab D. C. Microvoltmeter, and the temperature, are measured simultaneously. In the presence of ΔT the majority carriers exhibit a net drift to the sink (cold junction) thus giving this junction the sign of the majority carrier. The apparatus used is shown in Fig. 1.

Horne[3] has given a criterion for the reliability of Seebeck coefficient measurements; a plot of Seebeck voltage vs temperature difference giving a straight line through the origin, identifies a properly functioning device. The apparatus meets this requirements, see Fig. 4. Seebeck coefficient data for a typical sample of p type bismuth telluride and single crystal bismuth trisulfide are shown in Fig. 5 and Fig. 7, respectively. The values of Seebeck coefficient for the better n and p type bismuth telluride samples agree with those reported.

1.4 Figure of Merit

The figure of merit, calculated from equation 13 using the results for the better bismuth telluride material (Table I), is 1.08×10^{-3} deg^{-1}. These results give a Z of 1.03×10^{-5} deg^{-1} for polycrystal bismuth trisulfide and a Z of 1.7×10^{-5} deg^{-1} for single crystal bismuth trisulfide.

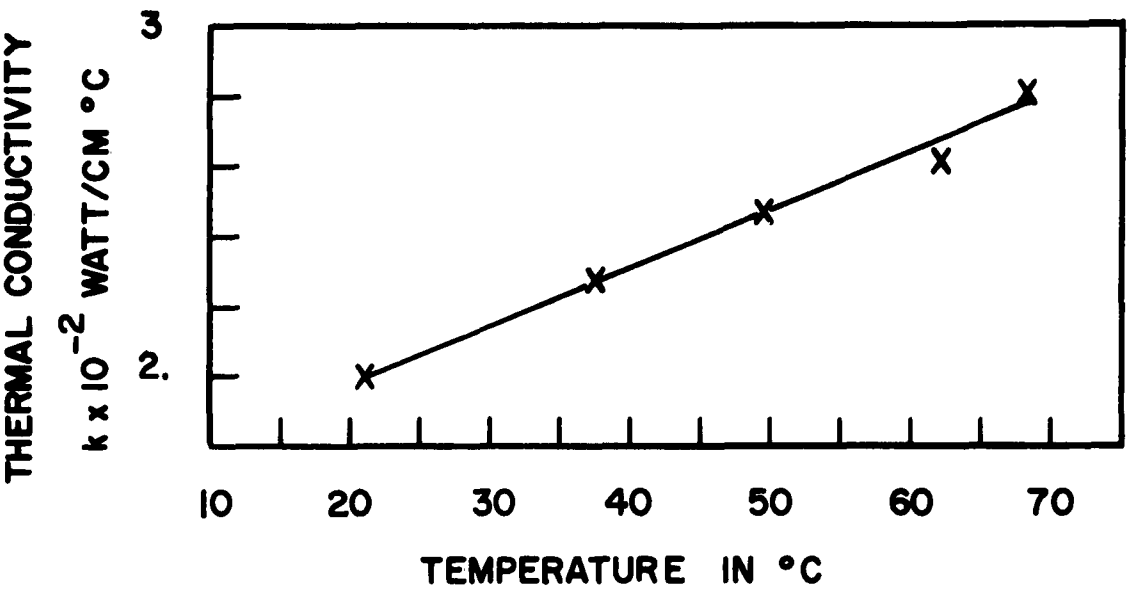

Fig. 6 Thermal conductivity vs temperature for single crystal $Bi_2 S_3$

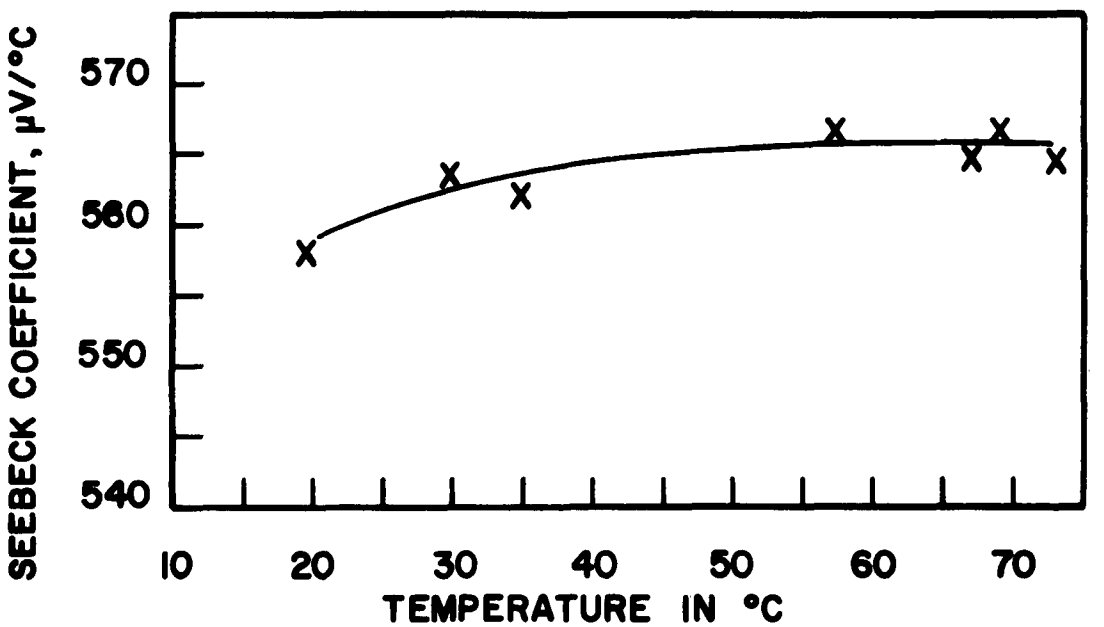

Fig. 7. Seebeck coefficient vs temperature for single crystal Bi_2S_3

References

1. S. S. Ballard, K. A. McCarthy and W. C. Davis, Rev. Sci. Inst. 21, 905 (1950).

2. A. D. Stuckes, Phys. Rev. 107, 427 (1951).

3. R. A. Horne, Rev. Sci. Instr. 31, 459 (1960).

4. A. F. Ioffe, Semiconductor Thermoelements and Thermoelectric Cooling, Infosearch, Ltd., London, (1957).

5. S. Nishioka, Memoirs of College of Science, University of Kyoto, A25, 147 (1954).

6. Bulletin, American Smelting and Refining Co., New York, (1959).

7. C. B. Satterthwaite and R. W. Ure, Jr., Phys. Rev. 108, 1164 (1957).

8. First Eighteen-month Progress Report, Selenides Project, Lee Gildart and D. F. Clifton, University of Kentucky, Lexington, Ky., (1958).

9. H. J. Goldsmid, Proc. Phys. Soc. Lond, B69, 203 (1956).

10. N. A. Goriunova and B. T. Kolomiets, Zh. Tekh. Fiz. 25, 984 (1955).

11. N. A. Goriunova and B. T. Kolomiets, Zh. Tekh. Fiz. 25, 2069 (1955).

12. J. Black, E. M. Conwell, L. Seigle and C. W. Spencer, J. Phys. Chem. Solids 2, 240 (1957).

13. M. Telkes, J. Appl. Phys. 18, 1116 (1947).

14. T. C. Harman, B. Paris, S. E. Miller, H. L. Goering, J. Phys. Chem. Solids 2, 181 (1951).

15. P. P. Konorov, Zh. Tekh. Fiz. 26, 1126 (1956).

16. N. A. Goriunova, B. T. Kolomiets and A. A. Malkova, Soviet Phys. Tech. Phys. 1, 1583 (1957).

17. B. D. Cullity, M. Telkes, and J. Norton, J. Metals 188, 47 (1950).

18. A. F. Ioffe and A. R. Regel, Progress in Semiconductors, Vol. 4, John Wiley and Sons, Inc., New York (1960).

19. International Critical Tables, 5, 221, McGraw-Hill Book Co., Inc, (1929)

20. J. Appel, Progress in Semiconductors, Vol. 5, John Wiley and Sons, Inc., New York (1960).

21. T. C. Harman, J. H. Cahn, and M. J. Logan, J. Appl. Phys. 30, 1351 (1959).

PART IV

ELECTRICAL TRANSIENT BEHAVIOR AND THE SWITCHING EFFECT IN ANTIMONY TRISULFIDE

We give here a conclusion of subject matter covered in Technical Note AFOSR-121[15] summarizing experiments by which the important time and electric field dependent characteristics associated with the "switching effect" in stibnite were measured.

Additional experiments are described by which temperature dependent properties, pre-breakdown pulses, and the conductivities before and after switching were determined. Finally, certain physical properties applicable to semiconducting and dielectric stibnite are examined.

Stibnite, Sb_2S_3, at the stoichiometric composition, undergoes dielectric breakdown with applied fields of approximately 10^6 volts per cm, which is of the same order as the breakdown fields for most dielectric materials. Furthermore, following the removal of the applied field, the conductivity of the stibnite sample remained unchanged.

However, it was discovered in this laboratory that samples of stibnite containing 1 to 4 per cent by weight excess antimony undergo breakdown with a much smaller field, about 1000 volts/cm ; and with removal of the field the sample resistance is found to be about four orders of magnitude smaller. This behavior is unlike that of

most dielectrics, which ordinarily either show chemical decomposition, or else do not show a permanent change in resistances.

In addition to the above effect it was also found that the original high resistance of the samples could be restored by heating. It is this reversible breakdown or "switching effect" which motivated these investigations.

4.1 Structure and Physical Constants of Stibnite

Stibnite is naturally occurring mineral, commonly used as a source of antimony. It has a bright metallic luster, and a well-defined crystalline character. It is readily produced in the laboratory by direct reaction of sulphur and antimony at about 650°C[5, 6]. Various properties and constants of interest are given below:

Chemical Formula:	Sb_2S_3
Melting point: [3, 5, 6]	548°C
Energy gap: [3, 4, 14]	1.55-1.7 ev
Density: [3, 5, 6]	4.6 gm/cc
Dielectric constant: [3]	9.6
Resistivity: [3, 4]	10^9 ohm cm
Stoichiometric composition by weight:	71.69% Sb, 28.31 %S
Cleavage plane: [4, 7]	010

Stibnite crystalizes with an orthorhombic unit cell (see Fig. 1) having a = 10.20A, b = 11.28A and c = 3.83A. Sb_2S_3, Sb_2Se_3 and Bi_2S_3 are isomorphic with only slight differences in their lattice spacings. For stibnite the accepted space group is Vh^{16} (pbnm) or D_2h^{16}.

This structure (Fig.. 1) consists of sheets of Sb_2S_3 indefinitely extended in the plane parallel to the c-axis and roughly diagonal to the

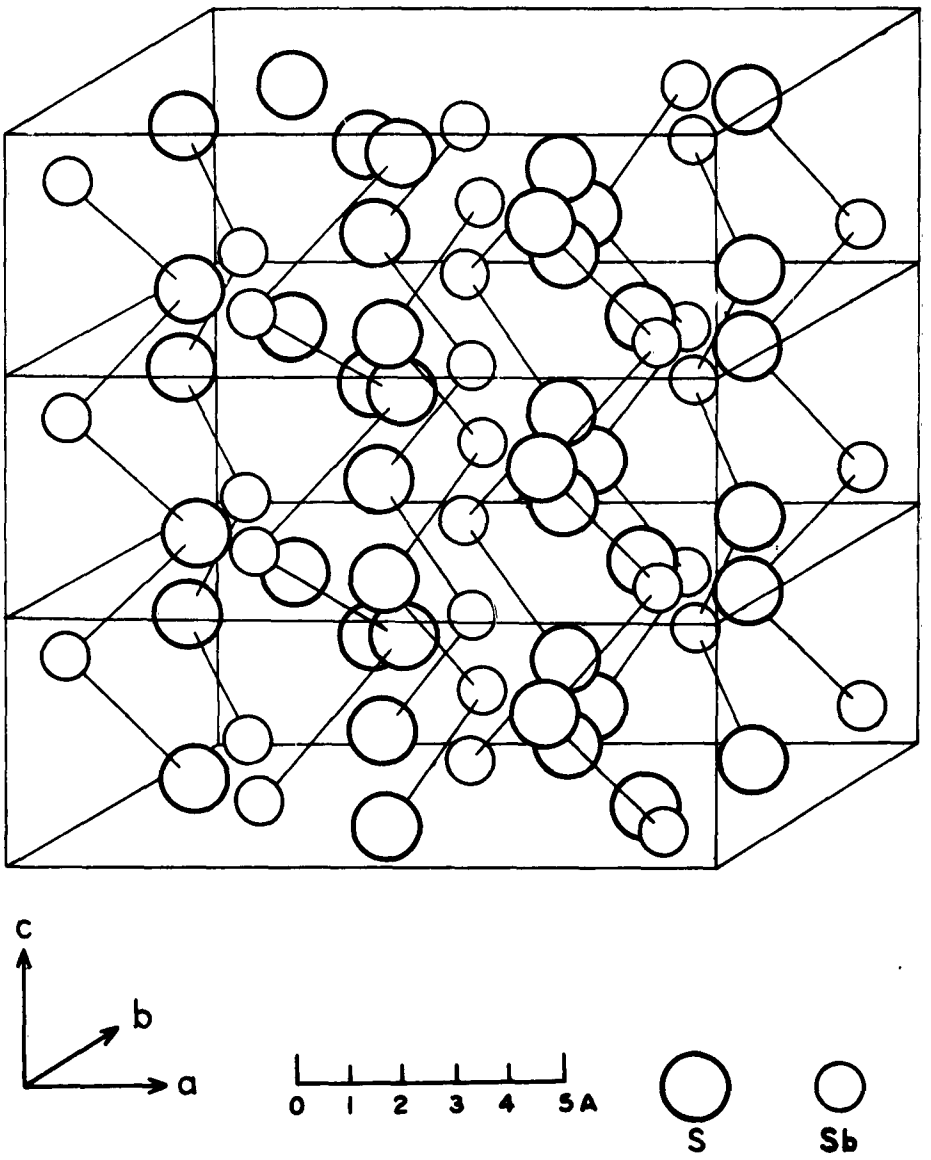

Figure 1.---Three unit cells of stibnite

a- and b- axis. In each sheet each Sb and each S atom is surrounded by three atoms of the opposite kind, at distances roughly equal to the sum of the neutral atomic radii. The separation between sheets, is, however, about half again greater, which results in unusually large interstices in the crystal. There is an open plane with approximate coordinates (110) which one would expect to be the principal plane of cleavage. However, this is not the case, and is explained by the fact at the edges of each unit cell there is a strongly bonded sulphur atom interrupting the otherwise loose bonding across this plane.

A phase diagram (Fig. 2) for the Sb-S system shows that antimony has only a limited solid solubility in stibnite, so that excess antimony above 3% or 4% implies free antimony in the crystals.

4.2 Preparation of Samples

The constituents are reacted directly by heating in an evacuated pyrex tube at 650°C. The resulting ingot is crushed, melted, and cast into a 2mm pyrex tube. The samples used in most of the experiments were sections of these castings. In some cases the sample was sealed into a pyrex tube and dropped through a hot zone, producing single crystals. Electrodes were attached to the samples by welding, pressure ppint contacts or using silver paste. The separation of the contacts varied from 0.5 mm to about 5.0 mm.

4.3 Examination of the Breakdown Transient

Initial experiments established that stibnite containing excess antimony displays electric breakdown when subjected to relatively low fields strengths of 1000 to 3000 volts per cm. It was further determined that the time required for transition from high (10^8 ohms)

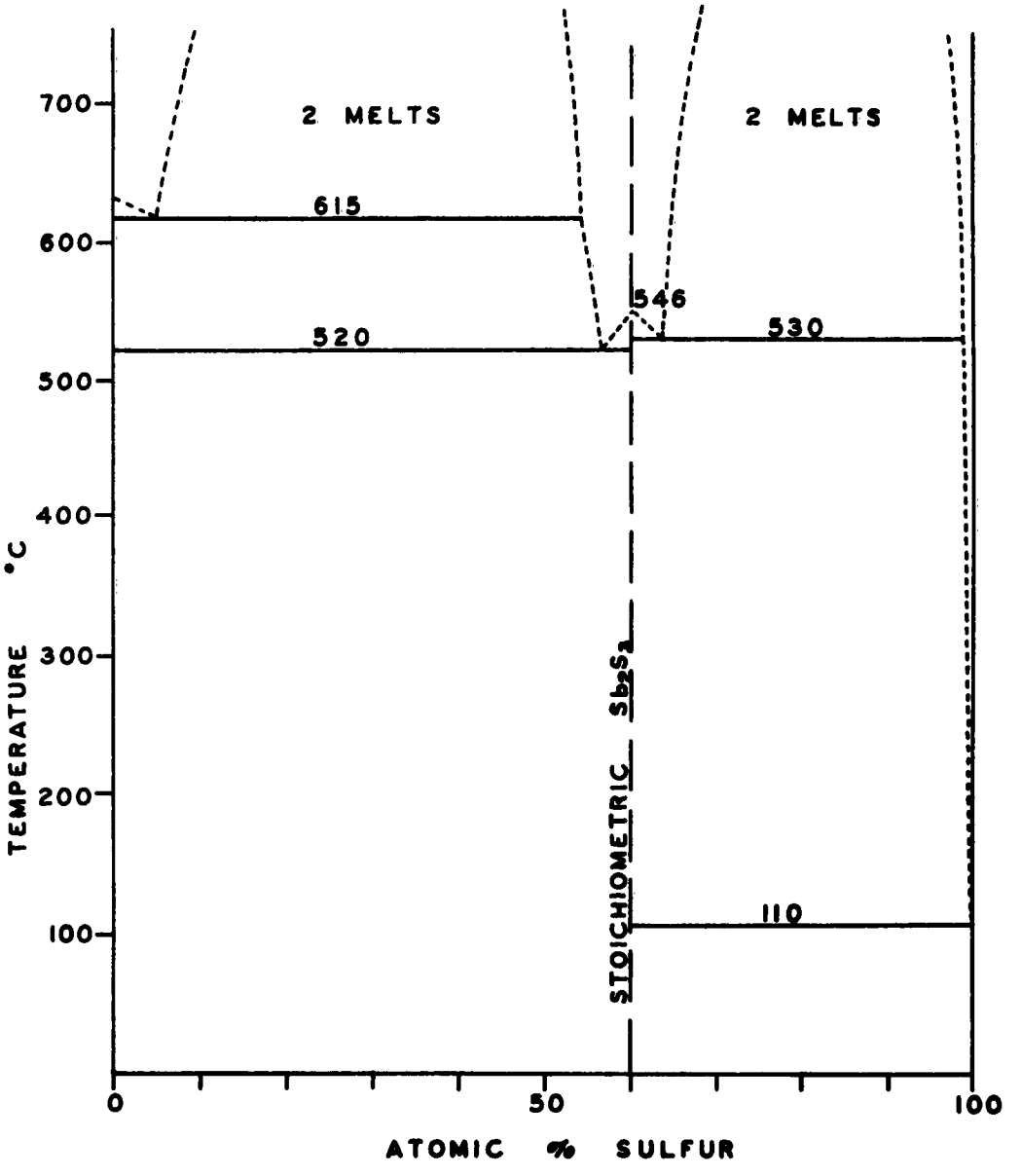

Figure 2. Phase diagram of the antimony sulfur system [5,6].

to low (10^4 ohms) resistance is very short. In order to obtain a measurement of this transition time and to determine the sample voltage at the instant of breakdown several experiments were devised based on the application of a high voltage sawtooth pulse to the sample and photographing the sample current trace from an oscilloscope. These experiments are described in some detail in Technical Note AFOSR-121[15]. A block circuit and some of the pertinent wave forms are shown in Figs. 7, 8, 11 and 12. The transition time is determined by referring to the one microsecond timing marks (Fig. 12). A simple method of calibrating sample voltage and current required only replacing the sample with a number of standard resistances and multiply exposing the resulting traces on a single negative. This negative can then be used as an overlay to determine the sample resistance, voltage, and current at any time within the trace.

Several hundred samples of various compositions were examined using this method. The duration of the breakdown transition from these experiments was about 1.5 microseconds. The limited high frequency response of the oscilloscope used only permits interpreting this as a maximum for the transition. More precise experiments subsequent to the last report have been completed and from these the duration of the transition is approximately 100 nanoseconds.

The breakdown duration was found to be independent of potential across the sample at the time of breakdown. Furthermore, there was no apparent relationship between breakdown time and the type of electrode, electrode separation, state of crystallization, composition or orientation in single crystals.

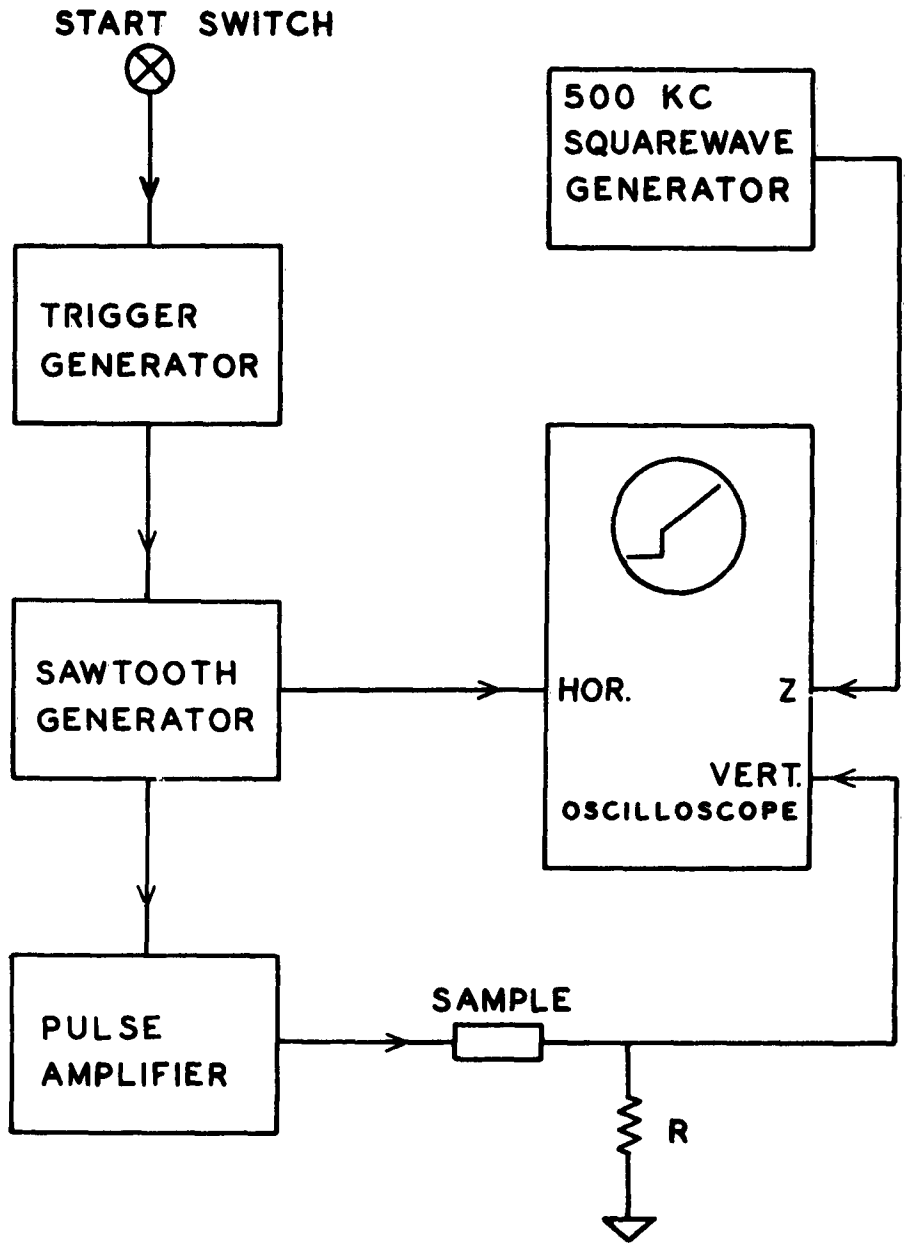

Figure 7. Block diagram of second timing circuit

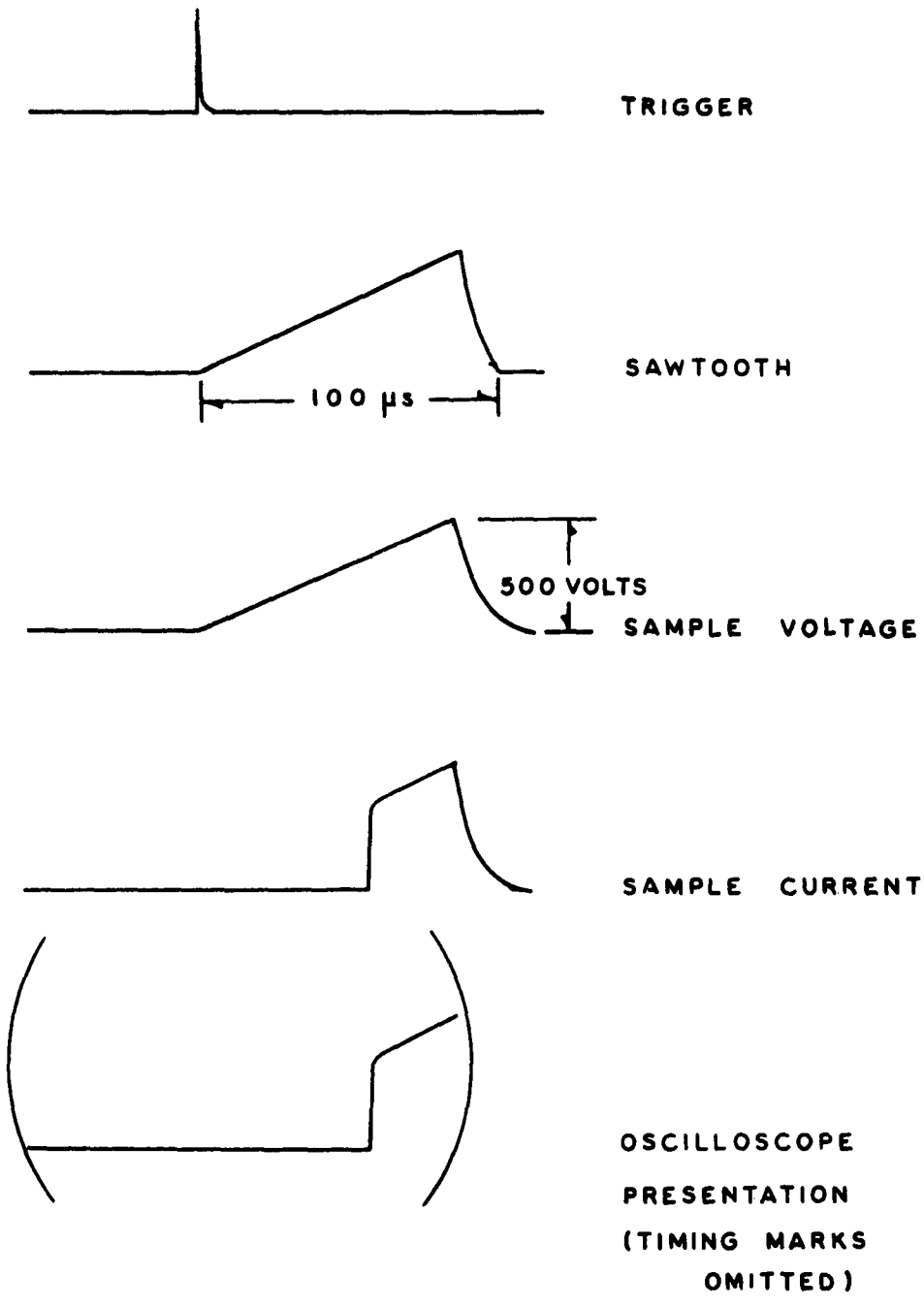

Figure 8. Waveforms in the timing circuit of Figure 7

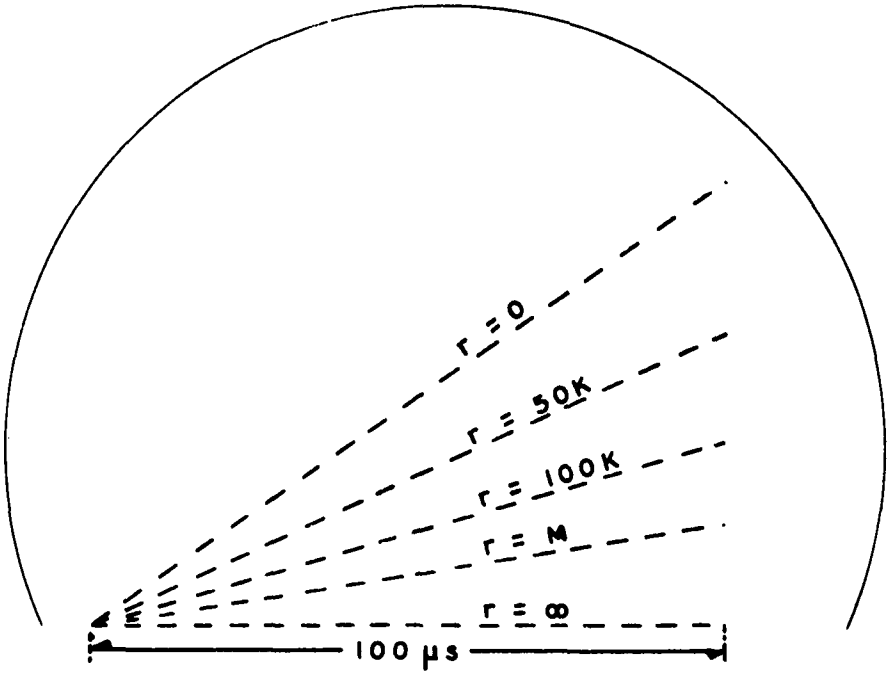

Figure 11. Calibration overlay for a 60K metering resistance

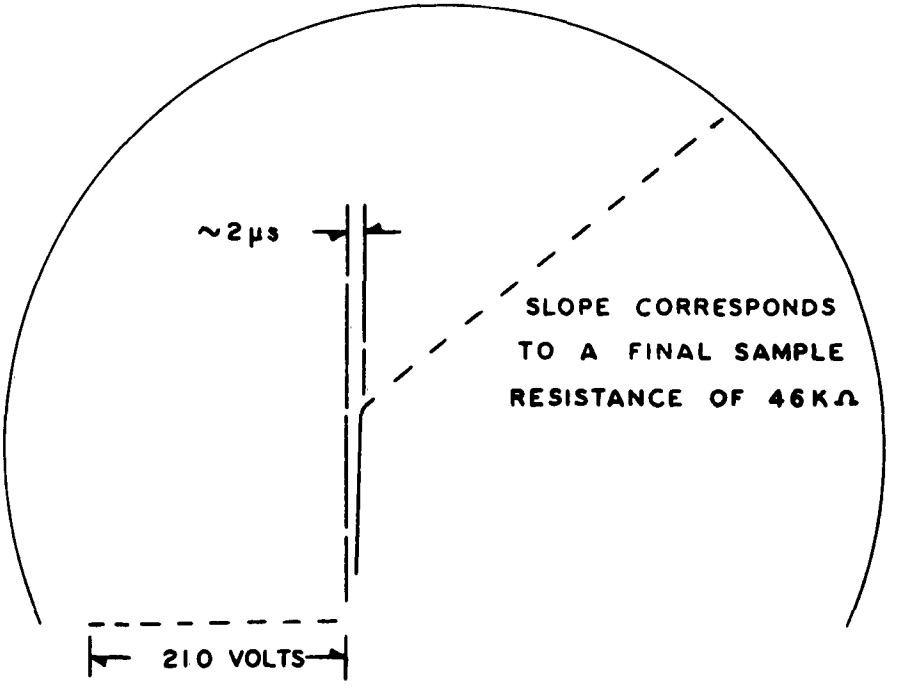

Figure 12. Typical breakdown trace

An orientation dependence was seen, however, in the case of breakdown field strength in single crystal samples. The required field for breakdown in the c-axis direction was approximately one-third that required along either the a or b axis. The breakdown field strength showed an approximately linear dependence on electrode separation and large contact effect (Fig. 13).

4.4 The Breakdown Path

The samples following breakdown were found to have a positive temperature coefficient of resistivity of approximately 0.004 per Centigrade degrees at room temperature. The possiblity arises that the electrodes were joined by a path of antimony metal following the breakdown. A series of measurements were made of the resistance samples following breakdown versus electrode separation. These data, combined with the known resistivity of antimony of 42 microhm-cm , give a cross-sectional area of about 2×10^{-10} cm^2 for a uniform antimony filament forming a path joining the two electrodes. Although attempts to measure its cross-sectional area have failed, the existence of such a metallic filament is indicated by the following experiment:

A sample was prepared with a fixed electrode and a moveable one as shown in Fig. 15. Several hundred volts were applied between these electrodes causing a breakdown to occur. An ohmmeter was then connected between the electrodes, and the sample surface was explored with the moveable probe. It was found by progressively excavating the material and exploring the revealed surfaces that a continuous conducting path could be traced through the sample to the fixed electrode about as shown in Fig. 15.

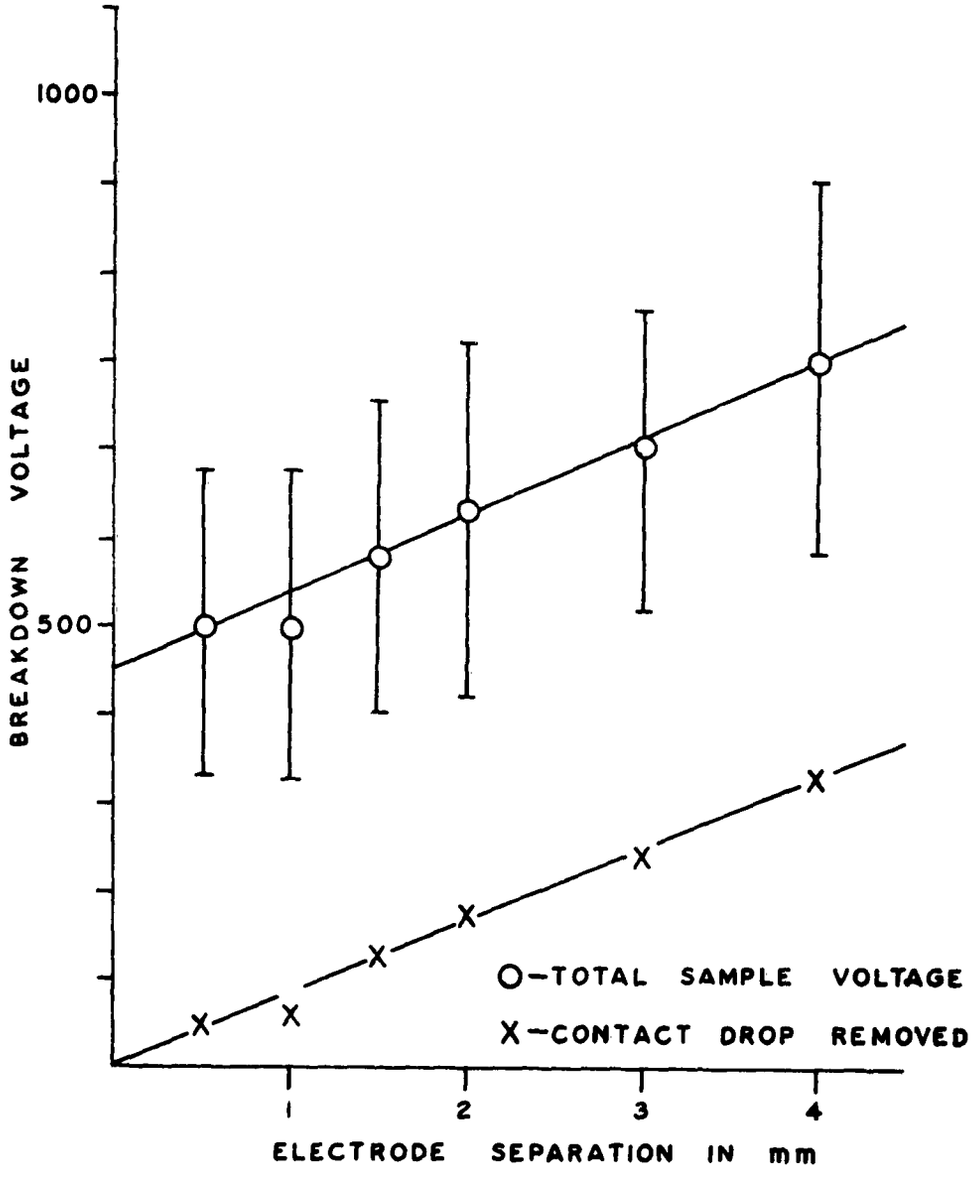

Figure 13. Breakdown voltage versus electrode separation

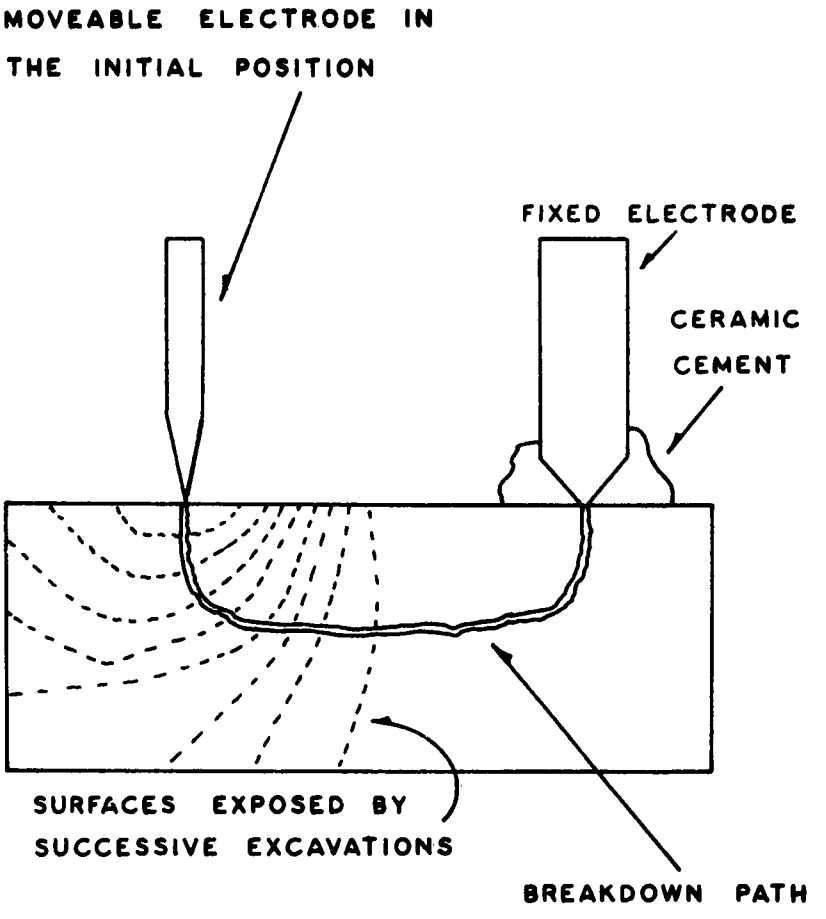

Figure 15. The breakdown path

There was no visible difference between the path and the adjacent material, therefore, it was not possible to detect the path by an optical method. Attempts to replicate the surface for electron micrograph examination failed. Initial X-ray diffraction measurements gave inconclusive data, although it is possible that a more carefully designed experiment may produce some useful results.

4.5 Effect of Temperature on Breakdown Behavior

The effect of temperature on breakdown field strength was studied in the range from 300° to 600°K. At the higher temperatures, measurements were difficult to obtain because of the tendency of the sample to anneal, i.e., to return to its high resistance state. Additionally, thermal activation greatly increases the sample conductivity making it difficult to apply large fields without appreciable Joule heating. Despite the wide scatter in the data resulting from these problems it was possible to obtain some useful conclusions. The general behavior of the mean data points plotted in Fig. 20 correlates rather well with a theory of Fröhlich and Simpson[11, 12]. This theory which is described in some detail in AFOSR-121 [15] predicts the breakdown field strength, F*, will vary with temperature according to the following expression.

$$F^* = C \exp(\Delta E / kT)$$

Where C is a constant and ΔE is the energy separation below the conduction band for trapping sites. The theory further provides that these trapping levels have many excited states within the interval ΔE below the conduction band edge. The data in Fig. 20 has been fitted with a least-squares line corresponding to a ΔE of 0.275 ev. The inter-

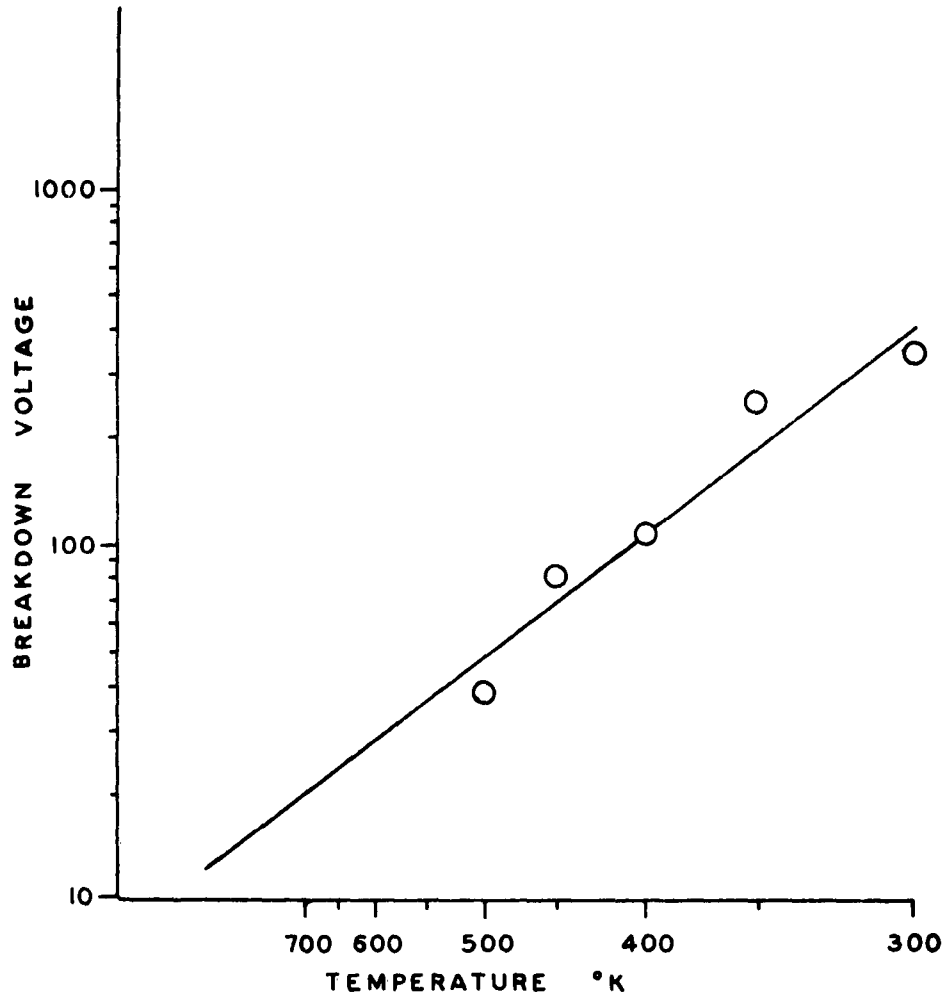

Figure 20. Breakdown voltage plotted logarithmically versus temperature plotted reciprocally.

change of energy between electrons in the excited states of the traps and lattice vibrations provides an outlet for the energy accepted from the applied field by conduction electrons. As the field or the temperature in this case is increased this energy exchange mechanism saturates allowing the conduction electron energy to increase to the point of electron-electron avalanching or breakdown.

4.6 Annealing Process

The samples of stibnite studied had a stable low resistance, following breakdown, in the range 3×10^4 to 10×10^4 ohms at room temperature. As stated previously, raising the temperature to the region between 100°C and 300°C and then cooling, restored the original high value of the resistance.

It was found that when the current through the sample is monitored while the sample is being heated, on the recovery part of the cycle, a temperature is reached at which the current may suddenly drop, and then jump back again. It may repeat this erratic behavior several times. The limiting value of the current swing, on the high resistance side, is the value of the normal thermal activation curve for the unbroken sample.

As the temperature was further increased, a point was reached at which the fluctuations disappear and the current became steady. This end point temperature occurred at about 200°C.

Oscilloscopic observation of the current through the sample during the above described annealing experiments showed that the duration of the annealing transition was very short, i.e., of the order of one microsecond, or about the same as for breakdown.

4.7 Delayed Breakdown

If a voltage, slightly smaller than that needed to induce immediate breakdown, is applied to a stibnite sample containing excess antimony, it is found that a breakdown will nevertheless eventually occur, the period of delay varying from microseconds to hours.

The delay time interval is shown in Fig. 22 to be roughly dependent on the reciprocal of the applied field, it being very long for fields, of about 200 volts per cm, and nearly zero for fields of about 6000 volts per cm.

Oscilloscope observation of this behavior revealed that "pre-breakdown" pulses of essentially constant amplitude occur at random times. These pre-breakdown pulses seemed to have the general behavior of these as described by McKay[13] in silicon p-n junctions and are interpreted as microplasmas or localized minute avalanche.

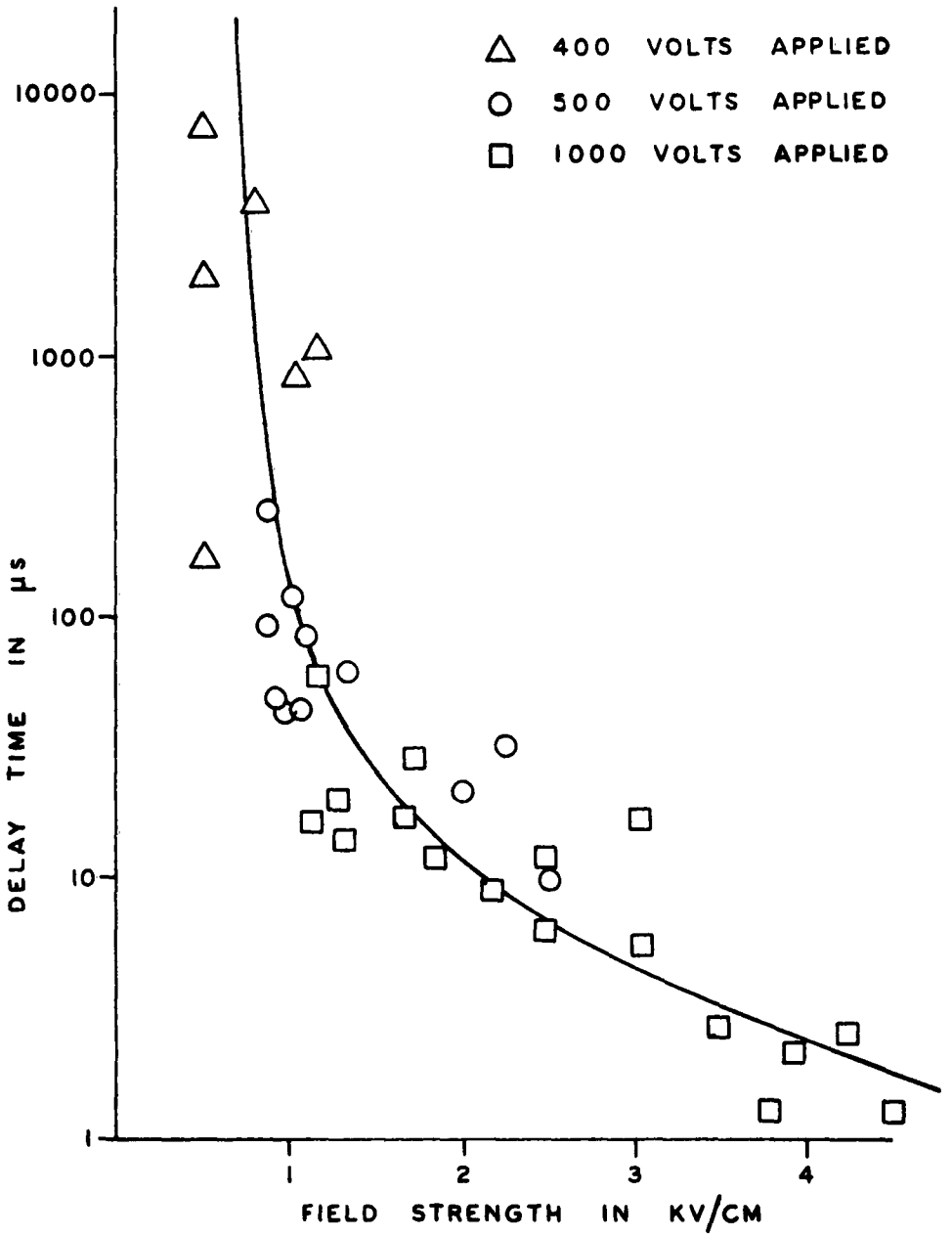

Figure 22. Breakdown delay time plotted logarithmically against sample field strength.

References

1. Von Hippel, A. and Alger, R., Phys. Rev. 76, 127 (1949).

2. Mott, N. F. and Gurney, R. W., Electronic Processes in Ionic Crystals, Clarendon Press, 1948, pp. 197-201.

3. Coblenz, A., Electronics 30, No. 11, 144 (157).

4. Ibuki, S. and Yoshimatsu, S., J. Phys. Soc. of Japan 10, 549 (1955).

5. Mellor, J. W., A Comprehensive Treatise on Inorganic and Theoretical Chemistry , IX, Longmans, Green and Co., 1925, pp. 553-55.

6. Hanson, M., Constitution of Binary Alloys, McGraw Hill, 1958, pp. 1160-61.

7. Wyckoff, R. W. G., Crystal Structures, Interscience, 1959, pp. V9.

8. Gottfried, C. and Schossberger, F., Strukturbericht, Akademische Verlagagasellschaft N. B. H., 1949, pp. 49-51.

9. Moller, H. G., Electrotechnik 3, 291 (1949).

10. Fletcher, R. C., Phys. Rev. 76, 1501 (1949).

11. Frölich, H. and Simpson, J. H., Advances in Electronics II, Academic Press, 1950, pp. 185-217.

12. Frölich, H., Proc. Roy. Soc. of London 188A, 521 (1947).

13. McKay, K. G., Phys. Rev. 94, 877 (1954).

14. Black, J., Conwell, E. M., Seigle, L., and Spencer, C. W., J. Phys. Chem. Solids 2, 240 (1957).

15. Davis, J. R. Jr., Technical Note, AFOSR-121, (1960).

PART V

APPARATUS FOR MEASURING RESISTIVITIES AND HALL COEFFICIENTS OF INTERMEDIATE RESISTANCE-VALUE SAMPLES

The apparatus for the measurements on intermediate-resistance-value samples uses the basic design set forth by Dauphinee and Mooser[1] combining an a. c. and a d. c. technique thus avoiding certain disadvantages of each alone, and is quite different from that described in Part I. The problem is one of measuring the current through the sample, the potential drop in the direction of current flow, and the Hall voltage across the width of the sample, on materials of intermediate resistance.

The apparatus constructed uses an isolating potential comparator circuit for comparing the potential drop, V_w, across a known resistance in series with the sample, to the Hall voltage, V_h, and the potential drop along the sample, V_r. Commercially built circuit choppers of special design[1], are used to compare the reference voltage V_w to V_r and V_h. One chopper converts the direct current through the reference resistor and the sample to square wave a. c. The other chopper allows a d. c. galvanometer to be used as a null indicator. A chopper frequency of 35 cps eliminates the Ettinghauser effect.

The measuring circuit is shown in Fig. 1. Thermal emf's produce d. c. current which are blocked by C_3.

The apparatus utilizes a permanent magnet having an effective field of about 7500 gauss in a half-inch gap, and a special sample holder permits samples to be changed quickly. This sample holder has five contacts either spring loaded or under screw tension. Two

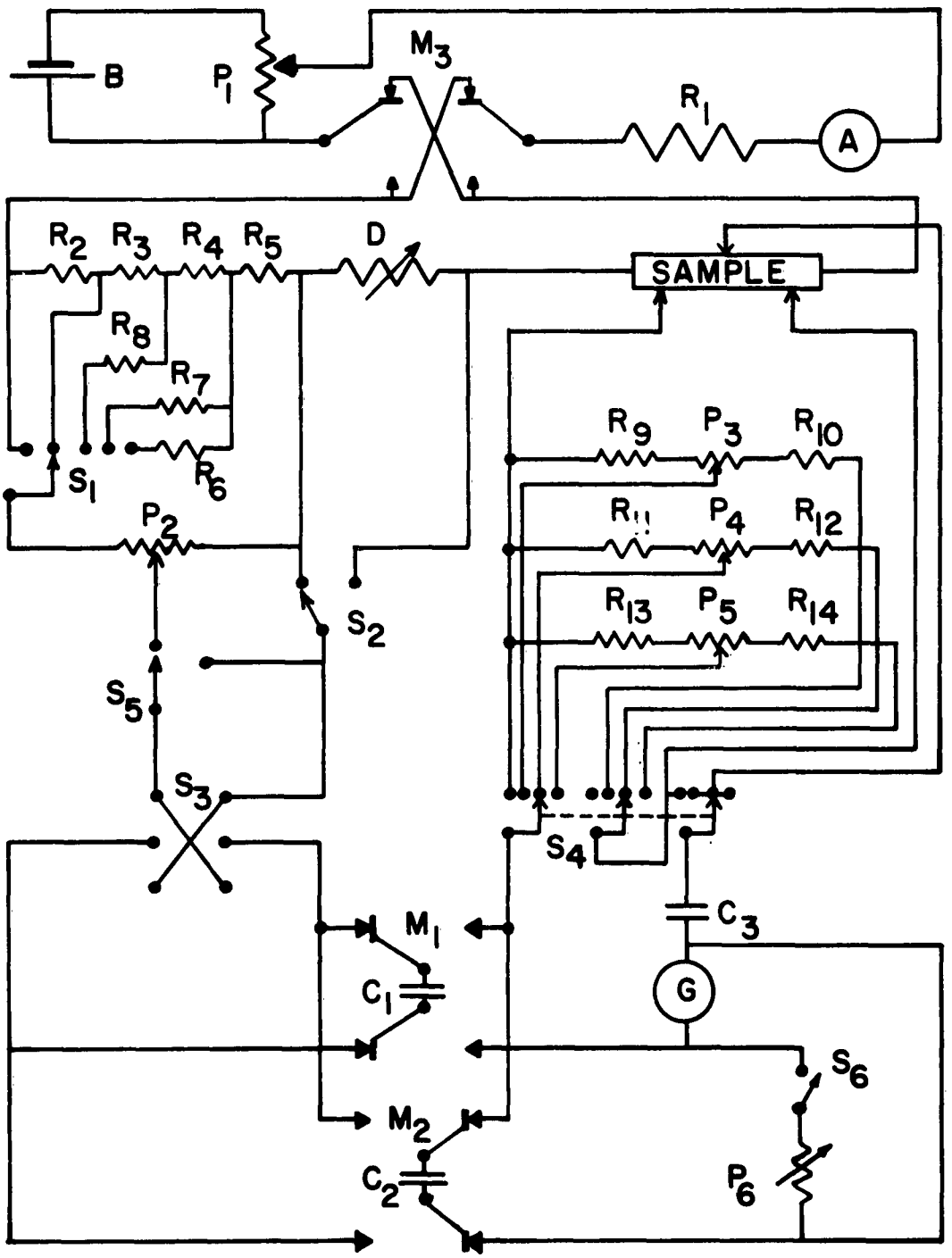

Fig. 1. Measuring Circuit

contacts at the ends of the sample are for current, two for potential measurement, and the remaining one is at the electrical center for Hall potentials.

Samples are cylindrical rods about 2 mm in diameter and 2 cm in length, but other shapes may be used. Contact is made to the sample by means of small lead beads welded to the surface of the sample. These lead beads are melted in a V of a current-carrying nichrome wire and touched to the surface after the oxide layer is driven from the surface of the bead, by the heat of the wire. The resulting contacts are ohmic and bonded well to the sample.

EXPERIMENTAL RESULTS

Bi_2Se_3 (p-type)

W_r (ohms)	W_h (ohms)	Resistivity ρ(ohm-cm)	Hall coefficient $R(m^3/coulomb)$	Hall mibility $\mu(m^2/volt\ sec)$
0.054	$5.9X10^{-4}$	$3.0X10^{-5}$	$1.5X10^{-6}$	0.050
0.068	$6.4X10^{-4}$	$3.8X10^{-5}$	$1.6X10^{-6}$	0.042
0.058	$5.3X10^{-4}$	$3.3X10^{-5}$	$1.3X10^{-6}$	0.039

As_2Te_3 (n-type)

0.044	$1.1X10^{-4}$	$2.5X10^{-5}$	$2.8X10^{-7}$	$1.1X10^{-2}$
0.19	$1.2X10^{-4}$	$1.1X10^{-4}$	$3.0X10^{-7}$	$2.7X10^{-3}$
0.20	$1.2X10^{-4}$	$1.1X10^{-4}$	$3.0X10^{-7}$	$2.7X10^{-3}$

HIGH-RESISTANCE SAMPLES

Attempts to measure the parameters on Sb_2Se_3 and Sb_2S_3 with this apparatus were unsuccessful due to high sample resistances. (See Part I of this report.)

References:

1 T. M. Dauphinee and E. Mooser, R. S. I. 26, 660 (1955).

PART VI

PAPERS PRESENTED AND PAPERS FOR PUBLICATION

6.0 Abstracts of Further Papers Presented Since July 1, 1958.

FIELD-INDUCED SWITCHING IN STIBNITE, D. M. Mattox and Lee Gildart, University of Kentucky. A stibnite crystal containing about 2 percent antimony can be made to switch repeatedly between the values of 10^4 and 10^{10} ohms purely by electrical means. Breakdown requires a voltage pulse of about a microsecond duration at fields of the order of 10^3 volts per cm, as has been described[1], the crystal then having a resistance of about 10^4 ohms. Restoration of the original resistance, 10^{10} ohms, can be accomplished by means of a) R. F. voltage pulses and b) low-frequency voltage pulses, at fields of about 10^3 volts/cm. The time required for restoration is about a millisecond. Breakdown and restoration thus constitute a complete, electrically induced switching cycle, which is indefinitely repeatible. Other Group V - Group VI compound semiconductors have been examined, but only stibnite containing excess antimony has been found to possess this behavior.

Paper presented at the April, 1959, meeting of the Physical Society, Washington, D. C. Abstract has been published in the Bulletin of American Physics Society, Series II, 4, 228 (1959).

---

1 Davis and Gildart, Bull. Am. Phys. Soc., Series II, Vol. 3.

The following contributed papers were presented at the spring meeting of the Kentucky Section, American Association of Physics Teachers, May 14, 1960, Lexington, Kentucky. Abstracts have been published in the American Journal of Physics, 28, No. 8, 761 (1960).

PREBREAKDOWN PULSES IN STIBNITE, J. R. Davis, University of Kentucky. When stibnite crystals are subjected to large electric fields there occurs a permanent drop in resistance of several orders of magnitude. With the application of somewhat reduced fields, short pulses of current are observed similar to those seen in reverse biased semiconductor junctions. The present paper describes several experiments in which the prebreakdown pulses and the breakdown transitions were examined oscillographically following the application of a fast rise time step pulse having an amplitude variable to 1500 v. A time delay was observed between the applied pulse and the inception of either breakdown or prebreakdown behavior. The delay time was found to be of the order of microseconds and inversely dependent on the field strength in the sample.

OPTICAL ABSORPTION BAND EDGE IN THIN Sb_2Se_3 FILMS ,

T. E. Johnson, University of Kentucky. Films of Sb_2Se_3 from 0.07 to 1.0μ thick were deposited by vacuum evaporation onto optically flat fused-quartz substrates. The films formed on heated substrates were polycrystalline with a preferred orientation of lattice planes; those deposited at room temperature were amorphous, as determined by x-ray diffraction. The optical transmission was measured over the range of 0.4 to 2.5μ with a Cary spectrophotometer, model 14. Film thicknesses were determined optically. Using an IBM 650 computer, the transmission data for the two film modifications were fitted to a theoretical double layer equation, giving the indices of refraction and absorption coefficients as functions of wavelength. The amorphous films show low absorption in the near infrared with a steeply rising edge at 1.5 ev. In the near infrared, the level of absorption in the crystalline films is somewhat higher with the onset of strong absorption occurring at 1.17 ev, in good agreement with the 1.2 ev value[1] observed for bulk single cyrstals. The structure of the band edge for the crystalline films is similar to that of the intrinsic band edge for silicon.

---

1 J. Black, E. M. Conwell, L. Seigle, and C. W. Spencer, J. Phys. Chem. Solids 2, 240 (1957).

THERMAL CONDUCTIVITY OF BISMUTH SULFIDE, J. M. Kline, University of Kentucky. Thermal conductivity of semiconducting materials is measured by an improved comparison technique and, in addition, the Seebeck coefficient is determined with this apparatus. Elimination of the usual errors and losses due to thermal conduction and radiation is realized by judicious choice of materials for the standard and radiation shield. Optimizing the size and shape of the sample and single crystal bismuth standard is discussed. Preliminary measurements on bismuth sulfide and other group V-VI compounds at room temperature are given and an accuracy of three percent is estimated for the method.

PRODUCTION OF Bi_2S_3 and Bi_2O_3 SAMPLES FOR SEMICONDUCTING STUDIES, D. M. Mattox, University of Kentucky. Very little reliable data can be found in the literature on the two semiconducting compounds Bi_2S_3 and Bi_2O_3 apparently due to the difficulties involved in their production. A Bi_2S_3 sample tends to develop excessive sulfur vapor pressure at temperatures above its melting point of 800°C while Bi_2O_3 in the molten form will dissolve or diffuse through common crucible materials. A method of reacting bismuth and sulfur in a closed Vycor tube under constant rotation is described. A method of growing a single crystal of Bi_2S_3 in the reacting tube and furnace is also described. A method of preparing thick films of Bi_2O_3 is outlined. Some preliminary measurements of semiconducting parameters of the two compounds are given.

REFINEMENTS IN TECHNIQUE OF MAKING DENSITY MEASUREMENTS ON SMALL CRYSTALLINE SAMPLES, Ralph O. Meyer, University of Kentucky. The pycnometer method of measuring density is used to attempt to detect a change in density of the order of 1/2% in small samples of Sb_2S_3 of approximately 20-mesh size. Emphasis is placed on obtaining the desired results with the simplest equipment possible. Three outstanding problems are discussed: (1) temperature measurement; (2) elimination of air bubbles from the particle-water mixture; and (3) obtaining the dry weight of the sample in the particle-water mixture. The density of the sample measured had a probable error of 0.06%

SPECULATIONS ON THE SWITCHING EFFECT IN STIBNITE, Lee Gildart, University of Kentucky. Alternately applied voltage and current pulses cause single crystals of stibnite, grown with about a one percent deficit of sulfur by weight, to "switch" between two resistance states repeatedly, i.e., between 10^9 and 10^4 ohms. There is approximately one sulfur vacancy per unit cell; the conductivity changes from semiconducting to metallic; and the dead time and switch times are of the order of fractions of a microsecond. It is conjectured that there are bistable states α and β for the antimony atoms, with α about 0.1 ev higher than β. Switching is believed to be a cooperative action in which there is a "micro" phase change along the conducting filament.

6.1 Papers for Publication

"Some semiconducting Properties of Bismuth Trisulfide and Bismuth Trioxide", D. M. Mattox, Technical Note, AFOSR-TN-60-1028, July 31, 1960.

"A Study of the Transient Behavior and the Switching Effect in Antimony Trisulfide", J. R. Davis, Technical Note, AFOSR-121, December 17, 1960.

"Energy Gaps in Bismuth Trioxide", D. M. Mattox and L. Gildart, Journal of Physics and Chemistry of Solids, Vol. 18, Nos. 2/3, pp. 215 (1961).

"Some Semiconducting Properties of Bismuth Trisulfide", L. Gildart, J. M. Kline and D. M. Mattox, Physics and Chemistry of Solids, Vol. 18, No. 4, pp. 286-289 (1961).

"Switching Phenomenon in Stibnite", J. R. Davis, Lee Gildart, and T. E. Johnson, (in preparation).

6.2 Patents Issued

"Synthetic Stibnite Crystal and Method for Producing Same", Lee Gildart and J. A. Powell, U. S. Patent No. 2, 968, 014.

PART VII

7.0 Personnel

The number of persons working on the project was maintained at about the level provided for in the budget. The staff and periods of service are as follows:

Lee Gildart	Principal Investigator	July 1, 1958- Sept. 30, 1960
J. R. Davis	Grad. Research Assistant	July 1, 1958 -March 1, 1959
T. E. Johnson	Grad. Research Assistant	July 1, 1958 -Aug. 1, 1961
D. M. Mattox	Grad. Research Assistant	July 1, 1958-March 31, 1961
J. M. Kline	Grad. Research Assistant	Sept. 1, 1958-Oct. 31, 1961
J. A. Stamper	Grad. Research Assistant	July 1, 1958-July 31, 1958
J. A. Powell	* Student Research Assistant	July 1, 1958-Aug. 1, 1959 June 1, 1960-Sept. 30, 1960
D. R. Read	Student Research Assistant	July 1, 1958-Dec. 31, 1959
R. W. Spurlock	Student Research Assistant	July 1, 1958-Nov. 30, 1959
R. O. Meyer +	Student Research Assistant	Aug. 1, 1959-April 30, 1960
P. W. Phillips	Student Research Assistant	July 15, 1960-July 31, 1960
A. L. Hamilton	Student Research Assistant	Aug. 1, 1960-Sept. 30, 1960
E. Mangelsen	Student Research Assistant	Feb. 15, 1960-April 30, 1960
K. A. Schneider	Instrument Maker	Available as needed
A. Kocsis	Instrument Maker	Available as needed

Dr. L. W. Gildart began a 24 month leave of absence on Sept. 1, 1960, to serve as a visiting professor at the Bandung Institute of Technology, Bandung, Indonesia, under a contract arrangement between the University of Kentucky and the ICA.

---

* Student Research Assistants are undergraduates who are on an hourly rate.
+ NSF Undergraduate Research Participant, June 8, 1959-Aug. 1, 1959.

7.1 Graduate Student Thesis Work

Contract support has enabled the Department to give substantial financial help to five graduate research assistants, working toward advanced degrees while engaged in the work of the project.

Mr. J.R. Davis, Jr., completed the requirements for the M.S. degree in Aug., 1960; the title of his thesis is "A Study of the Transient Behavior and the Switching Effect in Antimony Trisulfide". Mr. Davis is Director of Solid State Devices Research, Wesson Corporation, Lexington, Kentucky.

Mr. T.E. Johnson, Jr., completed the requirements for the Ph.D. in July, 1961, and accepted a position in solid state physics with United States Steel Corporation. His dissertation research deals with electrical and optical properties of Sb_2Se_3 and Sb_2S_3 and the theory of the low voltage breakdown in Sb_2S_3.

Mr. J.M. Kline is completing his Ph.D. research on Bi_2S_3 as a thermoelectric material.

Mr. D.M. Mattox completed the requirements for the M.S. degree in Aug., 1960, and accepted a research position in solid state physics at the Sandia Corporation. The title of his thesis is "Some Semiconducting Properties of Bismuth Trisulfide and Bismuth Trioxide".

Mr. J.A. Stamper completed the requirements for the M.S. degree in July, 1958, and accepted a research position in solid state physics at Texas Instrument. The title of his thesis is "Measurement of Hall Coefficients of Certain Compound Semiconductors".